

# **Synthesis of ferrocenyl conjugates of sulfa drugs and study as antimicrobial agents**

**By**

**Katleho Setlaba**



**Supervisor: Dr. Prinessa Chellan**

**Faculty of Science**

**Department of Chemistry and Polymer Science**

**March 2023**

## **Declaration**

By submitting this thesis electronically, I declare that the entirety of the work contained therein is my own, original work, that I am the sole author thereof (save to the extent explicitly otherwise stated), that reproduction and publication thereof by Stellenbosch University will not infringe any third-party rights and that I have not previously in its entirety or in part submitted it for obtaining any qualification.

Katleho Setlaba

March 2023

## Acknowledgements

First and foremost, I thank God for the knowledge, countless blessings, grace, and for helping me to carry out this research and complete this dissertation.

Secondly, I would like to express my deepest appreciation to my supervisor, Dr. Prinessa Chellan, for her expertise, invaluable guidance, and support throughout my MSc degree. Thank you for your patience, advice, and encouragement. I wouldn't be the researcher I am today without you.

I would like to acknowledge the following people for their assistance:

- Dr. Jaco Brand and Mrs. Elsa Malherbe (University of Stellenbosch) for the recording of the NMR spectra.
- Dr. Marietjie Stander (University of Stellenbosch) for mass spectral analyses.
- Dr. Dale Taylor and his team (H3D, University of Cape Town) for performing antiplasmodial screening.
- Dr. Lucinda Baatjies (Division of molecular biology and human genetics, Stellenbosch University) for performing antimycobacterial screening.
- Mr. Malcolm Ndlovu, under the supervision of Dr. Catherine Kaschula (University of Stellenbosch), for performing cytotoxicity studies.

A special thanks to Chellan Research group for insightful discussions in and outside the lab. I would also like to thank the Organometallic Research group for constructive criticism and discussions during our meetings.

A special thanks to my friend, Samantha Le Roux, for taking the time to proofread my chapters. Thank you for your constructive criticism.

I am grateful to Stellenbosch University Postgraduate Scholarship Programme (PSP) for their financial support. I also thank the Royal Society-African Academy of Sciences for funding this project.

Lastly, I would like to express my sincerest gratitude and appreciation to my family, especially my mother, Elsie Setlaba. Thank you for your love, encouragement, and support throughout this journey. To my sister and brother, Diketso Matamane, and Tshepo Setlaba, thank you.

**May God bless you all!!!**

## Conferences/Symposia contribution

1. **Oral presentation:** Katleho Setlaba, Prinessa Chellan, “*Synthesis and characterisation of ferrocenyl conjugates of sulfa drugs and study as antimicrobial agents*”, presented at the Western Cape Young Chemist Conference, Stellenbosch University, South Africa, 7620.

## Abstract

As humans have spread across the globe so have infectious diseases. Malaria and tuberculosis are among the most widespread infectious diseases, after Covid-19, affecting millions of people annually. Despite the effectiveness of the currently used antimalarial and anti-TB drugs, the emergence of drug resistance in the malaria parasite, *Plasmodium falciparum*, as well as multidrug resistant and extremely drug resistant forms of *Mycobacterium tuberculosis* is a growing problem and calls for the urgent need of new antimicrobial agents. In efforts to decrease the morbidity/mortality rates related to these diseases, it is important for these new antimicrobial drugs to target the resistant strains. A unique strategy in drug discovery today is drug repositioning, which involves the modification of known clinical drugs to rapidly identify new ones to treat other diseases. Looking at the current economic situation, this strategy could speed up the process of drug development to save costs. This study investigated the synthesis, characterisation, electrochemical and biological properties of new ferrocenyl amido sulfonamide complexes prepared from known sulfa drugs.

The new ferrocenyl organometallic complexes were prepared by the reaction of the primary amine functional group of sulfonamide compounds with ferrocenoyl chloride. All complexes were characterised using various spectroscopic and analytical techniques, such as  $^1\text{H}$  and  $^{13}\text{C}$   $\{^1\text{H}\}$  nuclear magnetic resonance (NMR) spectroscopy, infrared (IR) spectroscopy, electrospray ionisation-mass spectrometry (ESI-MS), cyclic voltammetry (CV), and reversed-phase high performance liquid chromatography (RP-HPLC).

The new complexes were tested for antiparasmodial activity against the chloroquine-sensitive NF54 strain of *Plasmodium falciparum*. Upon the introduction of the ferrocenyl moiety, the activity of selected sulfonamides was significantly enhanced, with some of the complexes being more active than their respective sulfa drugs. Complex **C2** displayed the best activity of all the complexes with an  $\text{IC}_{50}$  value of  $3.714\ \mu\text{M}$  followed by **C5** ( $\text{IC}_{50} = 5.822\ \mu\text{M}$ ). Thereafter, the complexes and their respective sulfa drugs were tested for antimycobacterial activity against the non-pathogenic Mc<sup>2</sup>155 and the pathogenic H37Rv strains of *Mycobacterium tuberculosis*. The complexes displayed better activities when tested against the strain H37Rv compared to results obtained for the Mc<sup>2</sup>155 strain. The complexes also displayed to be more potent than isoniazid against both strains.

In addition, the complexes were further screened for their cytotoxicity against the human embryonic kidney (HEK) and immortalised prostatic (PNT1A) cell lines and were found to be non-cytotoxic.

## Uittreksel

Soos mense oor die hele wêreld versprei het, so het aansteeklike siektes ook. Malaria en tuberkulose is van die mees wydverspreide aansteeklike siektes, na Covid-19, wat jaarliks miljoene mense affekteer. Ten spyte van die doeltreffendheid van die tans gebruikte antimalaria- en anti-TB-middels, is die oorsprong van middel weerstandigheid in die malariaparasiet, *Plasmodium falciparum*, sowel as multi-middel-weerstande en uiters middel-weerstandige vorms van *Mycobacterium tuberculosis* 'n groeiende probleem en is daar 'n dringende aanvraag na nuwe antimikrobiese middels. In pogings om die morbiditeit/sterftekoerse wat met hierdie siektes verband hou, te verlaag, is dit belangrik dat hierdie nuwe antimikrobiese middels die weerstandbiedende stamme teiken. 'n Unieke strategie in die ontdekking van geneesmiddels vandag is dwelmherposisionering, wat die wysiging van bekende kliniese middels behels om nuwes vinnig te identifiseer. As ons na die huidige ekonomiese situasie kyk, kan hierdie strategie die proses van geneesmiddelontwikkeling versnel om koste te spaar. Hierdie studie het die sintese, karakterisering, elektrochemiese en biologiese eienskappe van nuwe ferrosenielamido-sulfonamiedkomplekse wat van bekende sulfa middels berei is ondersoek.

Hierdie nuwe ferroseniel-organometaalkomplekse is berei deur die reaksie van die primêre amien funksionele groep van sulfonamide verbindings met ferrosenielchloried. Alle komplekse is gekarakteriseer deur gebruik te maak van verskeie spektroskopiese en analitiese tegnieke, soos  $^1\text{H}$  en  $^{13}\text{C}$   $\{^1\text{H}\}$  kernmagnetiese resonansie (KMR) spektroskopie, infrarooi (IR) spektroskopie, elektrospoei ionisasie-massaspektrometrie (ESI-MS), sikliese voltammetrie (CV), en omgekeerde-fase hoë werkverrigting vloeistofchromatografie (RP-HPLC).

Die komplekse is getoets vir antiplasmodiese aktiwiteit teen die chlorokien-sensitiewe NF54-stam van *Plasmodium falciparum*. Met die inlywing van die ferroseniel-eenheid is die aktiwiteit van geselekteerde sulfonamiede aansienlik verhoog, met sommige van die komplekse wat meer aktief was as hul onderskeie sulfa-middels. Kompleks **C2** het die beste aktiwiteit van al die komplekse vertoon met 'n  $\text{IC}_{50}$  waarde van  $3.714\ \mu\text{M}$  gevolg deur **C5** ( $\text{IC}_{50} = 5.822\ \mu\text{M}$ ). Daarna is die komplekse en hul onderskeie sulfa-middels getoets vir antimikobakteriële aktiwiteit teen die nie-patogeniese Mc<sup>2</sup>155 en die patogeniese H37Rv-stamme van *Mycobacterium tuberculosis*. Die komplekse het beter aktiwiteite in die stam H37Rv vertoon in vergelyking met dié in die Mc<sup>2</sup>155-stam. Die komplekse het ook getoon om sterker as isoniazied in beide stamme te wees.

Verder is die komplekse getoets vir hul sitotoksiteit teen die menslike embrioniese nier (HEK) en geïmmobiliseerde prostaat (PNT1A) sellyne en is gevind dat dit nie-sitotoksies is nie.



## List of Abbreviations

<b>3D7</b>	Chloroquine-sensitive <i>Plasmodium falciparum</i> strain
<b>ACT</b>	Artemisinin-based combination therapy
<b>ADME</b>	Absorption, distribution, metabolism, elimination
<b>AMK</b>	Amikacin
<b>AMR</b>	Antimicrobial resistance
<b>ATR</b>	Attenuated Total Reflectance
<b>C<sub>p</sub></b>	Cyclopentadienyl ring
<b>CQ</b>	Chloroquine
<b>CS</b>	Cycloserine
<b>CYP</b>	Cytochrome P450
<b>Dd2</b>	Chloroquine-resistant <i>Plasmodium falciparum</i> strain
<b>DMF</b>	<i>N, N</i> -dimethylformide
<b>DMSO</b>	Dimethylsulfoxide
<b>DOT</b>	Directly observed therapy
<b>E<sub>1/2</sub></b>	Half-wave potentials
<b>EMB</b>	Ethambutol
<b>E<sub>pa</sub></b>	Anodic peak potentials
<b>E<sub>pc</sub></b>	Cathodic peak potentials
<b>Fc</b>	Ferrocene
<b>FcOHTAM</b>	Hydroxyferrocifen
<b>FcTAM</b>	Ferrocifen
<b>FQ</b>	Ferroquine
<b>GI</b>	Gastrointestinal
<b>GTS</b>	Global Technical Strategy
<b>HEK</b>	Human embryonic kidney
<b>HEPS</b>	4-(2-hydroxyethyl) -1-piperazineethanesulfonic acid
<b>HIV</b>	Human Immunodeficiency Virus
<b>HPLC</b>	High-performance liquid chromatography
<b>IC<sub>50</sub></b>	Half-maximal inhibitory concentration
<b>INH</b>	Isoniazid
<b>IPTp</b>	Intermittent preventative treatment in pregnancy

<b>IR</b>	Infrared Spectroscopy
<b>IRS</b>	Indoor residual spray
<b>ITNs</b>	Insecticide-treated mosquito nets
<b>KAN</b>	Kanamycin
<b><i>M. smeg</i></b>	<i>Mycobacterium smegmatis</i>
<b><i>M. tb</i></b>	<i>Mycobacterium tuberculosis</i>
<b>MIC</b>	Minimum inhibitory concentration
<b>MLCT</b>	Metal-to-ligand charge transfer
<b>MS</b>	Mass Spectrometry
<b>NAC</b>	N-acetylcysteine
<b>NADH</b>	Nicotinamide adenine dinucleotide
<b>PBS</b>	Phosphate-buffered saline
<b>pLDH</b>	Plasmodium lactate dehydrogenase
<b>PZA</b>	Pyrazinamide
<b>R<sup>2</sup></b>	Correlation coefficient
<b>RIF</b>	Rifampicin
<b>ROS</b>	Reactive oxygen species
<b>SP</b>	Sulfadoxine-Pyrimethamine
<b>TB</b>	Tuberculosis
<b>TBAP</b>	Tetrabutylammonium perchlorate
<b>TLC</b>	Thin layer chromatography
<b>WHO</b>	World health organisation
<b>δ</b>	Chemical shift

## Table of Contents

<b>Declaration.....</b>	<b>i</b>
<b>Acknowledgements .....</b>	<b>ii</b>
<b>Conferences/Symposia contribution.....</b>	<b>iii</b>
<b>Abstract.....</b>	<b>iv</b>
<b>Uittreksel.....</b>	<b>vi</b>
<b>List of Abbreviations .....</b>	<b>viii</b>
 <b>Chapter 1: Literature review .....</b>	 <b>1</b>
1.1 Malaria .....	1
1.1.1 The life cycle of the Plasmodium parasite.....	2
1.1.2 Prevention, Diagnosis, and Treatment.....	3
1.2 Tuberculosis .....	6
1.2.1 The pathogenesis of <i>Mycobacterium tuberculosis</i> .....	7
1.2.2 Treatment: Past and currently used drugs.....	8
1.3 Sulfonamides .....	12
1.4 Metals in medicine .....	14
1.4.1 Metallodrugs as antimicrobial agents .....	15
1.4.2 Sulfonamide complexes as anti-microbial agents .....	17
1.5 Ferrocene .....	20
1.5.1 Ferrocene-based antimalarial agents .....	23
1.5.2 Ferrocene based antitubercular agents.....	25
1.6 Problem Statement .....	26
1.7 Aim and objectives.....	26
1.7.1 Aim .....	26
1.7.2 Specific objectives:.....	26
1.8 Thesis lay-out .....	28

1.9 References .....	28
<b>Chapter 2: Synthesis and characterisation of ferrocenyl derivatives of sulfonamides ...</b>	<b>38</b>
2.1 Introduction .....	38
2.2 Results and discussion.....	40
2.2.1 Synthesis .....	40
2.2.2 Characterisation .....	44
2.3 Electrochemical studies .....	50
2.4 Stability studies .....	52
2.5 Summary .....	57
2.6 Experimental .....	58
2.6.1 Chemicals and reagents .....	58
2.6.2 Materials and methods .....	58
2.6.3 A general synthetic method .....	58
2.6.4 Electrochemical studies .....	63
2.6.5 HPLC method and purity determination .....	63
2.7 References .....	63
<b>Chapter 3: <i>In vitro</i> biological evaluation of ferrocenyl derivatives of sulfonamide complexes .....</b>	<b>67</b>
3.1 Introduction .....	67
3.2 Results and discussion.....	69
3.2.1 Predicting lipophilicity .....	69
3.2.2 Turbidimetric solubility studies.....	75
3.2.3 <i>In vitro</i> antiparasmodial evaluation against <i>Plasmodium falciparum</i> .....	77
3.2.4 <i>In vitro</i> antimycobacterial evaluation against tuberculosis .....	79
3.2.5 <i>In vitro</i> cytotoxicity studies on healthy cells .....	81

3.2.6 Aqueous stability studies .....	83
3.3 Summary .....	85
3.4 Experimental .....	86
3.4.1 Turbidimetric Assay .....	86
3.4.2 Evaluation of <i>in vitro</i> activity against <i>Plasmodium falciparum</i> .....	86
3.4.3 Evaluation of <i>in vitro</i> activity against <i>Mycobacterium tuberculosis</i> .....	87
3.4.4 <i>In vitro</i> cytotoxicity on healthy cell lines .....	88
3.5 References .....	88
<b>Chapter 4: Conclusions and future work .....</b>	<b>93</b>
4.1 Conclusions .....	93
4.2 Future work .....	94
4.2.1 Mechanistic studies.....	94
4.2.2 Structural modifications .....	95
4.3 References .....	96

## Chapter 1: Literature review

### 1.1 Malaria

Malaria is an infectious disease caused by protozoan parasite species of the genus *Plasmodium*. Four of these species – *Plasmodium falciparum*, *Plasmodium vivax*, *Plasmodium malariae*, and *Plasmodium ovale* – are human malaria species transmitted from one person to another through the bite of an infected female *Anopheles* mosquito.<sup>1</sup> Over the past few years, human cases of malaria due to the *Plasmodium knowlesi* species (simian malaria parasite) have been reported, recognizing the species as the fifth causative agent of human malaria.<sup>2</sup> Malaria continues to be a threat to humans, causing nearly one million deaths each year. The Global Technical Strategy (GTS) for malaria, initiated in 2006, has been a clear success in decreasing the malaria mortality rate by half in 2015 from thirty in early 2000 and continued to decrease at a much slower rate.<sup>3</sup> However, disruption to services due to the Covid-19 pandemic, lead to a substantial increase with an estimated 241 million malaria cases and 627 000 deaths in 2020.<sup>4</sup> Increasing from 229 million cases and 409 000 deaths in 2019.<sup>5</sup> Figure 1.1, shows malaria case incidence rates by country in 2018.<sup>6</sup>

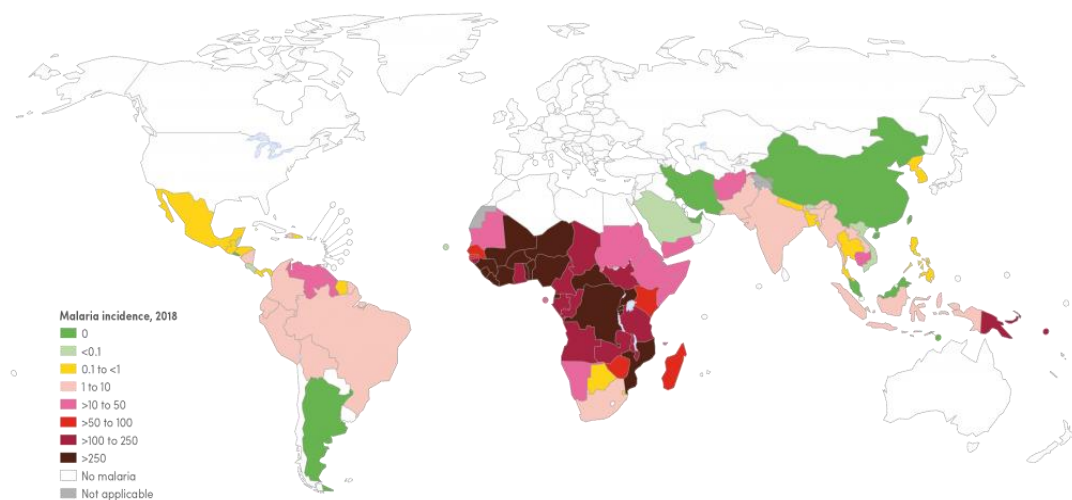


Figure 1.1: Map of malaria case incidence rate (cases per 1000 population at risk) by country, 2018.<sup>6</sup>

*Plasmodium falciparum* is the most life-threatening malaria species among the five *Plasmodium* species on the African continent, responsible for approximately 95% of all malaria deaths.<sup>7</sup> The *P. vivax* species is not as virulent as the *P. falciparum* species, but it has a wider geographic distribution owing to its ability to develop and survive at very low temperatures and high altitudes. In addition, it also has a dormant liver stage, called the hypnozoite, which enables the parasite to survive for a long period causing a relapse of symptoms. Infections due to *P. vivax* species are more common in areas outside Africa causing substantial morbidity. To discover new effective interventions it is essential to understand how the disease is transmitted and the pathology of the parasite.<sup>7</sup>

### **1.1.1 The life cycle of the Plasmodium parasite**

The life cycle of the Plasmodium parasite involves two hosts, the human and the female Anopheles mosquito (Figure 1.2).<sup>1</sup> The cycle within the human host begins when infective sporozoites with anticoagulant-containing saliva are injected into the human host by an infected female Anopheles mosquito. The infective sporozoites are slowly released into the bloodstream from the site of infection. Once the sporozoites reach the liver, they diffuse into hepatocytes where they undergo asexual replication to produce merozoites.<sup>8</sup> The invasive merozoites are released back into the bloodstream where they invade the red blood cells through multiple receptor-ligand interactions. The interactions initiate the blood stage which is responsible for clinical manifestation (e.g., fever). The merozoites grow and divide asexually into schizonts through the ring stage, trophozoites.<sup>9</sup> The schizonts burst to release new merozoites. With each multiplication cycle, some of the merozoites, instead of producing new merozoites, develop into male (microgametocytes) and female (macrogametocytes) gametocytes. The vector ingests the gametocytes as a blood meal, which fuse in the vector's stomach, generating zygotes.<sup>10</sup> The zygotes in turn mature into ookinetes which penetrate the midgut wall of the mosquito, where they grow into oocysts. The oocyst matures, bursts, and releases sporozoites which make their way to the mosquito's salivary glands, and the cycle is repeated.<sup>8</sup>





A clear understanding of the different stages of the parasite is essential in the design and development of antimalarial drugs. Minimum knowledge of the liver stage led to quinolones- primaquine and tafenoquine- being the only ones that target this stage with unknown mechanisms of action. However, in the case of asexual blood-stage research has discovered several processes as effective drug targets. This includes haemoglobin degradation and haeme detoxification, the folate biosynthesis pathway, and protein synthesis in the apicoplast.

Quinine, found in the bark of the cinchona tree, and its related compounds [quinine (QN), mefloquine (MFQ), chloroquine (CQ), and hydroxychloroquine (HCQ) Figure 1.4] were the first drugs to be used for the treatment of malaria. Out of the quinolone compounds, CQ stands out as being the most effective, yet inexpensive antimalarial drug used. This group of compounds is believed to inhibit  $\beta$ -haematin formation in the digestive vacuole of the parasite.

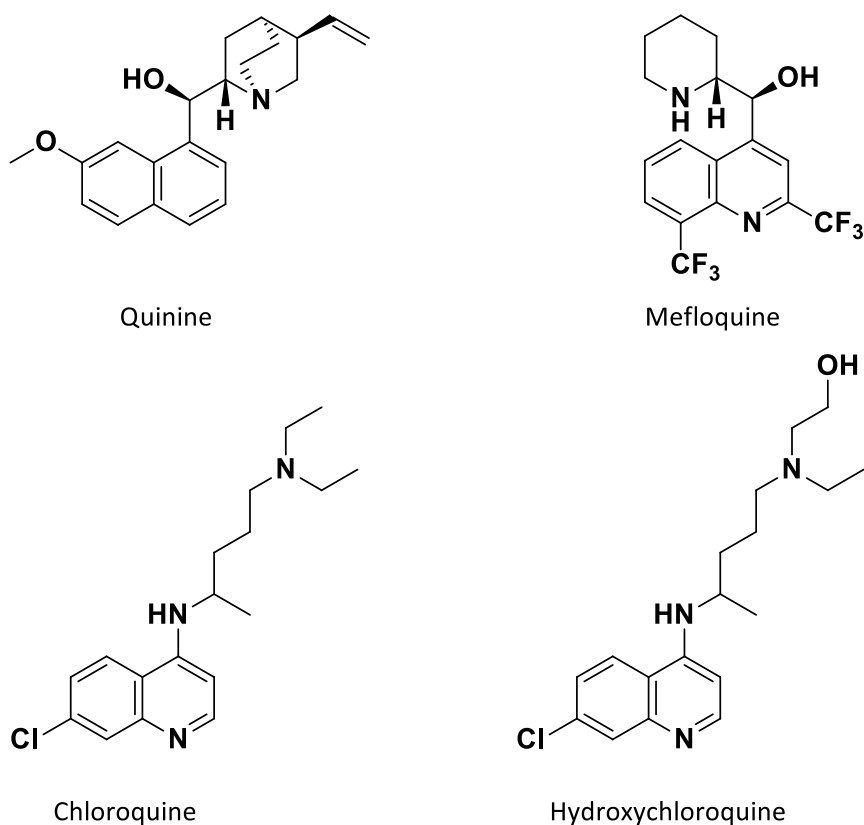


Figure 1.4: Quinoline-based antimalarials.

Antifolates are known to inhibit the formation of enzymes in the folate biosynthesis pathway, which is essential for malaria parasite survival.<sup>13</sup> This group of compounds is more potent when administered as a combination or pair and is mainly categorized into dihydropteroate synthase (DHPS) inhibitors (sulfadoxine, Sulfaline, or dapsone) and dihydrofolate reductase (DHFR) inhibitors (pyrimethamine, proguanil, or chlorproguanil) (Figure 1.5). Resistance to antifolates is caused by point mutations in the targeted enzyme. However, sulfadoxine-pyrimethamine is still used in combination with artesunate.

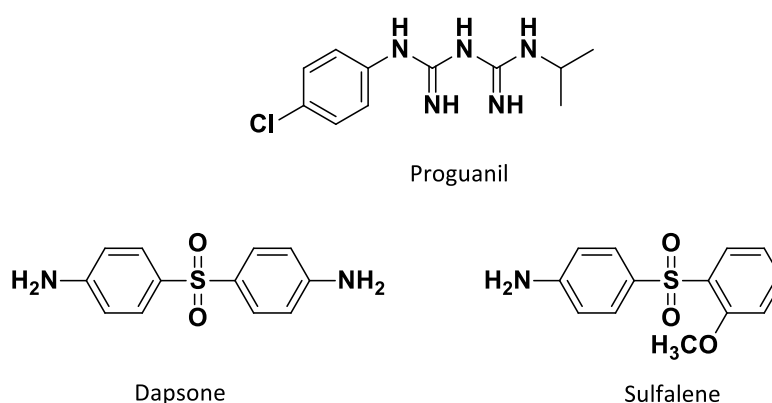


Figure 1.5: Class I (bottom) and II (top) antifolates used to treat malaria.

To date, the most effective treatment against malaria infections is the Artemisinin-based combination therapy (ACT). Artemisinin is isolated from the Chinese sweet wormwood plant and was traditionally used to treat fever. Artemisinin derivatives are fast acting and highly potent antimicrobial agents against all erythrocytic stages of the malaria parasite.<sup>14</sup> This is attributed by their ability to generate reactive oxygen species (ROS) or carbon-centred free radicals as they become active.<sup>15</sup> Although artemisinins are highly potent and fast-acting drugs, they have a very short half-life. Hence artemisinins are often administered in combination with long-lasting drugs. According to the world health organisation (WHO), the first-line treatment for *P. falciparum* includes artemether-lumefantrine, artesunate-amodiaquine, dihydroartemisinin-piperaquine, and artesunate-pyronaridine.<sup>5</sup> Although ACT is recognized as the most effective treatment against malaria infection, incidences of greater than 20% failure due to drug resistance have recently been reported.<sup>16</sup> Emphasizing the need for the design and development of novel antimalarial agents with an alternative mechanism of action.

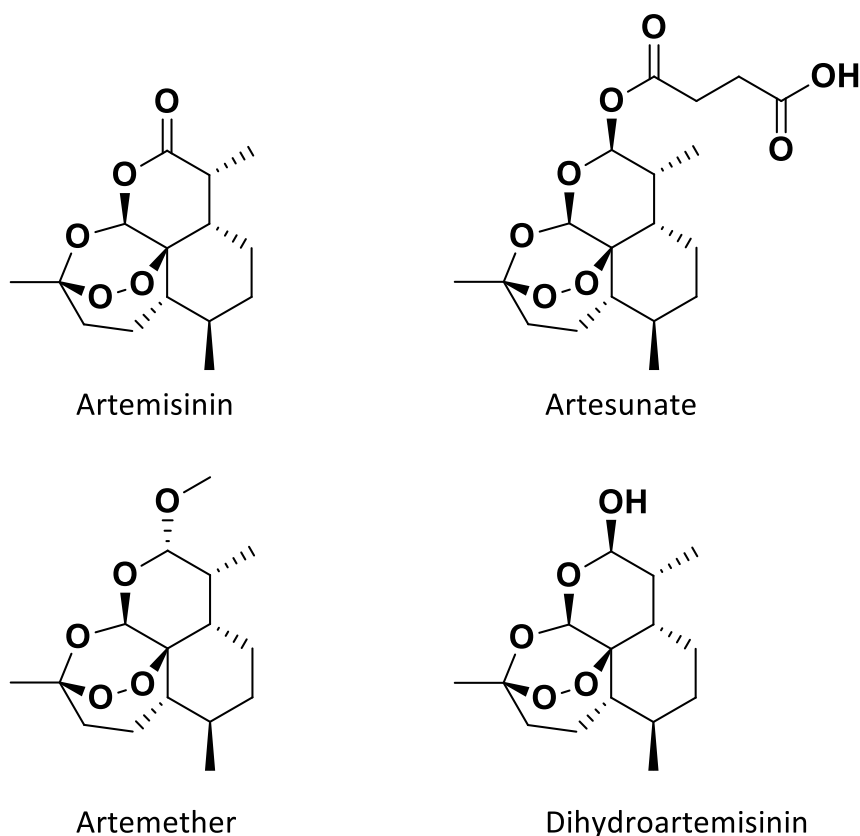


Figure 1.6: Artemisinin and derivatives.

## 1.2 Tuberculosis

Tuberculosis (TB), a well-adapted human bacteria, is an infectious disease caused by a single infectious agent *Mycobacterium tuberculosis* (*Mtb*), which was first identified by Robert Koch in 1882.<sup>17,18</sup> The airborne bacteria primarily affects the lungs (pulmonary TB), but can also spread to other parts of the body such as the spine, lymph nodes, kidneys, and the central nervous system (extrapulmonary TB). Despite being a curable and preventative disease, tuberculosis remains a major public health problem and it was declared a global health emergency by the World Health Organization (WHO) in 1993.<sup>19,20</sup> According to the World Health Organization, 5.9 million people were diagnosed with TB and 1.3 million deaths were recorded in 2020.<sup>21</sup> Furthermore, it was estimated that one-third of the world's population is infected with *Mycobacterium tuberculosis* and is at risk of re-activation of the disease. Sub-Saharan Africa has the highest cases of TB per capita, which is mainly driven by the human immunodeficiency virus (HIV). Figure 1.7, shows the estimated TB incidence in 2020.<sup>21</sup>

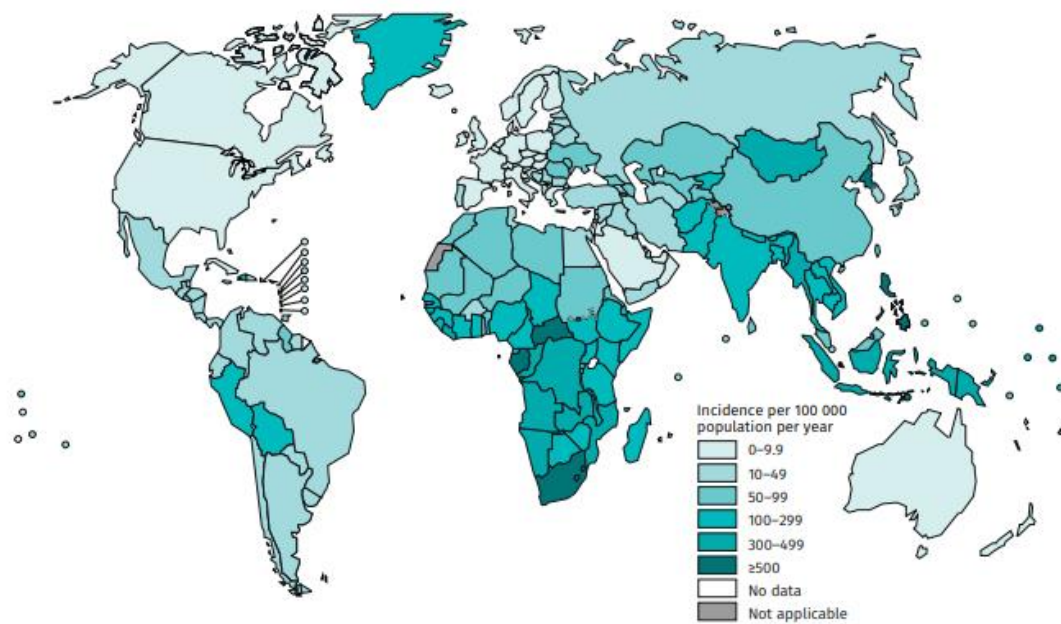


Figure 1.7: The estimated TB incidences in 2020 according to WHO.<sup>21</sup>

### 1.2.1 The pathogenesis of *Mycobacterium tuberculosis*

Infection starts when an uninfected person inhales water droplets containing *Mycobacterium tuberculosis* bacilli expelled into the atmosphere through coughing or sneezing by the infected person.<sup>22</sup> The macrophages in the alveoli ingest the mycobacteria. At this phase, the destruction of mycobacteria is dependent on the intrinsic capacity of the host phagocyte and the virulence factors of the ingested bacteria. The immune system subsequently stimulates the release of monocytes and other inflammatory cells to form dynamic organized structures called granulomas. Granulomas do not necessarily destroy bacteria but serve as an effective means to contain the spread of bacteria.<sup>22,23</sup>

As cellular immunity develops, the mycobacteria grow and cause a disruption of the macrophages and little tissue damage. Consequently, T-cells immunity develops antigen-specific T-lymphocytes, which proliferate and activates the macrophages to suppress the extracellular growth of mycobacteria. This enclosed infection is known as latent TB (Persistent TB) and remains throughout a host's life in a non-transmitted/asymptomatic state.<sup>17,24</sup> In addition, at this point infection may also be destroyed depending on the strength of the host's cellular immunity.

However, if a latently infected person's immune system becomes weakened by immunosuppressive drugs, HIV infection, malnutrition, aging, or other factors, then the granuloma center may serve as a rich medium in which *Mycobacterium* can progress in an uncontrolled manner. Hematogenous dissemination may also occur causing the formation of cavities which may further lead to the rupture of nearby bronchi allowing bacteria to spread through the airways to other parts of the lungs and body through the blood and lymphatic system. The person becomes infectious and requires antibiotic treatment to survive.<sup>25,26</sup>

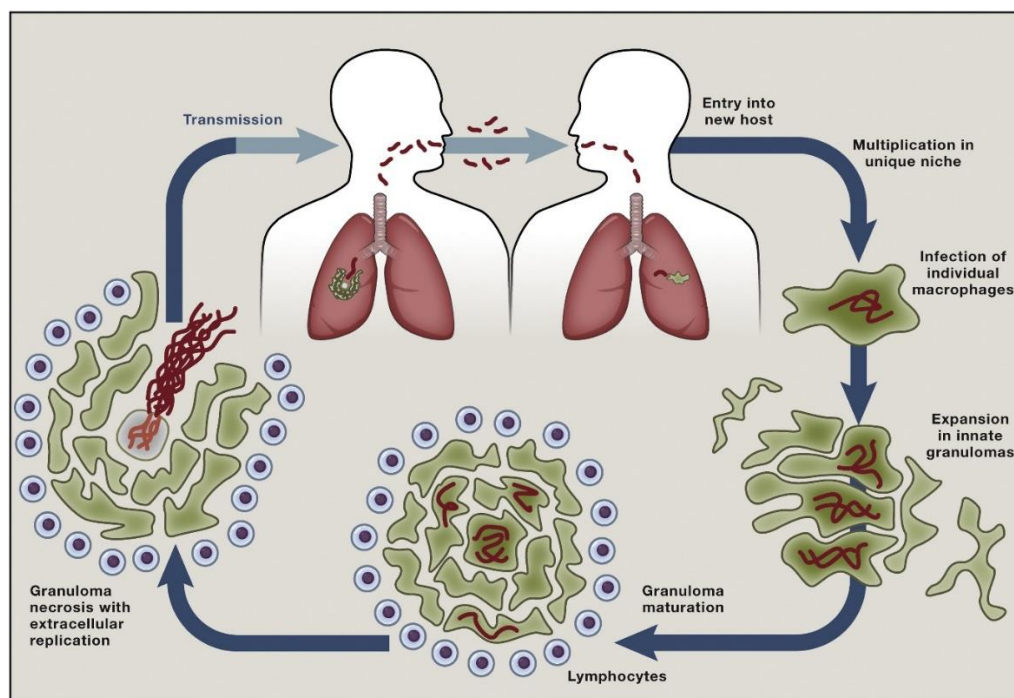


Figure 1.8: Pathogenesis of *Mycobacterium tuberculosis*.<sup>27</sup>

### 1.2.2 Treatment: Past and currently used drugs

Streptomycin was the first effective anti-tuberculosis agent to be discovered in the early 1940s.<sup>28,29</sup> Although it was proven to be active against the *Mycobacterium tuberculosis* strain, there were still controversies about its ability to persistently inhibit bacteria as a monotherapeutic agent. However, the vast appearance of drug resistance to streptomycin perpetuated the discovery and development of several TB drugs with different modes of action. These drugs include isoniazid (INH), pyrazinamide (PZA), cycloserine (CS), rifampicin (RIF), and kanamycin (KAN). The combined use of the above- mentioned drugs were found to be highly effective.

The standard treatment, recommended by the World Health Organization, for susceptible TB (DS-TB) regardless of HIV status involves a combination of the four first-line drugs, INH, RIF, PYZ, and ethambutol (EMB). The treatment starts with two months of intensive, directly observed therapy (DOT), with all four drugs followed by a continuous four months, continuation phase, of INH and RIF.<sup>30</sup>

Table 1: Summary of anti-TB first-line drugs.

<b>Drug</b>	<b>Route of administration</b>	<b>Mode of action</b>	<b>Resistance associated genes</b>	<b>Ref.</b>
<b>Isoniazid</b>	Oral	Inhibits the synthesis of mycolic acid.	katG, inhA	31–33
<b>Rifampicin</b>	Oral	Inhibits RNA synthesis through the inhibition of bacterial DNA-dependent RNA polymerase (RNAP).	rpoB	34,35
<b>Pyrazinamide</b>	Oral	First hydrolyzed into Pyrainoic acid, which inhibits the renal excretion of uric acid.	pncA, rpsA, panD, clpC1	36
<b>Ethambutol</b>	Oral	Inhibits the biosynthesis of polysaccharides on the mycobacterial cell wall by suppressing the arabinosyltransferase enzyme.	embB, ubiA	37,38

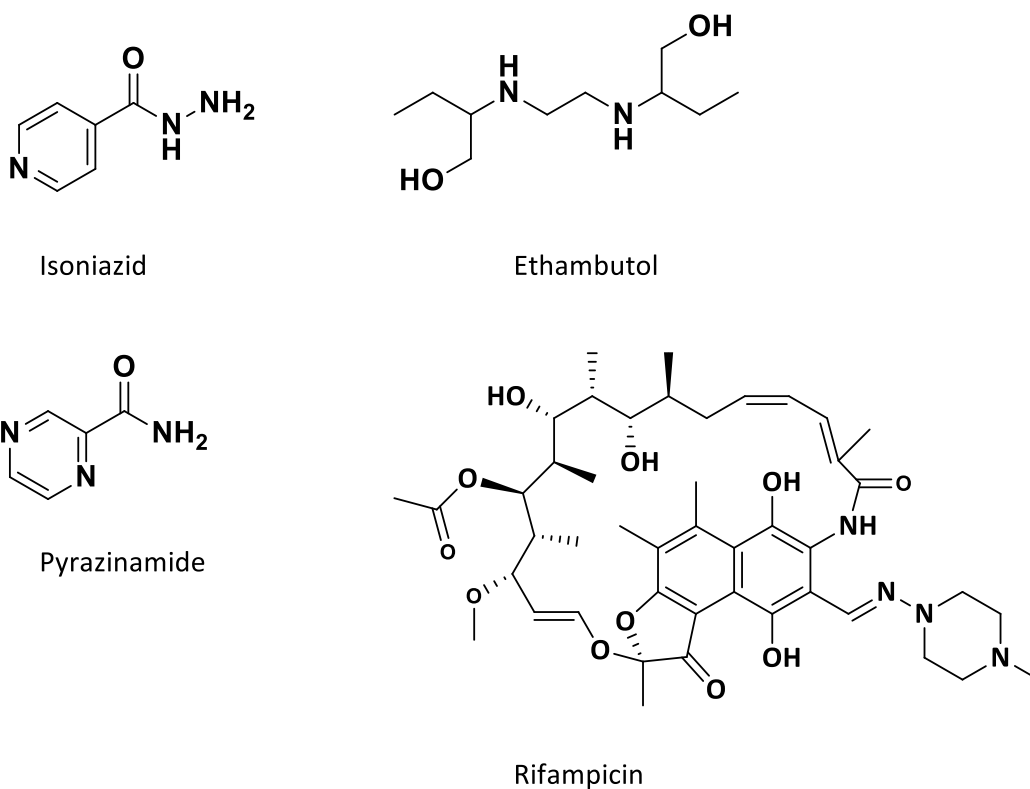


Figure 1.9: First-line drugs against DS-TB.

TB drugs were developed more than 40 years ago and taking this into consideration, they have some severe side effects associated with them subsequently lead to poor therapy compliance. In addition to poor therapy compliance, the long therapy duration and the required number of drug doses contributed to the appearance of multidrug-resistant, defined as resistant to INH and RIF, and extensively drug-resistant, which is defined as resistant not only to INH and RIF but also to fluoroquinolone drugs<sup>39,40</sup> and one of the second-line injectables agents CM, KAN or amikacin (AMK).<sup>41,42</sup>

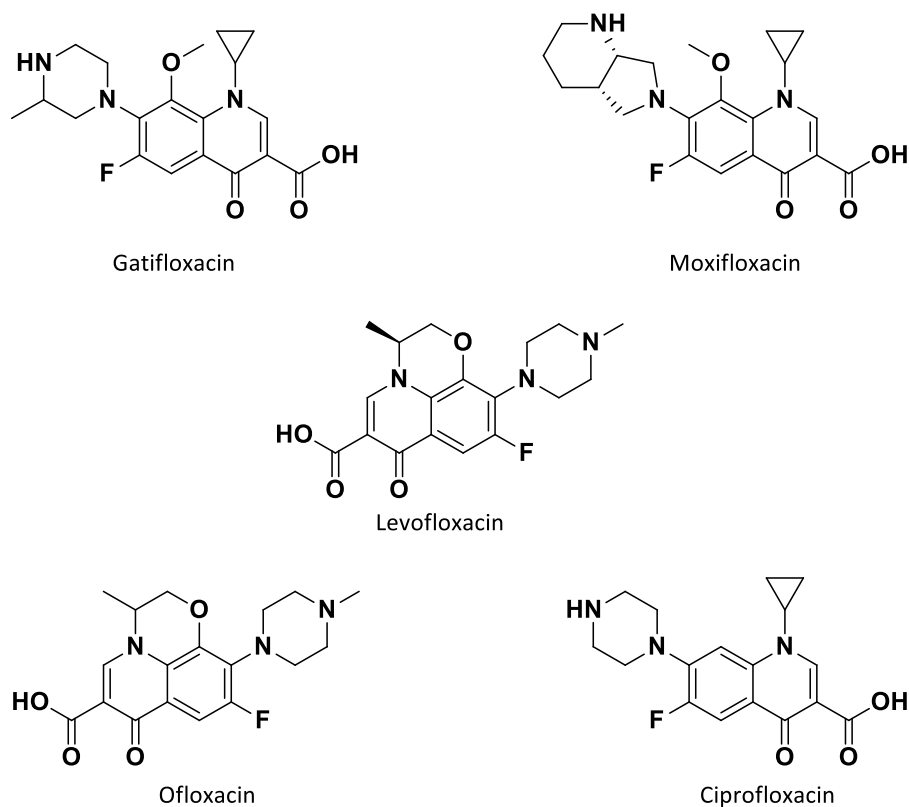


Figure 1.10: Second-line fluoroquinolone based anti-TB drugs.<sup>40</sup>

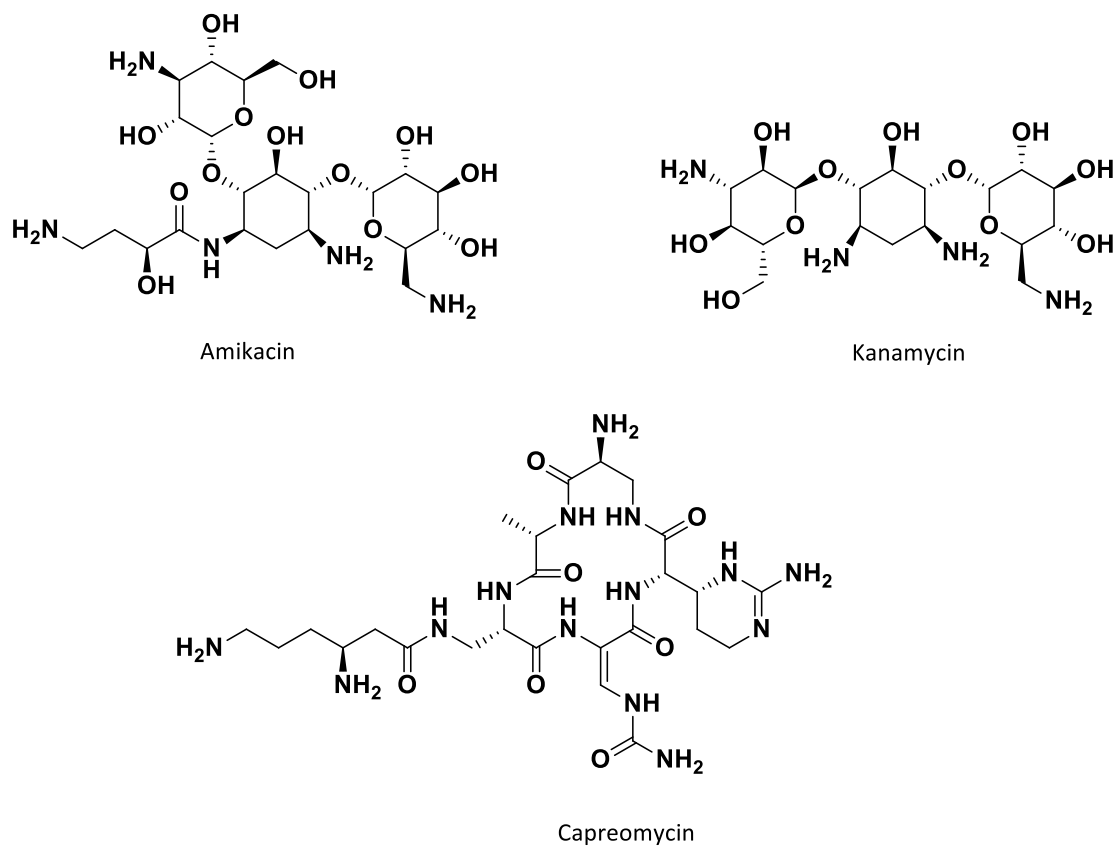


Figure 1.11: Second-line injectable drugs for treatment of drug resistant TB.<sup>42</sup>



### 1.3 Sulfonamides

In the early 1930s, a German scientist, Gerhard Domagk proposed that protosil (Figure 1.12a), an azo dye, was able to inhibit bacterial infections.<sup>43</sup> Shortly after his proposal, it was established that protosil is hydrolysed *in vivo* forming the active antimetabolite, sulfanilamide (Figure 1.12b). Sulfanilamide not only become widely used as a therapeutic agent, but it also served as a lead compound for chemists to design and synthesize compounds with higher biological activity. After its extensive structural modifications, it was shown by substituting one of the hydrogen atoms of the  $\text{SO}_2\text{NH}_2$  group with a heterocyclic ring resulted in compounds that not only proved to be more potent than sulfanilamide but also exhibited a broader spectrum of biological activity in addition to the well-known antibacterial effect.<sup>44</sup> Taking into consideration that there are currently more than 150 FDA-approved sulfur-containing drugs, it goes without saying that sulfonamides are still of great significant relevance in the pharmaceutical industry.

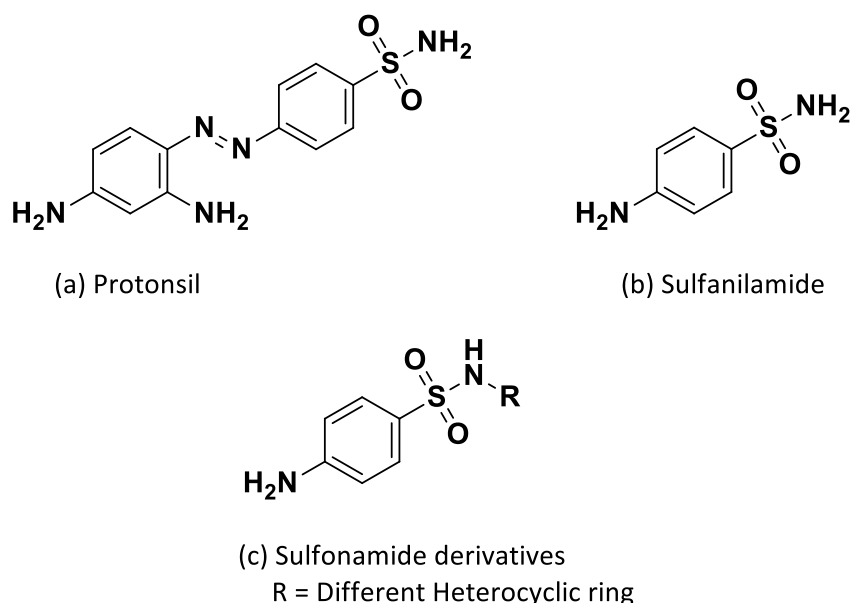
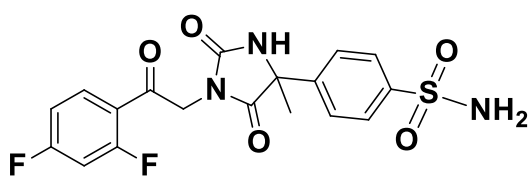


Figure 1.12: Chemical structure of (a) Protosil; b) biologically active, Sulfanilamide; c) the general structure of sulfonamides.

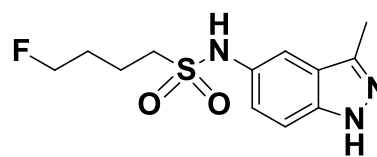
As a result of their increasing biological application, many different methods have been developed for their (sulfonamides) synthesis. The most common classical method involves the nucleophilic reaction between primary or secondary amines and sulfonyl chloride in the presence of a base.<sup>44</sup> However, the substrate in the method, sulfonyl chlorides are often very difficult to handle or store due to their instability.<sup>45</sup> Sulfonyl chlorides can also be prepared from sulfonic acids or thiols.<sup>46</sup> Furthermore, several metal-catalysed reactions like the use of Pd,<sup>47</sup> Rh,<sup>48</sup> and Cu<sup>49</sup> as transition metal catalysts can be used to generate sulfonamides in good yields.<sup>44,50</sup>

Sulfonamides inhibit dihydropteroate synthase (DHPS) by locking into the para-aminobenzoic acid (PABA) pocket of the enzyme through their similar chemical structures, preventing PABA to enter the reaction site and thereby forming a dihydropteroate analogue that cannot be used in the following step of the folate biosynthesis pathway.<sup>51,52</sup> Following that bacteria cannot internalize exogenous folate, this decrease in tetrahydrofolate (THF) results in mutations in DNA synthesis, which additionally results in cell death.<sup>52</sup>

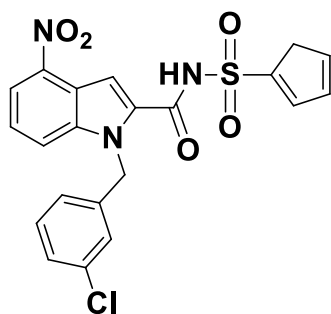
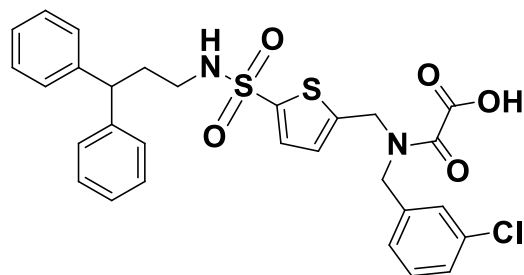
However, the development of more potent antibiotics,  $\beta$ -lactams, and increasing drug resistance have led to the discontinuation of sulfonamides as monotherapeutic agents in the treatment of malaria. Although sulfonamides are not specifically incorporated into present TB therapy, there are several sulfur and sulfonyl-containing compounds (Figure 1.13) reported to be active against *Mycobacterium tuberculosis* strains.<sup>53,54</sup>



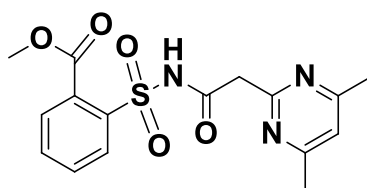
**A:** Noncovalent DprE1 inhibitor



**B:**  $\beta$ -Ketoacyl-ACP synthase I inhibitor

C: *Mtb* RNA polymerase inhibitor

D: Protein tyrosine phosphate inhibitor



E: Inhibits the branched chain amino acid synthesis

Figure 1.13: Sulfonyl containing compounds reported to be active against *Mycobacterium tuberculosis*.<sup>53,54</sup>

## 1.4 Metals in medicine

Metal ions and their complexes have been used since ancient times as therapeutic agents.<sup>55</sup> Salvarsan (Figure 1.14), an arsenic-containing organometallic complex, is the first metal complex to be synthesised and effectively used as a therapeutic agent in treatment of syphilis.<sup>56</sup> It was, however, the discovery of cisplatin (Figure 1.14), an anticancer drug that stimulated the development of metal-based compounds. Despite the success of these complexes and many others proving effective, often intuitively, metal complexes are still associated with toxicity.<sup>56,57</sup>

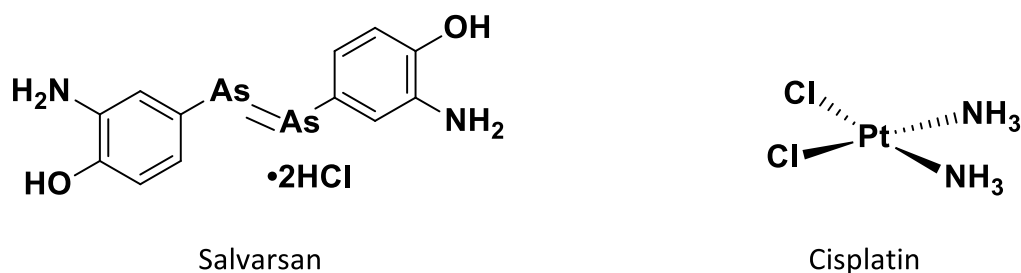


Figure 1.14: Structures of early organometallic complexes salvarsan and cisplatin.

However, through ongoing research, metal complexes have been shown to interact with biomolecules through mode(s) of action that are not seen in purely organic compounds. This is attributed by their electronic properties, reactivity, stereochemical features, three-dimensionality, ligand exchange, as well as their catalytic and photophysical activities, which is often limited in organic compounds.<sup>58</sup>

#### 1.4.1 Metallodrugs as antimicrobial agents

Although much of the research in metal-based compounds have been focused on the development of anticancer agents, recently there has been an interest in these compounds as potential antimicrobial agents because of their remarkable selectivity towards parasitic biomolecules compared to the host's biomolecules.<sup>59</sup> In light of these studies, Sanchez et al.,<sup>60</sup> synthesised rhodium- and ruthenium chloroquine complexes and evaluated them as potential antimalarial agents. The rhodium complex displayed similar antimalarial activity compared to chloroquine diphosphate (CQDP), whereas the ruthenium complex (Figure 1.15) displayed better activity than CQDP against both the CQ-sensitive and -resistant strains of *P. falciparum*.<sup>60</sup> Based on the promising results, Sanchez et al.,<sup>61</sup> further synthesised ruthenium (II)-arene complexes of CQ (Figure 1.15) and tested these against various strains of *P. falciparum*. The complexes displayed higher activities than CQDP in all four CQ-sensitive (FcB1, 3D7, PFB, and F32) and three CQ-resistant (w2, Dd2, and K1) strains of *P. falciparum*, showing that the complexes are able to interfere with the parasite's resistance mechanisms.<sup>61</sup>

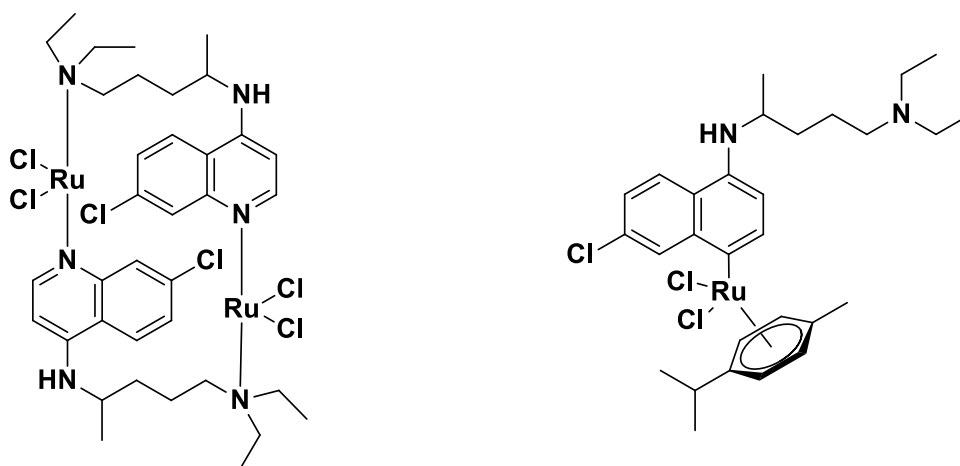


Figure 1.15: Ruthenium chloroquine complexes isolated by Sanchez et al. in efforts of finding better antimalarial agents.<sup>60,61</sup>

In efforts to obtain transition metal complexes with better efficacy and broader biological applications, Isabel et al., then synthesised vanadium and copper complexes containing 8-hydroxyquinoline and tested against various strains of *mycobacterium tuberculosis*. The complexes displayed better antitubercular activity than some of the second line anti-TB drugs including ethambutol and kanamycin, with MIC values of  $< 4.1 \mu\text{M}$ .<sup>62</sup>

Furthermore, Priya et al.,<sup>63</sup> prepared Co (II), Ni (II), Cu (II), and Zn (II) complexes with benzothiazole ligands and evaluated their antimycobacterial activity. The complexes (MIC =  $0.8 \mu\text{g/mL}$ ) were found to be 8x more potent than streptomycin (MIC =  $6.25 \mu\text{g/mL}$ ).<sup>63</sup> Recently, Debora et al.,<sup>64</sup> synthesised silver complexes containing thiosemicarbazones and phenanthroline ligands and evaluated their antitubercular activity. The complexes exhibited better activity than their corresponding thiosemicarbazone ligands and silver nitrate salt. Similar in the previous study, the complexes exhibited better activity than the currently used second line drugs.<sup>64</sup>

### 1.4.2 Sulfonamide complexes as anti-microbial agents

The study of metal-based compounds containing sulfonamide derivatives as ligands have mainly been focused on their evaluation against gram-positive (*Staphylococcus aureus* and *Bacillus cereus*), gram-negative (*Escherichia coli* and *Pseudomonas aeruginosa*) bacterial strains, various fungi strains and as carbonic anhydrase inhibitors.<sup>65</sup> There has been little interest in these types of complexes as potential therapeutic agents against malaria and tuberculosis. Quintana et al.,<sup>66</sup> synthesised cyhetrenyl and ferrocenyl complexes (Figure 1.16) containing sulfonamide ligands and evaluated their activities as anti-tuberculosis agents against the *M. tb* Mc<sup>2</sup> 6230 strain. The cyrhentrenyl complexes ( $\text{MIC}_{99} = 186.2\text{--}197.6\ \mu\text{M}$ ) exhibited better antimycobacterial activity than the ferrocenyl complexes ( $\text{MIC}_{99} = 259.1\text{--}281.7\ \mu\text{M}$ ). Based on structure-activity relationships, the antimycobacterial activity was linked to the electron-withdrawing and electron-donating effects of cyrhentrenyl and ferrocenyl moieties respectively.<sup>66</sup>

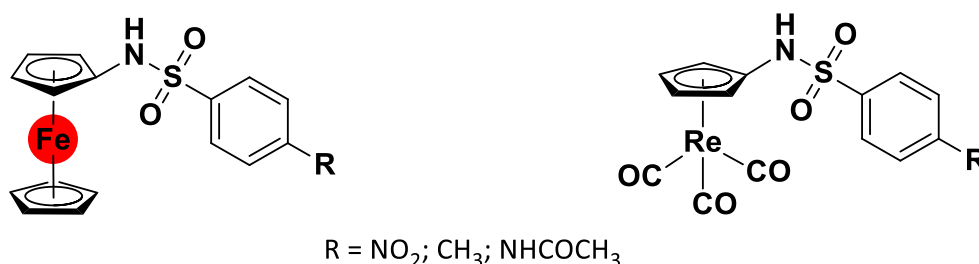
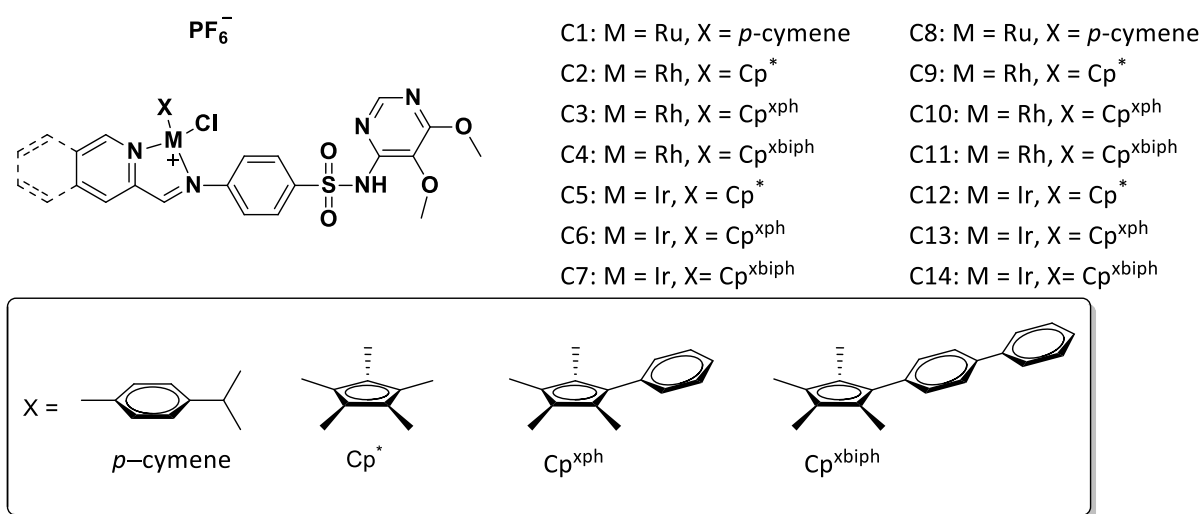


Figure 1.16: Organometallic-sulfonamide derivatives synthesised by Quintana et al.,<sup>66</sup> as potential anti-TB agents.

Similarly, Mondelli et al.,<sup>67</sup> synthesised a series of cobalt complexes containing various sulfonamide derivatives as ligands with the general formula  $[\text{Co}(\text{L})_2]\cdot\text{H}_2\text{O}$  (where L is sulfapyridine, sulfadimethoxine, sulfamerazine, sulfamethazine, sulfamethoxazole or sulfamethizole) and tested the compounds against *M. tuberculosis*. The complexes displayed similar antimycobacterial activity ( $\text{MIC} > 25\ \mu\text{g/mL}$ ) to that of the free ligands except for sulfamethizole ( $\text{MIC} = 12.5\ \mu\text{g/mL}$ ). Similar results were obtained with nickel sulfonamide complexes.<sup>68</sup> The poor antimycobacterial activity was linked to the low lipophilic character of the complexes.

In 2018, Chellan et al.,<sup>51</sup> synthesised half-sandwich Ru (II), Rh (III) and Ir (III) complexes containing quinolyl- and pyridyl-imino-sulfadoxine derived ligands (Figure 1.17). The *in vitro* biological activities of the complexes were evaluated against the 3D7 chloroquine-sensitive (CQS), Dd2 chloroquine-resistant (CQR), NF54 late-stage gametocyte (LSG) strains of *P. falciparum* as well as against the G3 and H37Rv strains of *Trichomonas vaginalis* and *M. tuberculosis* respectively. In general, the rhodium complexes were more active than the iridium complexes, whereas the ruthenium complexes were mostly inactive.



Heterocyclic moiety = Pyridyl

Heterocyclic moiety = Quinolyl

Figure 1.17: Sulfadoxine organometallic complex synthesised by Chellan et al.,<sup>51</sup> as potential antimicrobial agents.

All of the complexes exhibited no or limited activity against *Trichomonas vaginalis* G3 strain. In the *M. tuberculosis* assay, the rhodium pyridyl complexes were more active than the iridium complexes. Complexes 2, 3, 10, 13 and 14 were more active than sulfadoxine, displaying IC<sub>50</sub> values of less than 6.25 μM in comparison to 50 μM. This clearly shows that conjugation of organometallic fragments enhances biological activity. The complexes were also more active than pyrimethamine, however, none of them was as active as rifampicin and isoniazid.

However, in the parasitic assay, a reverse trend in activity was observed for the quinolyl complexes, where the rhodium complexes were more active than the iridium complexes. Interestingly, all Rh (III) and Ir (III) containing complexes were active against both the sexual and asexual stages of the parasite life cycle, whereas sulfadoxine, pyrimethamine and chloroquine were inactive. This further substantiate the role of organometallic fragments in metal-based drugs. Based on the structure-activity relationship, antiparasmodial activity was associated with increase in lipophilicity, size of the aromatic imino-group, number of substituents on the  $C_p^*$  ring and the rate of the chloride-water exchange.

In search of better organometallic sulfonamide complexes, Kotzé et al.,<sup>69</sup> further investigated whether the neutral *N, N*-chelated complexes would be more active than their cationic analogues, previously synthesised by Chellan et al.<sup>51</sup> Ir (III) complexes containing pyridyl- and quinolyl-sulfadoxine derived ligands (Figure 1.18) were synthesised by replacing the heteroatomic imino-group with the amido-group.

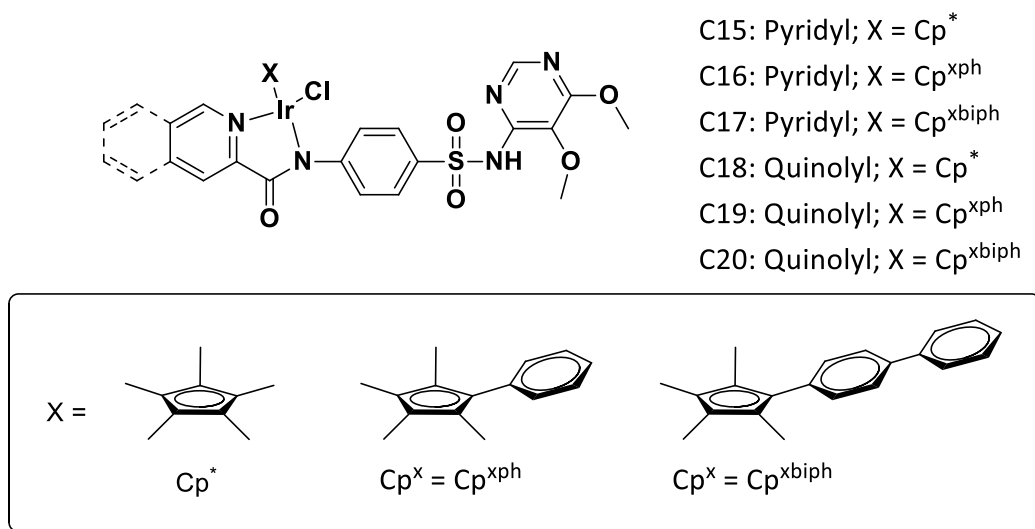


Figure 1.18: Organo-iridium sulfadoxine complexes synthesised by Kotzé et al.,<sup>69</sup> as potential antimicrobial agents.



The *in vitro* biological activities were evaluated against the 3D7-CQS, Dd2-CQR, and the pyrimethamine resistant-chloroquine sensitive (HB3) strains of *P. falciparum* as well as against the H37Rv strain of *M. tuberculosis*. A decrease in antimycobacterial activity was observed, with the most active complex C17, displaying MIC<sub>99</sub> value of 34.3  $\mu$ M after 14 days. In the parasitic assay, the percentage inhibition of the complexes was initially assessed at a concentration of 80  $\mu$ M. The quinolyl complexes exhibited better percentage inhibition than the pyridyl analogues, with complexes 18 and 20 showing inhibition percentages of > 90% in all strains. Thereafter, the IC<sub>50</sub> values were determined, of which C20 exhibited the best activities with IC<sub>50</sub> values of 0.78, 1.09 and 0.83  $\mu$ M in the 3D7-CQS, Dd2-CQR and HB3 strains of *P. falciparum* respectively.

## 1.5 Ferrocene

Ferrocene is one of the most studied organometallic compounds with diverse applications in catalysis<sup>70,71</sup>, sensing<sup>72,73</sup>, material science<sup>74</sup>, electroactive materials<sup>75</sup>, and aerospace materials. This is a consequence of its fascinating properties namely its remarkable stability in aqueous and aerobic media, electrophilicity, super aromaticity, solubility in organic solvents, and ease of functionalization. In addition, the lipophilic character and electrochemical behavior of ferrocene make it very attractive for biological applications, especially for grafting with bioactive or existing organic scaffolds. The lipophilic character improves the absorption of the organic scaffolds, by enhancing rapid and efficient diffusion across cell membranes into the nuclear complex. Furthermore, its electrochemical behavior, the ability to undergo one-electron oxidation leads to the formation of ferrocenium radical cation (Figure 1.19), which consequently generates reactive oxygen species (ROS) through a Fenton-like reaction under physiological conditions (scheme 1.2) leading to oxidative DNA damage.<sup>76</sup>

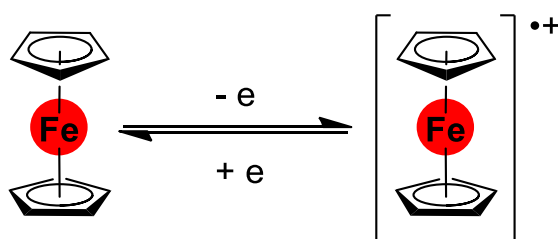


Figure 1.19: The redox reaction of ferrocene.



Scheme 1.1: Fenton chemistry

Ferrocene (Fc) has been shown to be a non-toxic compound. The study of its metabolism has demonstrated that a specific haemoprotein in the liver, cytochrome P450 (CYP), hydroxylates the iron compound to hydroxyferrocene, which is unstable in physiological media leading to the excretion of solvated ions.<sup>77</sup> Later, several reports proposed ferrocene-based compounds as a potential treatment for iron-deficient patients, which led to the discovery of ferrocerone (Figure 1.20 A).<sup>77</sup> Although no longer employed clinically, it was the first ferrocene-based compound to be clinically approved. Brynes et al.,<sup>78</sup> further explored the potential of ferrocene derivatives for the first time as a chemo-immunotherapeutic for lymphocytic leukemia P-388 in the late 1970s. A library of ferrocene derivatives bearing amine and amide groups was synthesised and orally administered to mice. Although the activity of the compounds was found to be significantly low, the study gave conclusive evidence that the incorporation of the ferrocene moiety into an appropriate carrier could potentially provide an agent with enhanced antitumor activity (Figure 1.20 B).<sup>78</sup> The study undoubtedly stimulated the synthesis and evaluation of ferrocene derivatives for antiproliferative purposes.

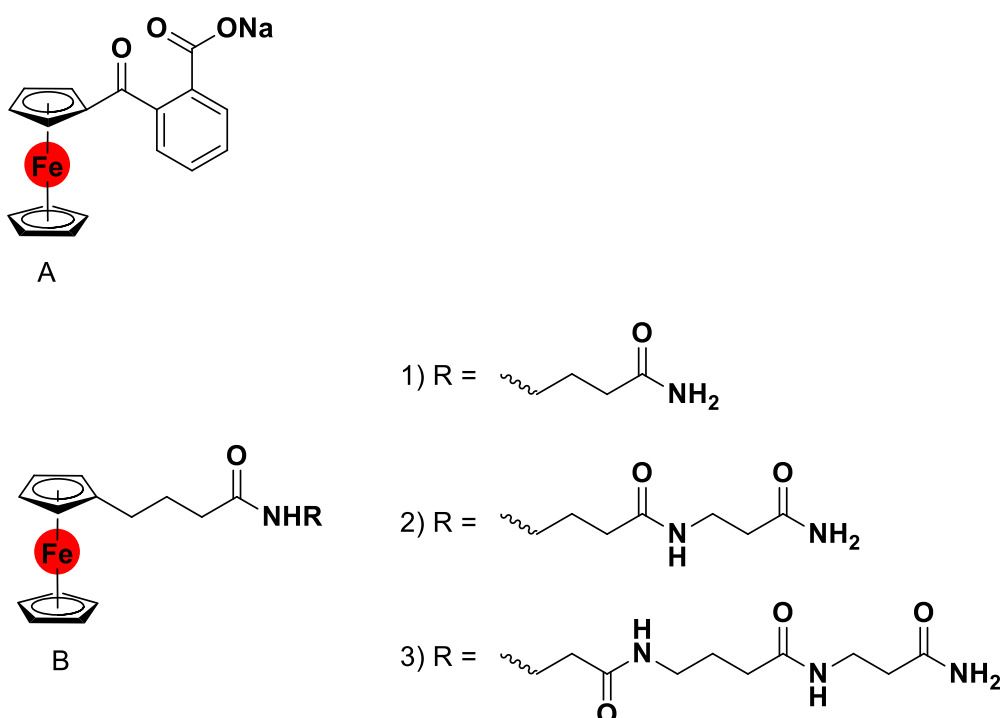


Figure 1.20: (A) Ferrocerone; (B) Ferrocene polyamides tested against lymphocytic leukemia.<sup>77,78</sup>

Since then, several types of ferrocene derivatives have been synthesised and biologically examined for their *in vivo* and *in vitro* anticancer activity. In 1996, Jaouen et al.,<sup>79</sup> synthesised a library of ferrocene derivatives using the “bioisosteric” approach by substituting the phenyl group of tamoxifen (TAM, Figure 1.21) with the ferrocene moiety. The derivatives, ferrocifen (Fc-TAM) and hydroxyferrocifen (Fc-OH-TAM)-an active hydroxylated metabolite of Fc-TAM-showed sensational biological activity in both MCF-7 (hormone dependant) and MDA-MB-231 (hormone-independent) breast cancer cells compared to the parent drugs<sup>77,80,81</sup>. The increased activity is associated with enhanced lipophilicity towards the estrogen receptor and the stronger cytotoxic effects induced by the ferrocene moiety. Besides the anticancer derivatives, several other ferrocene derivatives were proven to exhibit antifungal, antiviral, antiparasitic, and antibacterial properties<sup>82</sup>.

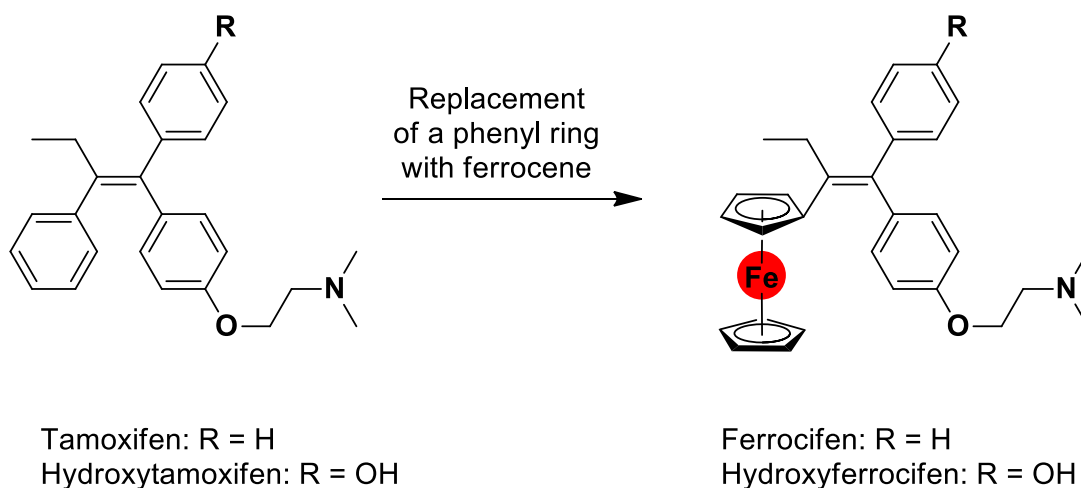


Figure 1.21: Incorporation of ferrocene into tamoxifen.<sup>79,80</sup>

### 1.5.1 Ferrocene-based antimalarial agents

The same strategy developed by Gerard Jaouen in anticancer therapy was further extended to antimalarial therapy in the mid-1990s. Although the incorporation of metals into organic scaffolds has been historically proven to have a profound effect on biological activity<sup>7</sup>, it should be emphasized that it might not be effective in some cases. For instance, the incorporation of ferrocene into mefloquine, quinoline, artemisinin, and atovaquone led to lower antimalarial activity compared to the parent compounds.<sup>83–85</sup> Additionally, it was also observed that linking ferrocene to chloroquine through (i) ionic interactions, (ii) alkylation of the quinolone nitrogen or (iii) conjugation to terminal nitrogen lead to lower antimalarial activity compared to the parent compound, chloroquine<sup>86,87</sup> (Figure 1.22). However, through extensive structural modifications, the incorporation of ferrocene into the lateral chain of chloroquine resulted in the discovery of ferroquine (FQ) (Figure 1.23).<sup>87</sup>

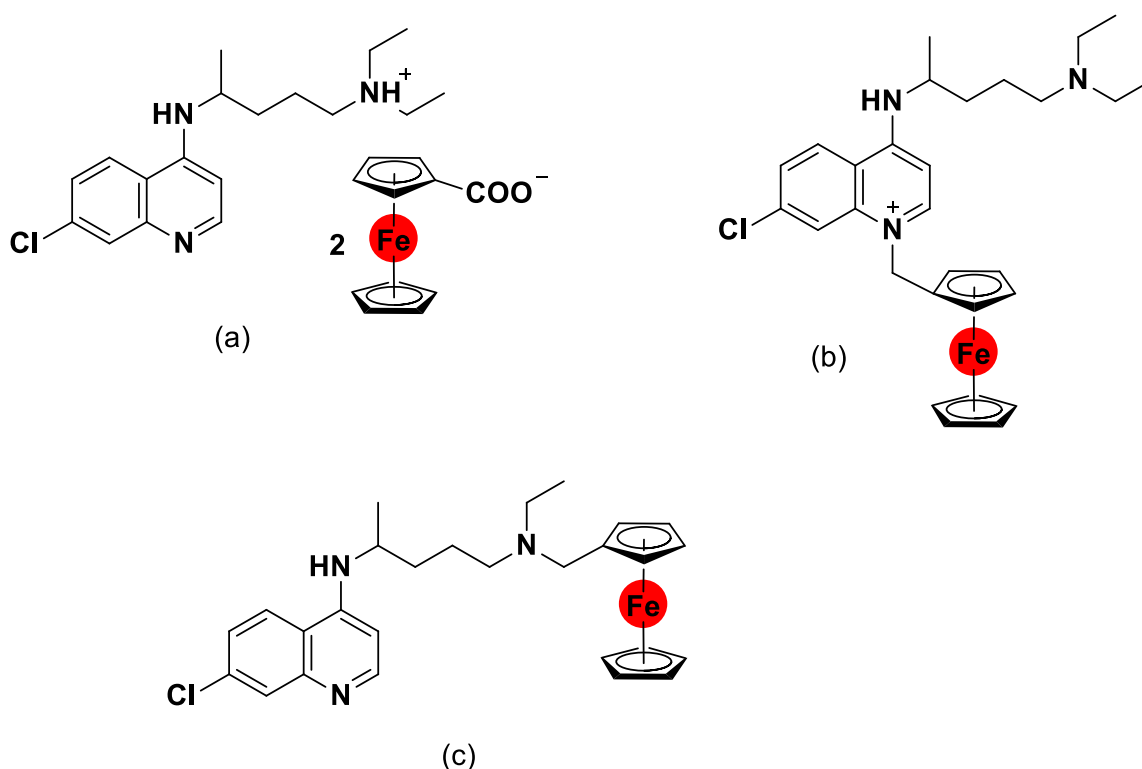
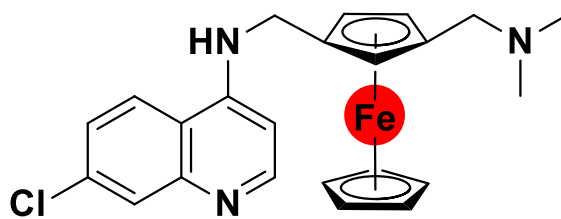


Figure 1.22: The type of linkage has a significant impact on the activities of FQ derivatives.<sup>87</sup>

FQ is highly active against both chloroquine-sensitive and chloroquine-resistant *P. falciparum* strains.<sup>88</sup> The potency of FQ, in the sensitive strain, was comparable to that of CQ. However, in the resistant strain, FQ was found to be 22 times more potent than CQ. The in vivo studies against *P. berghei* and *P. vickie* infected mice showed the high potency of FQ regardless of the mode of administration and/or the susceptibility of the strains to CQ, which further emphasized the good bioavailability of the drug.<sup>88</sup>



Ferroquine

Figure 1.23: Chemical structure of ferroquine.<sup>88</sup>

Following the successful discovery of ferroquine, several attempts were made to modify FQ to gain access to new molecular frameworks. Biot et al.,<sup>89</sup> synthesised ferroquine derivatives substituting one of the methyl groups with a hydroxyl group, closely mimicking hydroxy-CQ. The derivatives, with  $IC_{50}$  values of 133.2, 30.0, and 20.4 nM respectively, have been shown to be more active than CQ ( $IC_{50} = 138.9$  nM) against the CQ-resistant W2 strain. However, it was less effective than FQ ( $IC_{50} = 9.7$  nM).<sup>89</sup> Furthermore, the investigation of ciprofloxacin hybrids exemplified the idea that both the ester group and ferrocene are required for antiparasmodial activity.<sup>90</sup> All the synthesised derivatives were more active than ciprofloxacin and doxorubicin with one the hybrids exhibiting a 15 – 30 fold increase in efficacy against both the CQ-sensitive 3d7 and CQ-resistant W2 strains,  $IC_{50} = 1.7$  and 1.5  $\mu$ M respectively.<sup>90</sup> The synthesised compounds exhibited potent antiparasmodial activity, with some showing better activity than CQ. However, none of them exhibited similar or better antiparasmodial effects than FQ.

### 1.5.2 Ferrocene based antitubercular agents

Owing to the advance of ferroquine, the strategy of repositioning known clinical drugs have also been applied in search for better antimycobacterial agents. Pelinski et al.,<sup>91</sup> synthesised ferrocenyl diamines (Figure 1.24) with two/three carbon atom spacers between the two amino groups and evaluated them against *Mycobacterium tuberculosis*. The compounds exhibited promising antitubercular activity comparable to that of EM, both displaying MIC values of 8  $\mu\text{g/mL}$ .<sup>91</sup> However low antimycobacterial activity was observed when cyclohexyl is incorporated as a spacer. The group further synthesised ferrocenyl amide derivatives of nicotinamide and pyrazinamide which displayed good antitubercular activity in the sub-micromolar range, displaying MIC values less than 0.76  $\mu\text{M}$ . (Figure 1.25).<sup>92</sup>

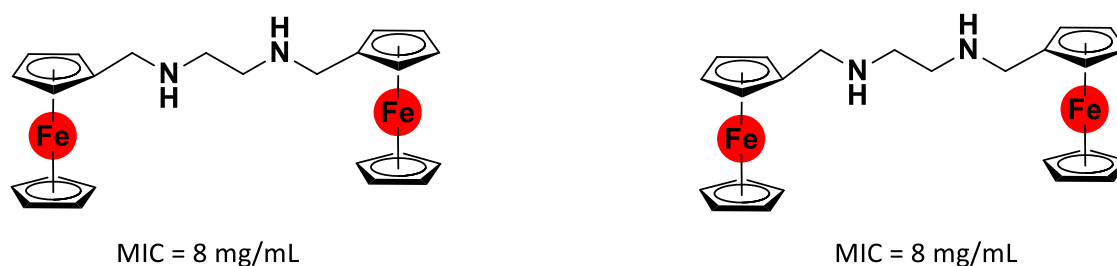


Figure 1.24: Ferrocenyl diamines synthesised by Pelinski et al.<sup>91</sup>

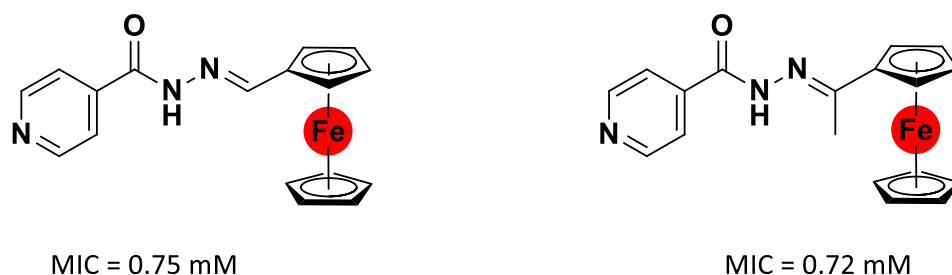


Figure 1.25: Ferrocenyl amides derivatives synthesised by Pelinski et al.<sup>92</sup>

## 1.6 Problem Statement

Malaria and tuberculosis are pervasive infectious diseases and continues to be a major global health problem, particularly in developing countries. Despite extensive efforts to eradicate these diseases, emergence of drug resistant strains to conventional antimalarial and antimycobacterial drugs respectively hinders the efficacy of these drugs and thus highlights the urgent need for the development of new effective drugs. Drug repurposing has recently become an increasing popular strategy for developing new drugs by the attachment and/or incorporation of transition metals into the scaffolds of known clinical drugs and has proven to enhance biological activity in drug-resistant strains relative to the parent drugs.

As previously discussed, the sulfonamide pharmacophore has been well-documented to display diverse biological activities. However, there's very little interest on metal-based sulfonamide complexes as antimalarial and/or antitubercular agents. This project therefor aims to evaluate SAR studies of ferrocene derivatives of sulfonamides as potential antimicrobial agents.

## 1.7 Aim and objectives

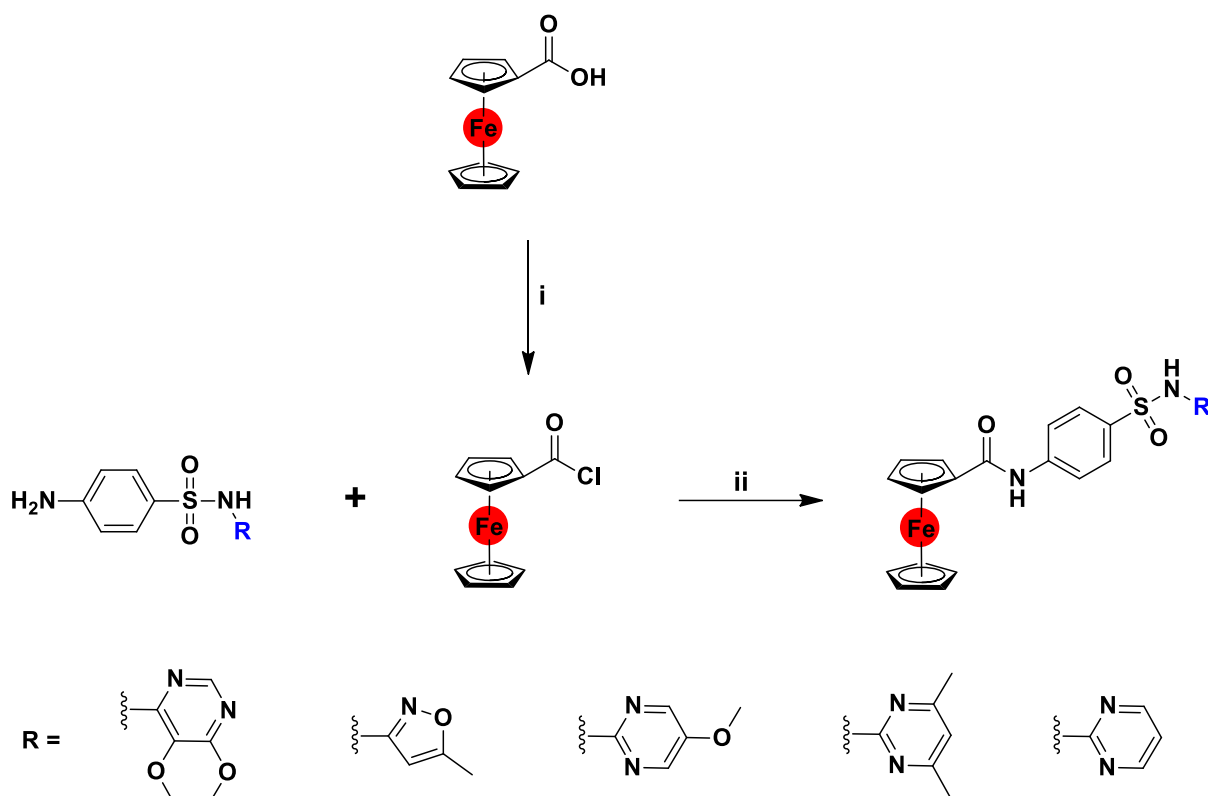
### 1.7.1 Aim

The overall aim of this project was to use the concept of derivatising known therapeutic agents to synthesise and characterise a library of new ferrocenyl derivatives of sulfonamides and evaluate their *in vitro* biological activity as potential antimicrobial agents.

### 1.7.2 Specific objectives:

#### 1.7.2.1 Synthesis

Five amido - ferrocene derivatives **C1 – C5** were synthesised from ferrocene carboxylic acid and the appropriate sulfonamide drug according to the scheme below.



Scheme 1.2: General synthetic approach for amides via acyl chloride. Reagents and reaction conditions: (i)  $(\text{COCl})_2$ , DMF (cat.),  $\text{CH}_2\text{Cl}_2$ ,  $0^\circ\text{C}$  to r.t, 4h. (ii) Pyridine, MeCN,  $0^\circ$  to r.t, 24h.

#### 1.7.2.2 Characterization

All complexes were characterized using the following spectroscopic and analytical techniques: proton and carbon nuclear magnetic resonance (NMR) spectroscopy, infrared spectroscopy (IR), mass spectrometry (MS), and high-performance liquid chromatography (HPLC).

#### 1.7.2.3 Study of physicochemical properties

Physico-chemical properties of the new complexes were studied using various techniques. UV-Vis and NMR spectroscopy was used to determine the stability of the compounds in organic solvent dimethylsulfoxide (DMSO), in water, and under physiological conditions. Turbidimetric assays were used to measure the solubility of the complexes in an aqueous environment.



#### 1.7.2.4 Biological evaluation

The *in vitro* antimicrobial activities of the compounds were determined by measuring the IC<sub>50</sub> values against different strains of *Plasmodium falciparum* and *Mycobacterium tuberculosis*. Toxicity was evaluated against human embryonic kidney (HEK) and the human prostatic PNT1A cell lines. The compounds were compared to determine how the incorporation of a highly hydrophobic compound, choice of metal, as well as the charge on the metal affected biological activity.

## **1.8 Thesis lay-out**

### *Chapter 1*

This chapter focuses on the traits of malaria and tuberculosis as well as the current treatment options. It emphasizes the emergence and spread of resistance strains and highlights the need for the development of new antimicrobial agents. It also covers the history of metallodrugs, their link to antimicrobial agents and the role ferrocene plays in modern drug discovery.

### *Chapter 2*

The synthesis and characterisation of the target compounds are described in this chapter. Electrochemical properties and solution stability studies in DMSO are also discussed.

### *Chapter 3*

The investigation into the physico-chemical properties of the compounds is discussed. These include lipophilicity, aqueous solubility as well as the stability of the compounds in aqueous media. Moreover, the results from the *in vitro* testing on the *Plasmodium falciparum* and *Mycobacterium tuberculosis* strains as well as the cytotoxicity studies on healthy cells are discussed.

### *Chapter 4*

The results obtained from the study are summarized in the present chapter. Conclusions are also presented and recommendations are offered for future work.

## **1.9 References**

- 1 A. G. Maier, K. Matuschewski, M. Zhang and M. Rug, *Plasmodium falciparum*,

- Trends Parasitol.*, 2019, **35**, 481–482.
- 2 A. Amir, F. W. Cheong, J. R. de Silva, J. W. K. Liew and Y. L. Lau, Plasmodium knowlesi malaria: Current research perspectives, *Infect. Drug Resist.*, 2018, **11**, 1145–1155.
- 3 C. A. Moxon, M. P. Gibbins, D. McGuinness, D. A. Milner and M. Marti, New Insights into Malaria Pathogenesis, *Annu. Rev. Pathol. Mech. Dis.*, 2020, **15**, 315–343.
- 4 WHO, *World Malaria Report 2021*, 2021.
- 5 World Health Organization, *World Malaria Report: 20 years of global progress and challenges*, 2020.
- 6 WHO Global, *World malaria report 2019*, 2019.
- 7 P. F. Salas, C. Herrmann and C. Orvig, Metalloantimalarials, *Chem. Rev.*, 2013, **113**, 3450–3492.
- 8 A. S. I. Aly, A. M. Vaughan and S. H. I. Kappe, Malaria parasite development in the mosquito and infection of the mammalian host, *Annu. Rev. Microbiol.*, 2009, **63**, 195–221.
- 9 K. Haldar, S. C. Murphy, D. A. Milner and T. E. Taylor, Malaria: Mechanisms of erythrocytic infection and pathological correlates of severe disease, *Annu. Rev. Pathol.*, 2007, **2**, 217–249.
- 10 R. Tuteja, Malaria - An overview, *FEBS J.*, 2007, **274**, 4670–4679.
- 11 World Health Organization, Global Malaria Programme. Eliminating malaria. Geneva: World Health Organization, *World Heal. Organ.*, 2015, 243.
- 12 W. 2020, *World Malaria Report 2020*, 1997, 73.
- 13 A. Gregson and C. V. Plowe, Mechanisms of resistance of malaria parasites to antifolates, *Pharmacol. Rev.*, 2005, **57**, 117–145.
- 14 M. P. Grobusch and P. G. Kremsner, Uncomplicated malaria, *Curr. Top. Microbiol. Immunol.*, 2005, **295**, 83–104.
- 15 J. Wang, L. Huang, J. Li, Q. Fan, Y. Long, Y. Li, B. Zhou. Artemisinin directly targets malarial mitochondria through its specific mitochondrial activation. *Plos one*. **2010**

- ;5(3):9582.
- 16 C. Wongsrichanalai and S. R. Meshnick, Declining artesunate-mefloquine efficacy against falciparum malaria on the Cambodia-Thailand border, *Emerg. Infect. Dis.*, 2008, **14**, 716–719.
  - 17 W. Cruz-Knight and L. Blake-Gumbs, Tuberculosis: An overview, *Prim. Care - Clin. Off. Pract.*, 2013, **40**, 743–756.
  - 18 R. Loddenkemper, J. F. Murray, C. Gradmann, P. C. Hopewell and M. Kato-Maeda, History of tuberculosis, *ERS Monogr.*, 2018, **2018**, 8–27.
  - 19 R. R. Nathavitharana and J. S. Friedland, A tale of two global emergencies: Tuberculosis control efforts can learn from the Ebola outbreak, *Eur. Respir. J.*, 2015, **46**, 293–296.
  - 20 J. A. M. Tufariello, J. Chan and J. A. L. Flynn, Latent tuberculosis: Mechanisms of host and bacillus that contribute to persistent infection, *Lancet Infect. Dis.*, 2003, **3**, 578–590.
  - 21 G. WHO, Global tuberculosis report 2020, *Glob. Tuberc. Rep.*
  - 22 K. Matuschewski, Getting infectious: Formation and maturation of plasmodium sporozoites in the Anopheles vector, *Cell. Microbiol.*, 2006, **8**, 1547–1556.
  - 23 M. J. Fenton and M. W. Vermeulen, Immunopathology of tuberculosis: Roles of macrophages and monocytes, *Infect. Immun.*, 1996, **64**, 683–690.
  - 24 P. Glaziou, K. Floyd and M. C. Ravigliione, Global Epidemiology of Tuberculosis, *Semin. Respir. Crit. Care Med.*, 2018, **39**, 271–285.
  - 25 A. Koul, E. Arnoult, N. Lounis, J. Guillemont and K. Andries, The challenge of new drug discovery for tuberculosis, *Nature*, 2011, **469**, 483–490.
  - 26 I. Smith, Mycobacterium tuberculosis pathogenesis and molecular determinants of virulence, *Clin. Microbiol. Rev.*, 2003, **16**, 463–496.
  - 27 C. J. Cambier, S. Falkow and L. Ramakrishnan, Host evasion and exploitation schemes of Mycobacterium tuberculosis, *Cell*, 2014, **159**, 1497–1509.
  - 28 A. P. Carter, W. M. Clemons, D. E. Brodersen, R. J. Morgan-Warren, B. T. Wimberly and V. Ramakrishnan, Functional insights from the structure of the 30S ribosomal

- subunit and its interactions with antibiotics, *Nature*, 2000, **407**, 340–348.
- 29 M.A. Borovinskaya, S. Shoji, J. M. Holton, K. Fredrick, J. H Cate. A steric block in translation caused by the antibiotic spectinomycin. *ACS chemical biology*. **2007** Aug 10;2(8):545-52.
- 30 WHO, *Treatment of Tuberculosis: Guidelines*, World Health Organization, Geneva, Switzerland, 4th edn., 2010.
- 31 B. Lei, C. J. Wei and S. C. Tu, Action mechanism of antitubercular isoniazid: Activation by Mycobacterium tuberculosis KatG, isolation, and characterization of InhA inhibitor, *J. Biol. Chem.*, 2000, **275**, 2520–2526.
- 32 F. Bardou, C. Raynaud, C. Ramos, M. A. Lan  elle and G. Lan  elle, Mechanism of isoniazid uptake in Mycobacterium tuberculosis, *Microbiology*, 1998, **144**, 2539–2544.
- 33 M. Nguyen, C. Claparols, J. Bernadou, B. Meunier. A fast and efficient metal-mediated oxidation of isoniazid and identification of isoniazid–NAD (H) adducts. *ChemBioChem*. **2001** ;2(12):877-83.
- 34 A. Telenti, P. Imboden, F. Marchesi, L. Matter, K. Schopfer, T. Bodmer, D. Lowrie, M. J. Colston and S. Cole, Detection of rifampicin-resistance mutations in Mycobacterium tuberculosis, *Lancet*, 1993, **341**, 647–651.
- 35 B. G. R. Hartmann, P. Heinrich, M. C. Kollenda, B. Skrobranek, M. Tropschug and W. Weid, *GMELIYUE*, 1985, **24**, 1009–1014.
- 36 A. Scorpio and Y. Zhang, Mutations in pncA, a gene encoding pyrazinamidase/nicotinamidase, cause resistance to the antituberculous drug pyrazinamide in tubercle bacillus, *Nat. Med.*, 1996, **2**, 662–667.
- 37 B. P. O. DeRisi Joseph, Penland Lolita, S. Tyagi, F. R. Kramer, N. P. Group and B. P. O. DeRisi Joseph, Penland Lolita,    199 7 Nature Publishing Group <http://www.nature.com/naturemedicine>, *Group*, 1996, **4**, 303–308.
- 38 K. Mikusova, R. A. Slayden, G. S. Besra and P. J. Brennan, Biogenesis of the mycobacterial cell wall and the site of action of ethambutol, *Antimicrob. Agents Chemother.*, 1995, **39**, 2484–2489.
- 39 World Health Organization. WHO Treatment Guidelines for Drug- Resistant

- Tuberculosis 2016. *World Heal. Organ.* **2016**.
- 40 S. Tiberi, A. Scardigli, R. Centis, L. D'Ambrosio, M. Muñoz-Torrico, M. Á. Salazar-Lezama, A. Spanevello, D. Visca, A. Zumla, G. B. Migliori and J. A. Caminero Luna, Classifying new anti-tuberculosis drugs: rationale and future perspectives, *Int. J. Infect. Dis.*, 2017, **56**, 181–184.
  - 41 Robert C. Goldman, Kevin V. Plumley and Barbara E. Laughon, The Evolution of Extensively Drug Resistant Tuberculosis (XDR-TB): History, Status and Issues for Global Control, *Infect. Disord. - Drug Targets*, 2008, **7**, 73–91.
  - 42 A. Zumla, P. Nahid and S. T. Cole, Advances in the development of new tuberculosis drugs and treatment regimens, *Nat. Rev. Drug Discov.*, 2013, **12**, 388–404.
  - 43 W. Sneader, Sulfonamides (The History), *Van Nostrand's Sci. Encycl.*, 2007, 1–4.
  - 44 A. Kołaczek, I. Fusiarz, J. Lawecka and D. Branowska, Biological activity and synthesis of sulfonamide derivatives: A brief review, *Chemik*, 2014, **68**, 620–628.
  - 45 S. Caddick, J. D. Wilden and D. B. Judd, Direct Synthesis of Sulfonamides and Activated Sulfonate Esters from Sulfonic Acids, *J. Am. Chem. Soc.*, 2004, **126**, 1024–1025.
  - 46 K. Bahrami, M. M. Khodaei and M. Soheilzad, Direct conversion of thiols and disulfides into sulfonamides, *Tetrahedron Lett.*, 2010, **51**, 4843–4846.
  - 47 B. R. Rosen, J. C. Ruble, T. J. Beauchamp and A. Navarro, Mild Pd-catalyzed N - arylation of methanesulfonamide and related nucleophiles: Avoiding potentially genotoxic reagents and byproducts, *Org. Lett.*, 2011, **13**, 2564–2567.
  - 48 J. Chan, K. D. Baucom and J. A. Murry, Rh(II)-catalyzed intermolecular oxidative sulfamidation of aldehydes: A mild efficient synthesis of N-sulfonylcarboxamides, *J. Am. Chem. Soc.*, 2007, **129**, 14106–14107.
  - 49 W. Deng, L. Liu, C. Zhang, M. Liu and Q. X. Guo, Copper-catalyzed cross-coupling of sulfonamides with aryl iodides and bromides facilitated by amino acid ligands, *Tetrahedron Lett.*, 2005, **46**, 7295–7298.
  - 50 S. Mondal and S. Malakar, Synthesis of sulfonamide and their synthetic and therapeutic applications: Recent advances, *Tetrahedron*, 2020, **76**, 131662.

- 51 P. Chellan, V. M. Avery, S. Duffy, J. A. Triccas, G. Nagalingam, C. Tam, L. W. Cheng, J. Liu, K. M. Land, G. J. Clarkson, I. Romero-Canelón and P. J. Sadler, Organometallic Conjugates of the Drug Sulfadoxine for Combatting Antimicrobial Resistance, *Chem. - A Eur. J.*, 2018, **24**, 10078–10090.
- 52 O. G. Patel, E. K. Mberu, A. M. Nzila and I. G. Macreadie, Sulfa drugs strike more than once, *Trends Parasitol.*, 2004, **20**, 1–3.
- 53 Y. L. Janin, Antituberculosis drugs: Ten years of research, *Bioorganic Med. Chem.*, 2007, **15**, 2479–2513.
- 54 G. F. S. Fernandes, A. M. Thompson, D. Castagnolo, W. A. Denny and J. L. Dos Santos, Tuberculosis Drug Discovery: Challenges and New Horizons, *J. Med. Chem.*, 2022, **65**, 7489–7531.
- 55 K. J. Franz and N. Metzler-Nolte, *Chem. Rev.*, 2019, 119, 727–729.
- 56 H. Sakurai, Y. Yoshikawa and H. Yasui, Current state for the development of metallopharmaceutics and anti-diabetic metal complexes, *Chem. Soc. Rev.*, 2008, **37**, 2383–2392.
- 57 P. C. A. Bruijninx and P. J. Sadler, New trends for metal complexes with anticancer activity, *Curr. Opin. Chem. Biol.*, 2008, **12**, 197–206.
- 58 J. Karges, R. W. Stokes and S. M. Cohen, Metal complexes for therapeutic applications, *Trends Chem.*, 2021, **3**, 523–534.
- 59 M. Navarro, C. Gabbiani, L. Messori and D. Gambino, Metal-based drugs for malaria, trypanosomiasis and leishmaniasis: recent achievements and perspectives, *Drug Discov. Today*, 2010, **15**, 1070–1078.
- 60 R. A. Sánchez-Delgado, M. Navarro, H. Pérez and J. A. Urbina, Toward a novel metal-based chemotherapy against tropical diseases. 2. Synthesis and antimalarial activity in vitro and in vivo of new ruthenium– and rhodium– chloroquine complexes, *J. Med. Chem.*, 1996, **39**, 1095–1099.
- 61 C. S. K. Rajapakse, A. Martínez, B. Naoulou, A. A. Jarzecki, L. Suárez, C. Deregnaucourt, V. Sinou, J. Schrével, E. Musi, G. Ambrosini, G. K. Schwartz and R. A. Sánchez-Delgado, Synthesis, characterization, and in vitro antimalarial and antitumor activity of new ruthenium(II) complexes of chloroquine, *Inorg. Chem.*,

- 2009, **48**, 1122–1131.
- 62 I. Correia, P. Adão, S. Roy, M. Wahba, C. Matos, M. R. Maurya, F. Marques, F. R. Pavan, C. Q. F. Leite, F. Avecilla and J. Costa Pessoa, Hydroxyquinoline derived vanadium(IV and V) and copper(II) complexes as potential anti-tuberculosis and anti-tumor agents, *J. Inorg. Biochem.*, 2014, **141**, 83–93.
  - 63 P. P. Netalkar, S. P. Netalkar, S. Budagumpi and V. K. Revankar, Synthesis, crystal structures and characterization of late first row transition metal complexes derived from benzothiazole core: Anti-tuberculosis activity and special emphasis on DNA binding and cleavage property, *Eur. J. Med. Chem.*, 2014, **79**, 47–56.
  - 64 D. E. S. Silva, A. B. Becceneri, M. C. Solcia, J. V. B. Santiago, M. B. Moreira, J. A. Gomes Neto, F. R. Pavan, M. R. Cominetti, J. C. M. Pereira and A. V. G. Netto, Cytotoxic and apoptotic effects of ternary silver(i) complexes bearing 2-formylpyridine thiosemicarbazones and 1,10-phenanthroline, *Dalt. Trans.*, 2020, **49**, 5264–5275.
  - 65 A. J. Salmon, M. L. Williams, Q. K. Wu, J. Morizzi, D. Gregg, S. A. Charman, D. Vullo, C. T. Supuran and S.-A. Poulsen, Metallocene-based inhibitors of cancer-associated carbonic anhydrase enzymes IX and XII, *J. Med. Chem.*, 2012, **55**, 5506–5517.
  - 66 C. Quintana, G. Silva, A. H. Klahn, V. Artigas, M. Fuentealba, C. Biot, I. Halloum, L. Kremer, N. Novoa and R. Arancibia, New cyrhetrenyl and ferrocenyl sulfonamides: Synthesis, characterization, X-ray crystallography, theoretical study and anti-*Mycobacterium tuberculosis* activity, *Polyhedron*, 2017, **134**, 166–172.
  - 67 M. Mondelli, F. Pavan, P. C. De Souza, C. Q. Leite, J. Ellena, O. R. Nascimento, G. Facchin and M. H. Torre, Study of a series of cobalt(II) sulfonamide complexes: Synthesis, spectroscopic characterization, and microbiological evaluation against *M. tuberculosis*. Crystal structure of  $[\text{Co}(\text{sulfamethoxazole})_2(\text{H}_2\text{O})_2] \cdot \text{H}_2\text{O}$ , *J. Mol. Struct.*, 2013, **1036**, 180–187.
  - 68 M. Mondelli, V. Bruné, G. Borthagaray, J. Ellena, O. R. Nascimento, C. Q. Leite, A. A. Batista and M. H. Torre, New Ni(II)-sulfonamide complexes: Synthesis, structural characterization and antibacterial properties. X-ray diffraction of  $[\text{Ni}(\text{sulfisoxazole})_2(\text{H}_2\text{O})_4] \cdot 2\text{H}_2\text{O}$  and  $[\text{Ni}(\text{sulfapyridine})_2]$ , *J. Inorg. Biochem.*, 2008,

- 102, 285–292.
- 69 T. J Kotzé, T. J.; S. Duffy, S.; V. M Avery; A. Jordaan.; D. F Warner; L. Loots; G. S. Smith; P. Chellan. Synthesis and Antimicrobial Study of Organoiridium Amido-Sulfadoxine Complexes. *Inorg Chim. Acta* 2021, **517**.
- 70 R. C. J. Atkinson, V. C. Gibson and N. J. Long, The syntheses and catalytic applications of unsymmetrical ferrocene ligands, *Chem. Soc. Rev.*, 2004, **33**, 313–328.
- 71 L. X. Dai, T. Tu, S. L. You, W. P. Deng and X. L. Hou, Asymmetric catalysis with chiral ferrocene ligands, *Acc. Chem. Res.*, 2003, **36**, 659–667.
- 72 M. Devices, *Materials , Molecular Devices and Biomolecules*, 2008.
- 73 H. Beitollahi, M. A. Khalilzadeh, S. Tajik, M. Safaei, K. Zhang, H. W. Jang and M. Shokouhimehr, Recent Advances in Applications of Voltammetric Sensors Modified with Ferrocene and Its Derivatives, *ACS Omega*, 2020, **5**, 2049–2059.
- 74 P. Stepnicka. Ferrocenes: ligands, materials and biomolecules. *John Wiley & Sons*; 2008.
- 75 H. J. Xie, B. Gélinas and D. Rochefort, Redox-active electrolyte supercapacitors using electroactive ionic liquids, *Electrochem. commun.*, 2016, **66**, 42–45.
- 76 D. Osella, M. Ferrali, P. Zanello, F. Laschi, M. Fontani, C. Nervi and G. Cavigiolio, On the mechanism of the antitumor activity of ferrocenium derivatives, *Inorg Chim. Acta*, 2000, **306**, 42–48.
- 77 M. Patra and G. Gasser. The medicinal chemistry of ferrocene and its derivatives. *Nature Reviews Chemistry*. 2017;**1**(9):0066.
- 78 Ryan, Cooper and Tauer, Ferrocenyl Polyamines as Agents for the Chemoimmunotherapy of Cancer, *J. Med. Chem.*, 2013, **172**, 12–26.
- 79 C. P. and G. J. Siden Top, Jie Tang, Anne Vessieres, Daniele Carrez, Ferrocenyl hydroxytamoxifen: a prototype for a new range of oestradiol receptor site-directed cytotoxics, *Chem. Commun.*, 1996, 955–956.
- 80 G. Jaouen, A. Vessièrès and S. Top, Ferrocifen type anti cancer drugs, *Chem. Soc. Rev.*, 2015, **44**, 8802–8817.
- 81 P. Chellan and P. J. Sadler, Enhancing the Activity of Drugs by Conjugation to



- Organometallic Fragments, *Chem. - A Eur. J.*, 2020, **26**, 8676–8688.
- 82 B. S. Ludwig, J. D. G. Correia and F. E. Kühn, Ferrocene derivatives as anti-infective agents, *Coord. Chem. Rev.*, 2019, **396**, 22–48.
  - 83 C. Biot, L. Delhaes, L. A. Maciejewski, M. Mortuaire, D. Camus, D. Dive and J. S. Brocard, Synthetic ferrocenic mefloquine and quinine analogues as potential antimalarial agents, *Eur. J. Med. Chem.*, 2000, **35**, 707–714.
  - 84 L. Delhaes, C. Biot, L. Berry, L. A. Maciejewski, D. Camus, J. S. Brocard and D. Dive, Novel ferrocenic artemisinin derivatives: Synthesis, in vitro antimalarial activity and affinity of binding with ferroprotoporphyrin IX, *Bioorganic Med. Chem.*, 2000, **8**, 2739–2745.
  - 85 A. Baramée, A. Coppin, M. Mortuaire, L. Pelinski, S. Tomavo and J. Brocard, Synthesis and in vitro activities of ferrocenic aminohydroxynaphthoquinones against *Toxoplasma gondii* and *Plasmodium falciparum*, *Bioorganic Med. Chem.*, 2006, **14**, 1294–1302.
  - 86 C. Biot, W. Daher, C. M. Ndiaye, P. Melnyk, B. Pradines, N. Chavain, A. Pellet, L. Fraisse, L. Pelinski, C. Jarry, J. Brocard, J. Khalife, I. Forfar-Bares and D. Dive, Probing the role of the covalent linkage of ferrocene into a chloroquine template, *J. Med. Chem.*, 2006, **49**, 4707–4714.
  - 87 D. Dive and C. Biot, Ferrocene conjugates of chloroquine and other antimalarials: The development of ferroquine, a new antimalarial, *ChemMedChem*, 2008, **3**, 383–391.
  - 88 C. Biot, Ferroquine: a new weapon in the fight against malaria, *Curr. Med. Chem. Agents*, 2004, **3**, 135–147.
  - 89 C. Biot, W. Daher, N. Chavain, T. Fandeur, J. Khalife, D. Dive and E. De Clercq, Design and synthesis of hydroxyferroquine derivatives with antimalarial and antiviral activities, *J. Med. Chem.*, 2006, **49**, 2845–2849.
  - 90 F. Dubar, G. Anquetin, B. Pradines, D. Dive, J. Khalife and C. Biot, Enhancement of the antimalarial activity of ciprofloxacin using a double prodrug/bioorganometallic approach, *J. Med. Chem.*, 2009, **52**, 7954–7957.
  - 91 D. Andrianina Ralambomanana, D. Razafimahefa-Ramilison, A. C. Rakotohova, J. Maugein and L. Péliniski, Synthesis and antitubercular activity of ferrocenyl

- diaminoalcohols and diamines, *Bioorganic Med. Chem.*, 2008, **16**, 9546–9553.
- 92 G. M. Mague, J. Jakhlal, M. Ladyman, A. Vallin, D. A. Ralambomanana, T. Bousquet, J. Maugein, J. Lebibi and L. Pélinski, Synthesis and antimycobacterial activity of a series of ferrocenyl derivatives, *Eur. J. Med. Chem.*, 2011, **46**, 31–38.

## Chapter 2: Synthesis and characterisation of ferrocenyl derivatives of sulfonamides

### 2.1 Introduction

Malaria and tuberculosis (TB) are currently treated using combination therapy which involves the administration of two or more drugs as discussed in Chapter 1. This type of treatment has been highly effective, but the emergence of drug resistance, often accelerated by the misuse and overuse of antibiotics, hinders its efficacy. Modification of known clinical drugs through the attachment or incorporation of an organometallic moiety is a promising and attractive strategy for reactivating organic drugs, increasing biological activity and fighting drug resistance.<sup>1</sup> Over the last decade, excellent reviews on the modification of known clinical drugs through the incorporation of transition metals such as ruthenium, rhodium, osmium etc., have been published.<sup>1-3</sup> Several studies have also shown how the incorporation of metals into the organic framework of sulfonamide drugs can increase their biological activity as anticancer, antimicrobial, antifungal, and as carbonic anhydrase inhibitors.<sup>4-9</sup> However, metal-based sulfonamide complexes as antimalarial or anti-TB agents are extremely limited with the only examples from Mondelli et al.,<sup>10,11</sup> and Quintana et al.,<sup>12</sup> as discussed in Chapter 1, section 1.4.2, page 17.

Previous work within our research group, by Chellan et al.<sup>13</sup> and Kotzé et al.,<sup>14</sup> focusing on targeting drug resistant *P. falciparum* and *M. tuberculosis* strains, as discussed in Chapter 1, demonstrated how the incorporation of an organometallic moiety into sulfadoxine, a current antimalaria drug, can potentially restore its biological activity. Figure 2.1 illustrates few of the most promising complexes synthesised by them and most importantly, the complexes demonstrated no significant toxicity towards human embryonic kidney cells (HEK293), indicating selectivity towards the parasite.<sup>13</sup>

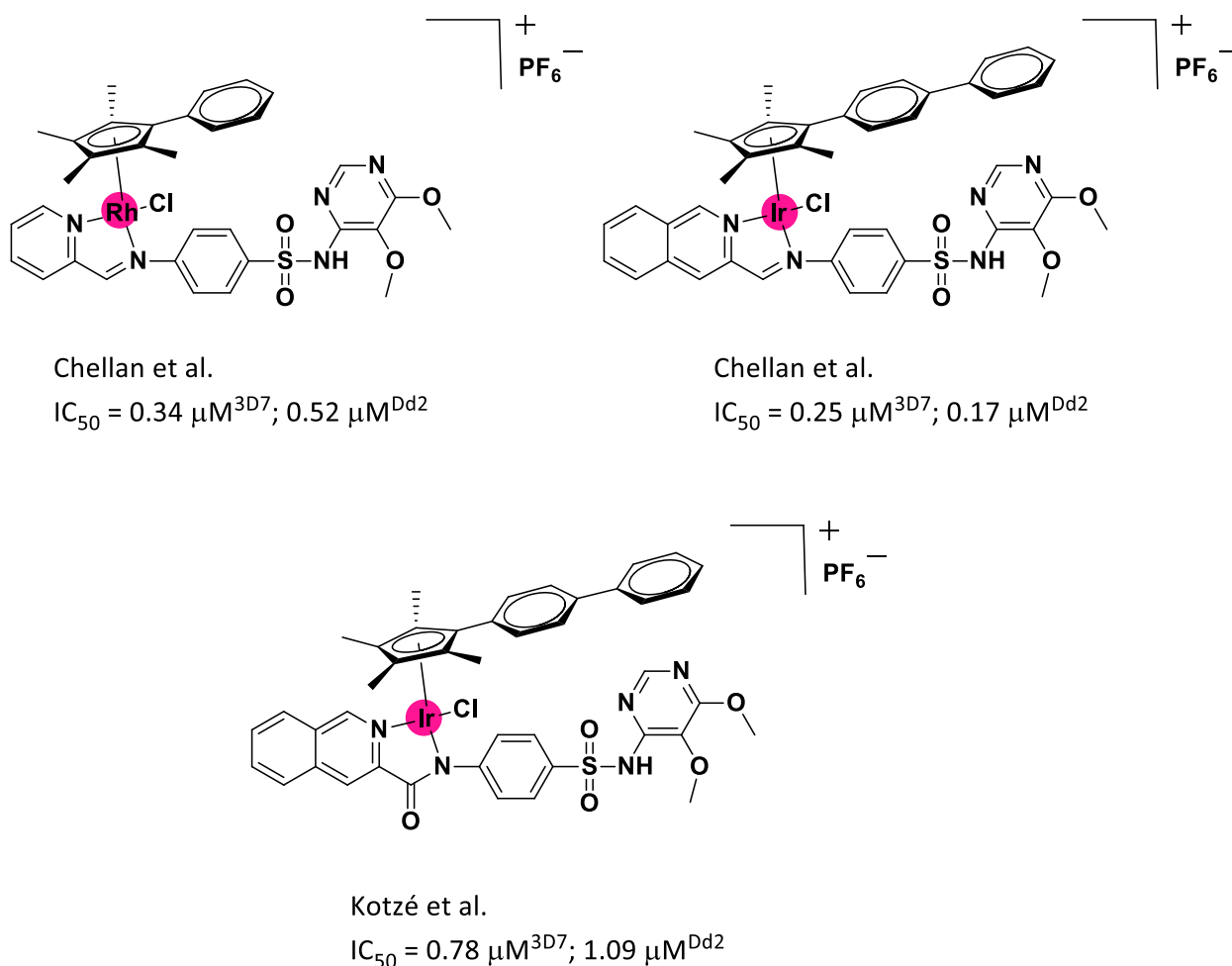


Figure 2.1: Organo-iridium and -rhodium complexes that have shown to improve the biological activity of sulfadoxine.<sup>13,14</sup>

Owing to the success of the aforementioned sulfonamides derivatives and our interest in ferrocene chemistry, this chapter will focus on the synthesis and characterisation of ferrocenyl sulfonamide derivatives, where ferrocene is linked to the sulfa drug via an amide functionality. The rationale for the incorporation of the amide functionality between the two entities is to design more stable organometallic complexes that are able to resist metabolic cleavage in physiological media until they reach their specific target site, resulting in better pharmacological activities.

## 2.2 Results and discussion

### 2.2.1 Synthesis

Novel ferrocenyl derivatives of sulfa-drugs (**C1-C5**) were prepared using a published literature method.<sup>14</sup> The method used a two-step reaction starting with commercially available ferrocene carboxylic acid as outlined in Scheme 2.1. The reaction mechanism is detailed in Figure 2.3. The ferrocene carboxylic acid undergoes a nucleophilic substitution when reacted with excess oxalyl chloride in anhydrous dichloromethane (DCM) under inert conditions. This reaction takes place in the presence of a catalytic amount of *N,N*-dimethylformide (DMF, 1-2 drops) to form the reactive ferrocenoyl chloride intermediate at room temperature. The rate of the reaction is improved by using the catalytic amount of DMF as it activates the oxalyl chloride, forming the Vilsmeier reagent, 1-chloro-*N,N*-dimethylmethaniminium chloride. The Vilsmeier reagent can then act as an electron-withdrawing group as well as a leaving group upon protonation to yield the desired acid chloride. The synthesised ferrocenoyl chloride was subsequently coupled with various sulfa-drugs (Figure 2.2) in the presence of pyridine, as a base for neutralising the hydrochloric acid formed, to drive the reaction towards product formation.

The reactions were monitored using TLC analysis. In general, TLC analysis indicated the consumption of the starting materials and the appearance of a new spot, which was slightly more polar than ferrocenoyl chloride but less polar than the respective amines. Initial synthesis attempts identified that there was no further change in spot distributions with respect to relative intensities observed on the TLCs when comparing reaction times of 24 and 48 hours. Therefore, subsequent reactions were terminated after 24 hours. In some reactions the product precipitated out of solution, which was then further washed with the reaction mixture to remove any unreacted starting materials. In the absence of precipitate formation, the reaction mixtures were worked up and crude residues isolated via recrystallisation or column chromatography. The complexes were successfully isolated as either orange or off-white powders in moderate to good yields (Table 2). The complexes isolated by recrystallization or column chromatography were obtained as orange powders whereas the complexes that precipitated out of solution were obtained as off-white powders. The complexes also displayed good solubility in dimethyl sulfoxide (DMSO) and DMF, but were insoluble in water and most organic solvents. Furthermore, all complexes were subjected to reversed-phase high performance liquid chromatography (RP-HPLC) and determined to have purities greater than 98%.

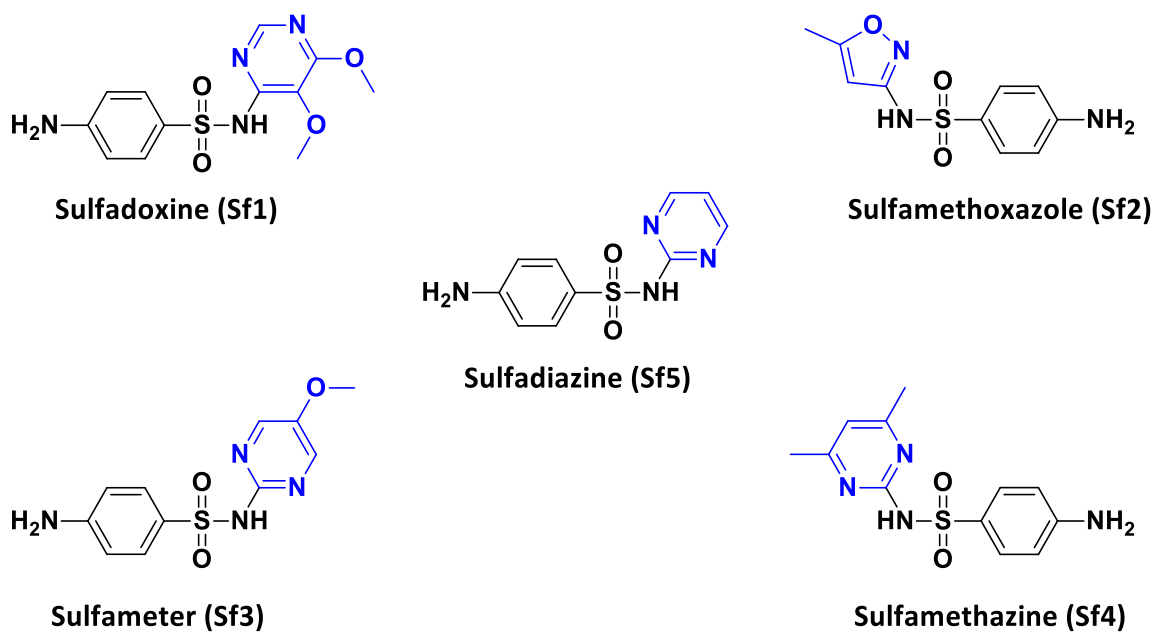
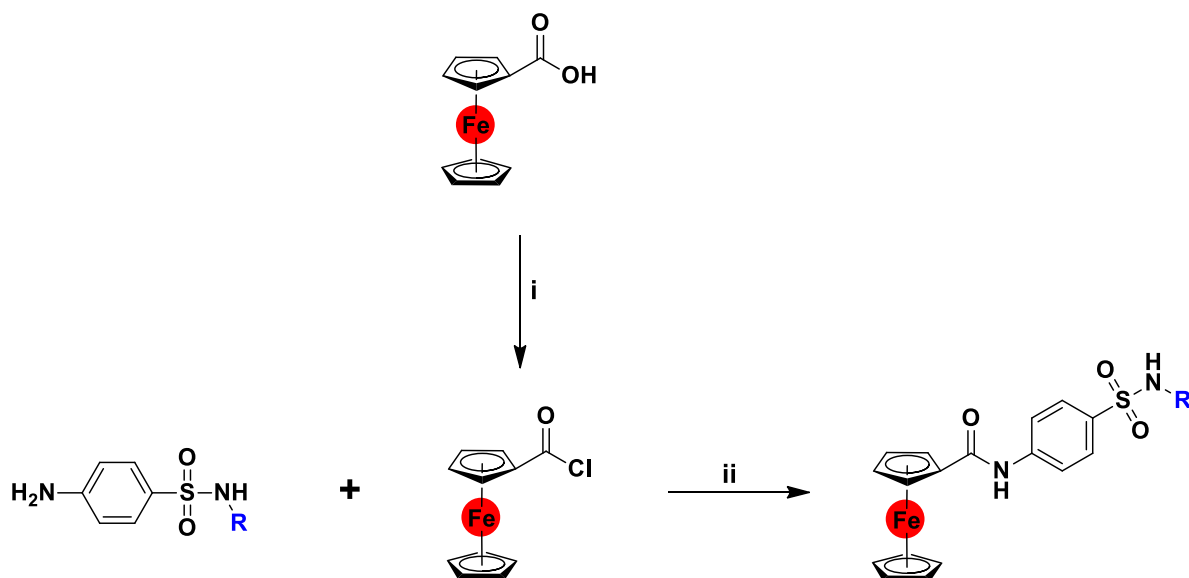


Figure 2.2: The selected sulfonamide drugs used for this study.



Scheme 2.1: General synthetic approach for amides via acyl chloride. Reagents and reaction conditions: (i) (COCl)<sub>2</sub>, DMF (cat.), CH<sub>2</sub>Cl<sub>2</sub>, 0°C to r.t., 4h. (ii) Pyridine, MeCN, 0°C to r.t., 24h.

The most likely mechanism for this reaction starts with the nucleophilic oxygen atom of DMF attacking the electrophilic carbonyl carbon of oxalyl chloride forming intermediate (**I**). Intermediate (**I**) then rearranges intramolecularly to form the ionic adduct (**II**), which subsequently loses CO<sub>2</sub> and CO (**III**) to yield the reactive electron-deficient iminium salt, the Vilsmeier reagent. Ferrocene carboxylic acid reacts with the reactive Vilsmeier reagent by attacking its electron-deficient carbon atom. Deprotonation occurs to form the intermediate (**IV**) and HCl. The nitrogen pushes its lone pairs towards the carbon atom, forcing the chlorine atom to leave, which subsequently attacks the carbonyl carbon of the intermediate (**VI**). Intramolecular rearrangement takes place (**VII**) forming the desired acid chloride and regenerating the catalytic DMF.

The nucleophilic sulfonamide attacks the partially positive carbonyl carbon of ferrocenoyl chloride, by acting as an electron pair donor, forming the unstable intermediate (**VIII**). The carbon-oxygen  $\pi$ -bond reforms and the chloride ion leaves (**IX**). Deprotonation then takes place through the removal of a hydrogen atom from nitrogen, forming the desired amide and HCl (which is neutralised by pyridine).

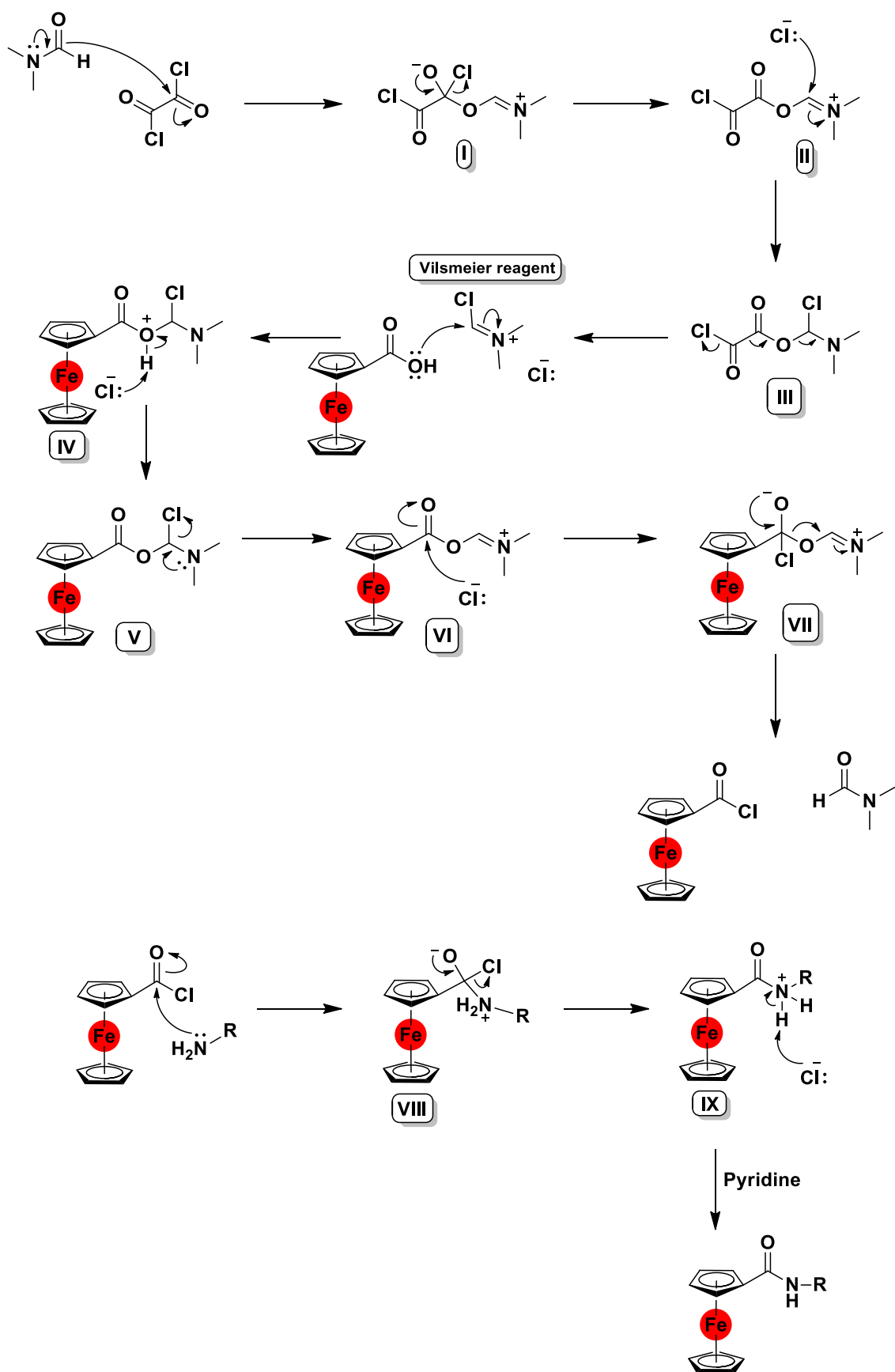


Figure 2.3: Proposed reaction mechanism of amide formation via acyl chloride with a catalytic amount of DMF.



Table 2.1 Physical appearance and yield of the synthesised complexes (C1–C5).

Compound	Physical appearance
<b>Fc-Sulfadoxine (C1)</b>	Orange powder
<b>Fc-Sulfamethoxazole (C2)</b>	Off-white powder
<b>Fc-Sulfameter (C3)</b>	Off-white powder
<b>Fc-Sulfamethazine (C4)</b>	Orange powder
<b>Fc-Sulfadiazine (C5)</b>	Off-white powder

### 2.2.2 Characterisation

The complexes **C1–C5** were characterised using various analytical techniques. These include  $^1\text{H}$  and  $^{13}\text{C}$   $\{^1\text{H}\}$  nuclear magnetic resonance (NMR) spectroscopy, infrared (IR) spectroscopy, electrospray ionisation mass spectrometry (ESI-MS), and reversed-phase high performance liquid chromatography (RP-HPLC). All characterisation data confirmed the successful synthesis of the desired complexes.

#### $^1\text{H}$ NMR Spectroscopy

The successful synthesis of the complexes was confirmed by  $^1\text{H}$  NMR spectroscopy, through the disappearance of the proton resonances for the primary amine in the parent sulfa drug and the appearance of the amide proton resonance,  $\text{H}_a$  of the complex (Figure 2.4). The  $\text{H}_a$  resonance is present as a singlet, integrating for one proton between  $\delta_{\text{H}}$  9.50 and 9.95 ppm, for all complexes. The broad singlet,  $\text{H}_g$ , of the sulfonamide moiety is present far downfield between  $\delta_{\text{H}}$  10.50 and 11.50 ppm. The broadness of the peak may be due to the presence of water in the  $\text{DMSO-d}_6$  NMR solvent –  $\text{H}_g$  is highly acidic, making it likely to exchange with water in the solvent.<sup>15</sup> The two methoxy groups of the dimethoxy-pyrimidine ring appeared as two singlets at  $\delta_{\text{H}}$  3.88 and 3.68 ppm, respectively, integrating for 3 protons each. The characteristic resonances for the ferrocenyl moiety resonate between  $\delta_{\text{H}}$  4.15 and 5.10 ppm. The singlet at  $\delta_{\text{H}}$  4.19 ppm, represents the lower unsubstituted  $\text{C}_p$  ring ( $\text{H}_b$ ), which integrates for 5 protons, while the resonances for  $\text{H}_c$  ( $\delta_{\text{H}}$  4.46 ppm) and  $\text{H}_d$  ( $\delta_{\text{H}}$  5.02 ppm) on the upper monosubstituted  $\text{C}_p$  ring are present as two singlets, both integrating for 2 protons. Predominantly, for monosubstituted ferrocenyl derivatives, these proton resonances are reported as triplets or doublets due to an AA'BB' spin system.<sup>16</sup> However, the observance of

these protons,  $H_c$  and  $H_d$ , as two singlets likely suggest that the complexes are fluxional at ambient temperature.

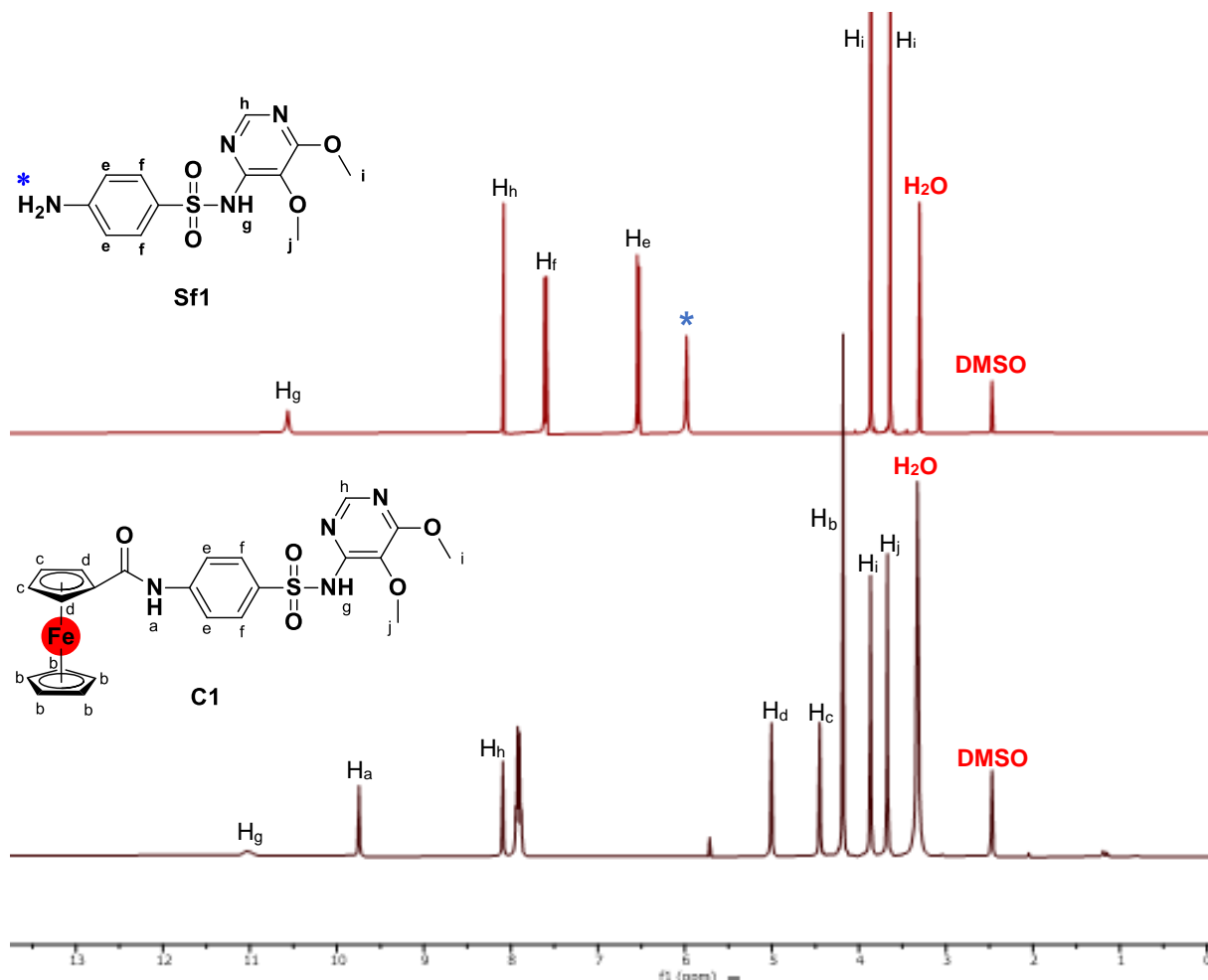


Figure 2.4: Stacked  $^1\text{H}$  NMR spectra of the parent sulfa drug, sulfadoxine (top), and the synthesised complex, **C1** (bottom), in  $\text{DMSO-d}_6$ .

In addition, the phenyl proton resonances of the *para*-substituted aromatic ring are shifted slightly downfield and appear to converge, from distinct doublets,  $H_e$  and  $H_f$ , in the sulfa drug into a multiplet integrating for 4 protons in the complex **C1** (Figure 2.5). This convergence may be due to the phenyl protons experiencing electron donating effects from the ferrocenyl moiety causing them to become more de-shielded. Lastly, the resonance in the aromatic region adjacent to the multiplet is assigned to the proton of the dimethoxy-pyrimidine ring, which remains unshifted upon the introduction of the ferrocenyl moiety.

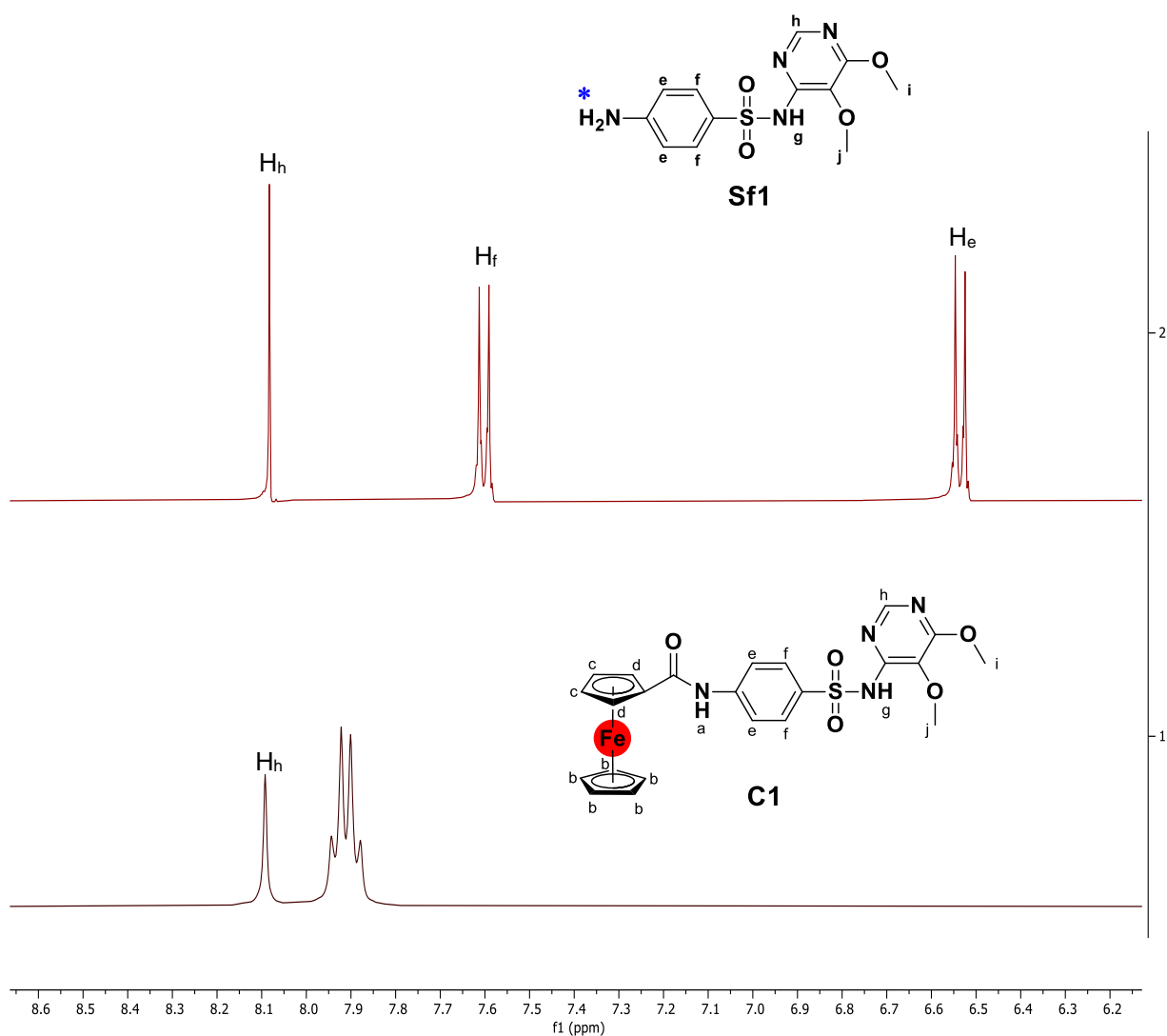


Figure 2.5: Stacked  $^1\text{H}$  NMR spectra of sulfadoxine (top) and **C1** (bottom) in the aromatic region, showing the convergence of the two doublets into a multiplet.

Other characteristic resonances observed in the spectra of the remaining complexes, **C2–C5**, are summarised in Table 2.2. The slightly lower chemical shift of the heterocyclic ring proton resonance of **C2** compared to the other complexes is likely due to less conjugation following that **C2** is the only complex bearing a five membered heterocyclic ring while the other complexes have a pyrimidine ring.

Table 2.2:  $^1\text{H}$  NMR chemical shifts of the heterocyclic rings and its substituents.

Complexes	NMR Chemical shifts (ppm)		
	$\text{OCH}_3$	$\text{CH}_3$	Heterocyclic ring protons
<b>C2</b>	-	2.27	6.11 (s, 3H)
<b>C3</b>	3.77	-	8.28 (s, 2H)
<b>C4</b>	-	2.26	6.76 (s, 1H)
<b>C5</b>	-	-	8.50 (d, 2H); 7.01 (m, 1H)

 $^{13}\text{C} \{^1\text{H}\}$  NMR spectroscopy

$^{13}\text{C} \{^1\text{H}\}$  NMR was used to further characterise the complexes. The NMR spectra of all complexes (**C1** – **C5**) appear to be quite similar, therefore the spectrum of **C3** (Figure 2.6) serves as a representative spectrum for all five complexes. The spectra of all complexes show a resonance corresponding to the carbonyl carbon at approximately  $\delta_c$  170.46 ppm, further confirming the presence of the amide functional group. All aromatic carbon atoms of the phenyl group resonate between  $\delta_c$  120 and 160 ppm as expected. The carbon atoms of the ferrocene moiety resonate between  $\delta_c$  69.00 and 76.05 ppm: one intense resonance for the five carbons of the unsubstituted  $\text{C}_p$  ring, two resonances for the four carbons of the substituted  $\text{C}_p$  ring, and one resonance for the quaternary  $\text{C}_p$  ring carbon. The methylene carbon of **C2** resonates at  $\delta_c$  12.53 ppm, while the methoxy carbons of **C1** and **C3** resonate at  $\delta_c$  54.45, 60.61, and 56.73 ppm, respectively. The higher chemical shift of the methoxy carbons compared to the methylene carbons is likely due to the electronegative oxygen atom withdrawing electrons to itself causing the carbons to be de-shielded.

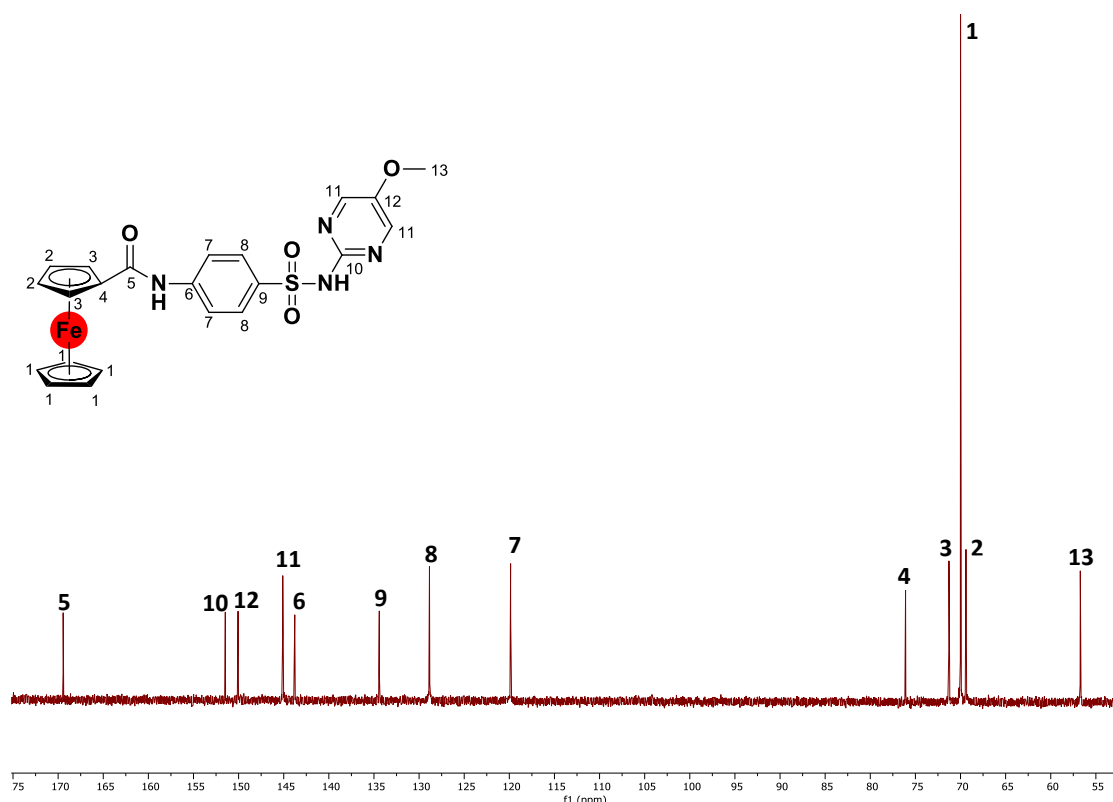


Figure 2.6:  $^{13}\text{C}$   $\{^1\text{H}\}$  NMR spectrum of complex **C3** in  $\text{DMSO-d}_6$ .

### Infrared Spectroscopy

Infrared spectroscopy is an analytical technique used to identify the functional groups present in a molecule based on their vibrations in the infrared region. Figure 2.7 shows the stacked IR spectra of the starting materials, ferrocene carboxylic acid and the sulfa drug as well as the synthesised complex **C2**. The infrared spectra of **C1** - **C5** are overall quite similar, therefore, the spectrum of **C2** is used as a representative spectrum for all five complexes. The absorption bands at  $3465.0\text{ cm}^{-1}$  and  $3375.6\text{ cm}^{-1}$  are assigned to the asymmetric  $\nu_{as}(\text{NH})$  and symmetric  $\nu_s(\text{NH})$  bands of the free  $\text{NH}_2$  group of the sulfonamide. Upon the introduction of ferrocenyl group, the disappearance of the  $\nu_{as}(\text{NH})$  and the appearance of a new band at  $3129.7\text{ cm}^{-1}$  is observed, confirming the deprotonation of the amine. A strong carbonyl  $\nu(\text{C=O})$  absorption band is seen at  $1669.3\text{ cm}^{-1}$  in **C2**, which is observed in the spectrum of ferrocene carboxylic acid as a very broad band at around  $1650\text{ cm}^{-1}$ . A  $\nu(\text{C-N})$  band is also observed at  $1250\text{ cm}^{-1}$ . The symmetric  $\nu_s(\text{S=O})$  and asymmetric  $\nu_{as}(\text{S=O})$  absorption bands of the sulfonyl group are observed in the regions  $1150 - 1180\text{ cm}^{-1}$  and  $1249 - 1361\text{ cm}^{-1}$ , respectively.

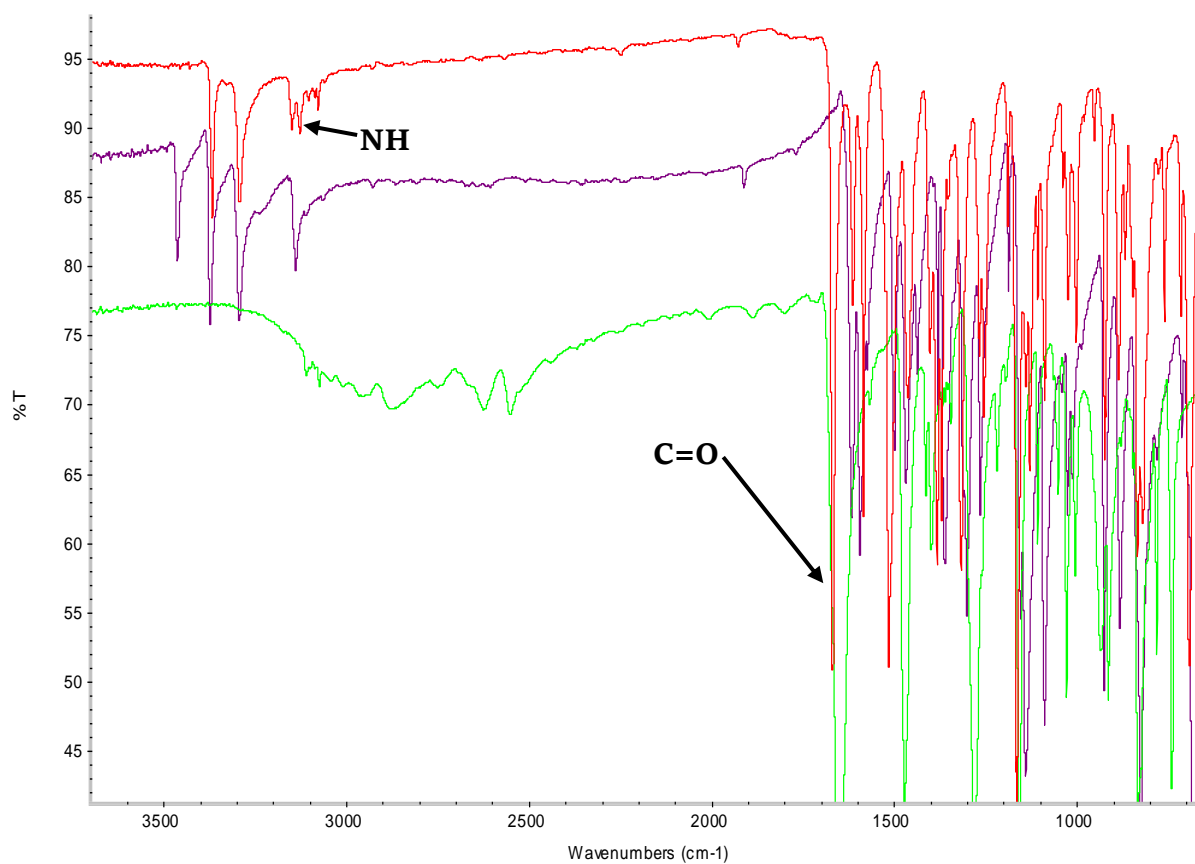


Figure 2.7: Infrared spectra of complex **C2** (red), sulfamethoxazole (purple), and ferrocene carboxylic acid (green).

### Mass Spectrometry

The mass spectra of the complexes were collected using Electrospray Ionisation-mass spectrometry (ESI-MS). The spectra of all complexes show base peak corresponding to the protonated molecular  $[M + H]^+$  ion peak. In addition, the sodium adduct ( $[M + Na]^+$ ) peaks were also observed. The determined experimental values agree favourably with the expected masses, confirming the integrity of the proposed structures. The values are summarised in Table 2.3 below.

Table 2.3: The calculated and experimentally determined m/z values for complexes **C1** – **C5**.

Complexes	Calculated M/z	M/z = [M + H] <sup>+</sup> (100%)	M/z = [M + Na] <sup>+</sup> (%)
<b>C1</b>	522.3546	523.0739	545.0563 (25%)
<b>C2</b>	465.3033	466.0523	488.0344 (55%)
<b>C3</b>	492.3286	493.0641	515.0464 (35%)
<b>C4</b>	490.3558	491.0842	513.0654 (15%)
<b>C5</b>	462.3026	463.0534	485.0358 (25%)

## 2.3 Electrochemical studies

As an additional technique, the electrochemical properties of complexes **C1** – **C5** were evaluated using cyclic voltammetry (CV). CV is an effective and a versatile technique used to understand the redox behaviour of bioactive complexes, which might provide insight into biological interactions involved as well as the effects that substituents could have on the ferrocene moiety in ferrocene derivatives.<sup>17,18</sup> Due to the limited solubility of the complexes in organic solvents, the measurements were carried out in 5% DMSO/MeCN (acetonitrile) solution (1.0 mM) containing 0.1 M tetrabutylammonium perchlorate [n-Bu<sub>4</sub>N][ClO<sub>4</sub>] (TBAP) as the supporting electrolyte. The redox potentials were measured at room temperature at a scan rate of 25 mV.s<sup>-1</sup>, under nitrogen atmosphere with ferrocene as the internal standard. The cyclic voltammogram of complex **C4** is shown in Figure 2.8 as a representative example, whereas the data of the other complexes are listed in Table 2.4.

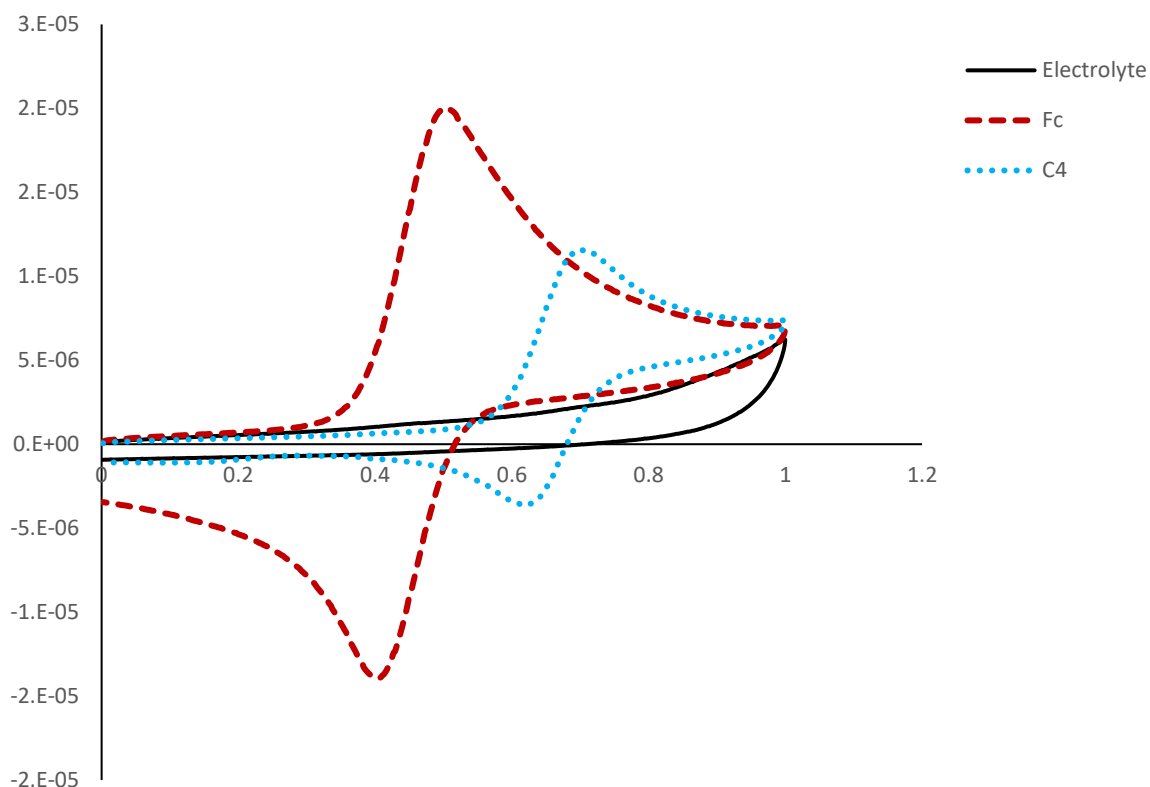


Figure 2.8: Cyclic voltammograms of the electrolyte (black solid line), ferrocene (dark red dashed line), and C4 (blue round dots) measured in 0.1 M tetrabutylammonium perchlorate on a glassy carbon working electrode at 25°C vs.  $\text{Fc}/\text{Fc}^+$  at a scan rate of 25  $\text{mV}\cdot\text{s}^{-1}$ .

Table 2.4: The redox potentials (V vs  $\text{Ag}/\text{Ag}^+$ ) of the standard reference, ferrocene, and complexes C1 – C5.

Compounds	$E_{\text{pa}}$ (V)	$E_{\text{pc}}$ (V)	$E_{1/2}$ (V)	$\Delta E_{\text{p}}$ (V)
<b>Ferrocene</b>	0,51	0,40	0,455	0,11
<b>C1</b>	0,72	0,62	0,67	0,10
<b>C2</b>	0,64	0,55	0,595	0,09
<b>C3</b>	0,70	0,60	0,65	0,10
<b>C4</b>	0,70	0,62	0,66	0,08
<b>C5</b>	0,72	0,61	0,665	0,11

The internal standard, ferrocene, exhibited one oxidation and one reduction wave during the forward and the back potential sweeps, indicating a single electron redox exchange. Complexes



**C1 – C5** exhibited similar one electron transfer processes with positive shifts in their half-wave potentials ( $E_{1/2}$ ) relative to ferrocene ( $E_{1/2}=0.455$  V), suggesting that the ferrocenyl moiety became slightly more difficult to oxidise.<sup>19</sup> Since the oxidation potentials of ferrocene derivatives are dependent on the electron-withdrawing or –donating ability of the substituent(s), preceding studies of mono-substituted ferrocene derivatives have shown that the presence of electron-donating groups increases the proclivity of the ferrocenyl moiety toward oxidation, whereas electron-withdrawing groups demonstrated the opposite.<sup>17</sup> Thus, the appearance of the anodic peaks of **C1 – C5** at higher potentials than that of ferrocene may be due to the presence of the amide group in close proximity to the ferrocene moiety, which likely reduces the electron density at the metal centre compared to the free hydrogen atom in the case of ferrocene.<sup>20</sup> The electron-withdrawing ability of the substituents is also shown to be dependent on the nature of the heterocyclic fragments, since the observed  $E_{1/2}$  value of 0.595 V suggests that **C2** is slightly easier to oxidise than **C1** and **C3-C5**, further emphasising that the amide bridge allows for electronic communication between the ferrocene and the sulfonamide moieties. This may likely be due to the heteroatom withdrawing electron density from the carbons in the ring, rendering the ring electron poor. Additionally, the substituents on the rings may also influence electron density within the rings.

Peak-to-peak separation ( $E_p$ ) values ranging between 80 – 110 mV were observed for the synthesised complexes, which are slightly larger than the theoretical value ( $E_p=57$  mV) for a reversible one electron transfer process.<sup>21</sup> Since the  $E_p$  value of 110 mV for the ferrocene compound was observed in a similar range under the same experimental conditions, this slight deviation might indicate a slower electron transfer due to the uncompensated solvent resistance effects rather than the complexes exhibiting a quasi-reversible process. In addition, to this, the increasing the scan rate led to a proportional increase in signal intensity but the scan rate did not have any impact on the reversibility of the process, further emphasising a reversible process which is diffusion-controlled.

## 2.4 Stability studies

It is important to understand the stability of compounds in solution for *in vitro* and *in vivo* biological applications. Biological assays are normally done in the presence of DMSO, which is quite possibly one of the most widely used organic solvents due to its nature, high viscosity, and its ability to solubilise a variety of compounds.<sup>22,23</sup>

The complexes were observed to change colour, from orange to dark brown, upon dissolution in DMSO under direct light as shown in Figure 2.9. However, no color change was observed in the absence of direct light or even at low temperature. The visible colour change, which is a possible indication of instability, raised some concerns in terms of the design and chemical modifications of these complexes. Initially the different heterocyclic fragments constituting the different sulfonamides derivatives were thought to be the cause of the colour change. However, since all the complexes were changing colour to the same extent, despite their differences in heterocyclic fragments, this was ruled out as a possible contributing factor.

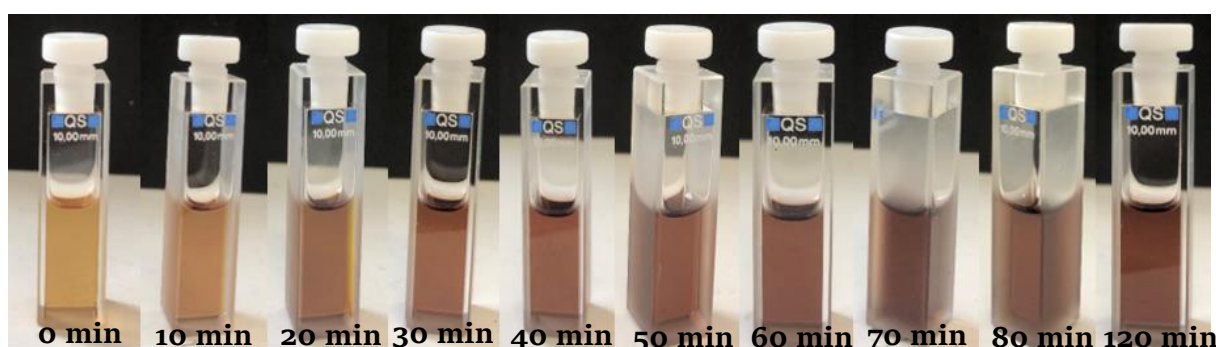


Figure 2.9: 1.0 mM solution of complex **C2** in DMSO solution.

To study these modifications, UV-Vis experiments were performed at 25°C in 10 min intervals over a period of 2 hours. A 1 mM stock solution of the compound in DMSO was exposed to natural light for 10 min before taking the next UV-Vis scan as shown Figure 2.10. The UV scan at 0 min (red) shows one main absorption band at 448 nm with a shoulder band at 330 nm. The absorption band at 448 nm is assigned to the d-d transitions of the ferrocene moiety.<sup>24,25</sup> As the color of the sample changes, a proportional appearance of a new absorption maxima (550 nm) and disappearance of the main absorption band (448 nm) is observed. In addition to this, the strong absorption shoulder band (330 nm) is gradually red shifted to longer wavelengths, further confirming the changes in the structural modifications of these complexes. The stability of the two moieties, ferrocene and sulfamethoxazole, were also separately monitored under the same experimental conditions, where both compounds were shown to be stable after 2 hours (Figure 2.11).

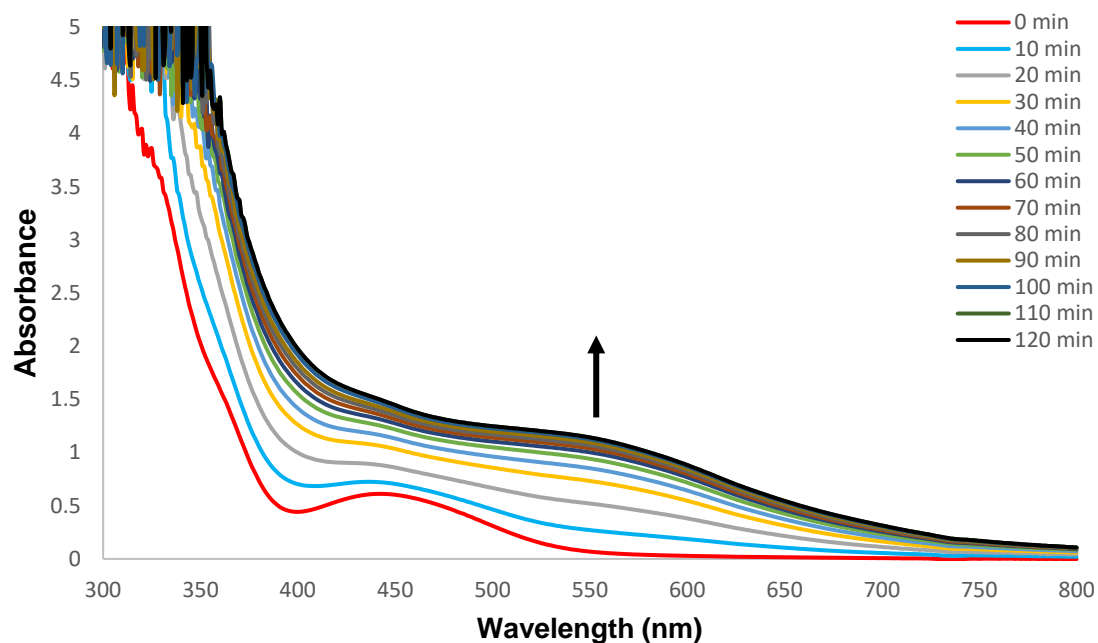


Figure 2.10: UV-Vis absorption spectra of **C2** in DMSO over a period of 2 hours in intervals of 10 min.

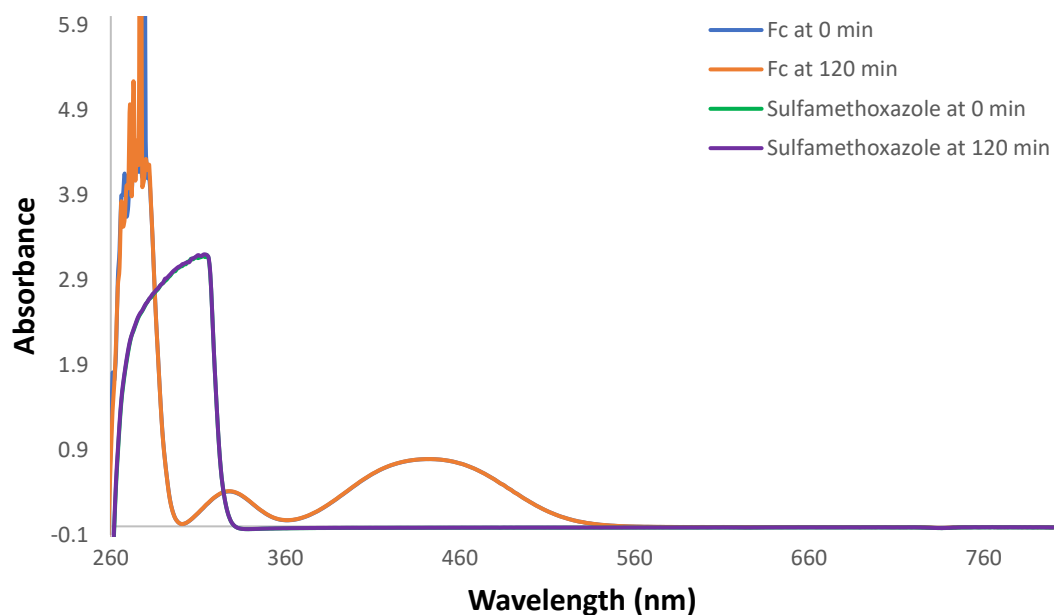


Figure 2.11: UV-Vis spectra of ferrocene (0 min and 120 min) and sulfamethoxazole (0 min and 120 min) in 100% DMSO.

Preliminary NMR experiments were then performed to gain more insight into these modifications in 1-hour intervals over a period of 5 hours (Figure 2.12). The broad amino

singlet of the sulfonamide at 11.34 ppm completely disappears after 3 hours and the sharp water signal at 3.34 ppm broadens with time. Since the NH of the sulfonamide is capable of hydrogen bonding to solvent molecules it might be interacting with water in the solvent. Furthermore, no significant changes in the ferrocene signals were observed after 3 hours. However, small shoulders were observed on the trailing edges of the main signals after 5 hours. In addition to this, the two doublets of the *para*-substituted phenyl protons in the aromatic region converged into a broad singlet. An appearance of a multiplet, adjacent to the newly formed broad singlet, with a disappearance of a sharp singlet at 6 ppm is also observed. The integration after 5 hours is not consistent with the number of protons in the proposed structure as expected.

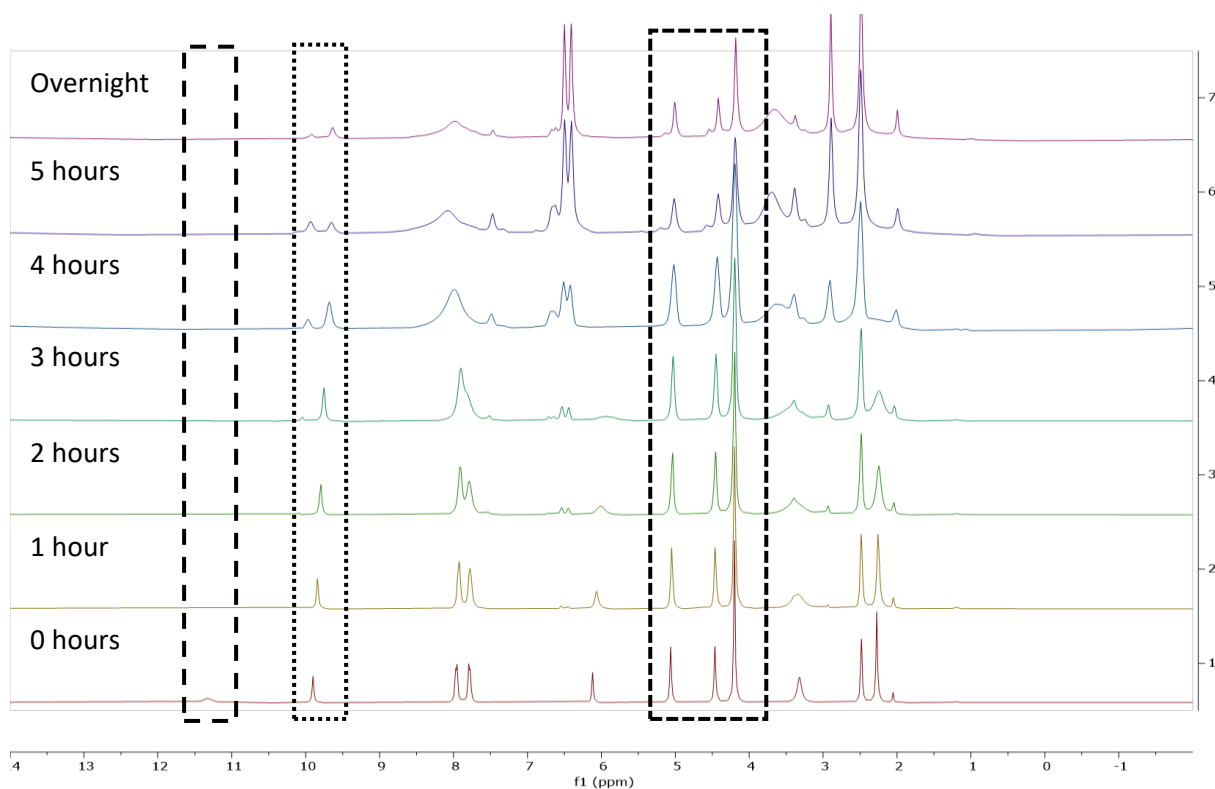


Figure 2.12: Stacked  $^1\text{H}$  NMR spectra of **C2** in  $\text{DMSO-d}_6$  in 1-hour intervals over a period of 5 hours.

To substantiate the complex NMR spectra, the same RP-HPLC method that was used to determine the purity of the complexes was applied. The experiment was designed in such a manner that the stock solutions were first exposed to light for 24 hours prior to injection. The chromatograms displayed two intense signals, emphasising the decomposition of the

complexes. The decomposed complexes were characterised using electrospray ionisation (ESI) spectrometry. The decomposition process was confirmed by the fact that some of the peaks observed in the decomposition spectra were not present in the original spectra of the target compounds. The spectra of the decomposition products show molecular ion peaks corresponding to the deprotonated molecular  $[M - H]^-$  ion and common multiple ion peaks which are summarised in Table 2.5. The mass spectrum of **dc5**, shown in Figure 2.13, is used as a representative and the proposed structures of the indicated fragmentation peaks are shown in Figure 2.14.

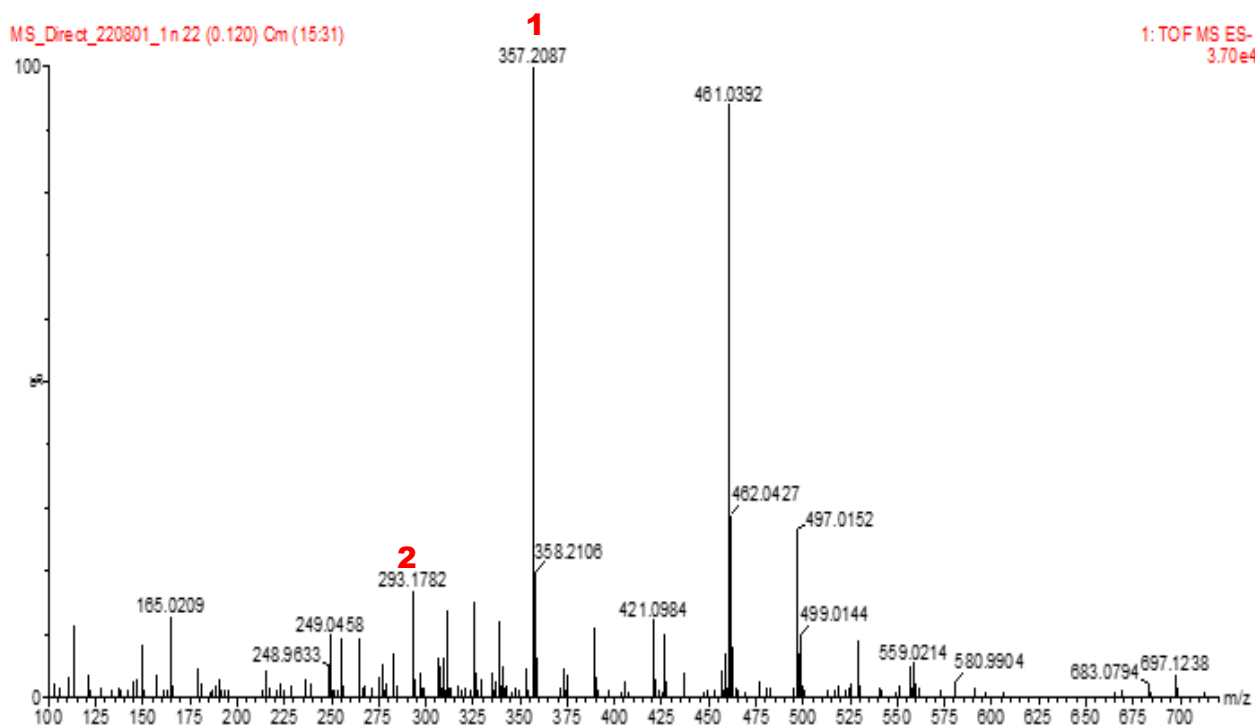


Figure 2.13: The mass spectrum of **dc5**.

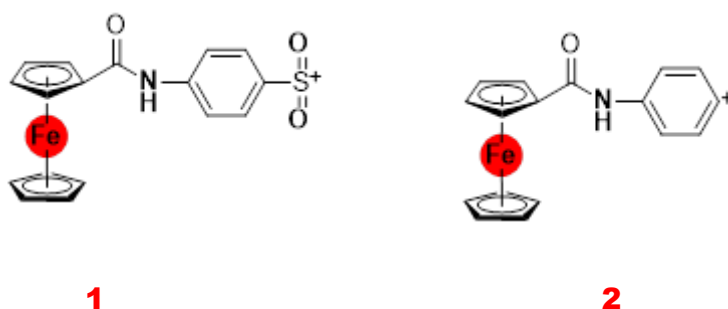


Figure 2.14: Proposed structures of **dC5** based on the m/z fragmentation values.

Table 2.5: Experimentally determined m/z values of the decomposed complexes and the common fragmentation peaks observed among the complexes.

Complexes	M/z = [M-H] <sup>-</sup>	Common fragmentation peaks
<b>dC1</b>	521.0606	293.1797; 165.0204
<b>dC2</b>	464.0353	357.2061; 293.1752; 165.0187
<b>dC3</b>	491.0480	357.2063; 293.1752; 165.0188
<b>dC4</b>	489.0678	357.2061; 293.1751
<b>dC5</b>	461.0392	357.2087; 293.1782; 165.0209

Based on the experimental m/z values and the proposed structures, two possible decomposition pathways are shown in Figure 2.15.

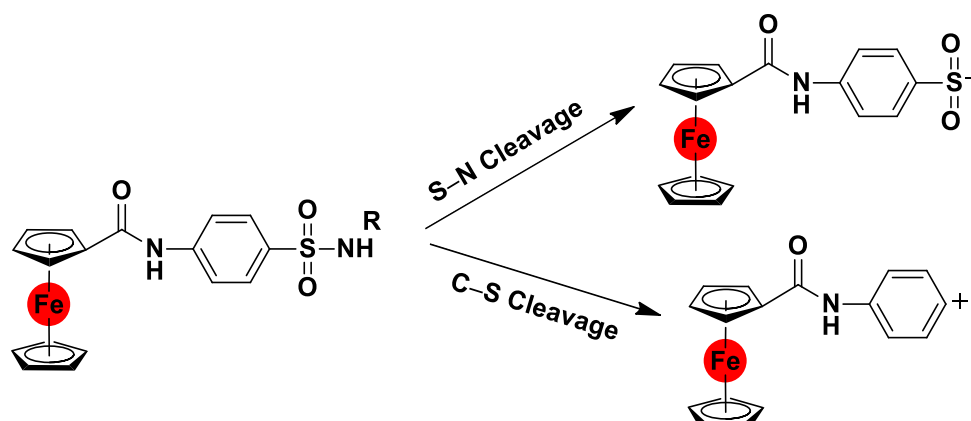


Figure 2.15: Proposed possible degradation pathways of the synthesised complexes in DMSO.

## 2.5 Summary

A small library of ferrocene derivatives of sulfonamides, each bearing an amide linker between the ferrocene and sulfonamide moieties, was successfully synthesised and isolated in moderate to good yields. The complexes were fully characterised using various spectroscopic and analytical techniques including <sup>1</sup>H, <sup>13</sup>C {<sup>1</sup>H} NMR spectroscopy, infrared spectroscopy, and mass spectrometry. The purity of the complexes was determined by reversed-phase HPLC and all complexes were confirmed to be in purities of greater than 98%. In addition, the electrochemical studies revealed that the complexes are slightly more difficult to oxidize than

the unsubstituted ferrocene. The complexes also showed stability to in DMSO for approximately 2 hours after which they started to degrade. Degradation was most commonly afforded through the cleavage of S-N and C-S bonds within the complexes.

## 2.6 Experimental

### 2.6.1 Chemicals and reagents

All chemicals and reagents were purchased from Sigma-Aldrich and were used without further purification. All solvents were also purchased from Sigma- Aldrich. The solvents were distilled and dried using standard methods before use and stored over molecular sieves. Reactions were monitored using aluminum-backed TLC silica gel plates in a variety of solvent systems using the ascending technique. TLC plates were visualised under ultraviolet light.

### 2.6.2 Materials and methods

All reactions were carried out under a nitrogen atmosphere using standard Schlenk line technique. Infrared (IR) absorptions were measured on the FT-IR spectrometer using Attenuated Total Reflectance (ATR).  $^1\text{H}$  and  $^{13}\text{C}$  Nuclear Magnetic Resonance (NMR) spectra were recorded on a 400 MHz Varian Unity Inova spectrometer at 25 degrees Celsius. The chemical shifts are reported in ppm and were referenced to dimethylsulfoxide- $\text{d}_6$  (2.50 ppm). The data were processed using MestReNova-14.1.1-24571. Mass spectrometry determinations were carried out using Electrospray Ionisation-mass spectrometry (ESI-MS) on a Waters API Quattro Micro triple quadrupole mass spectrometer with data recorded using the positive.

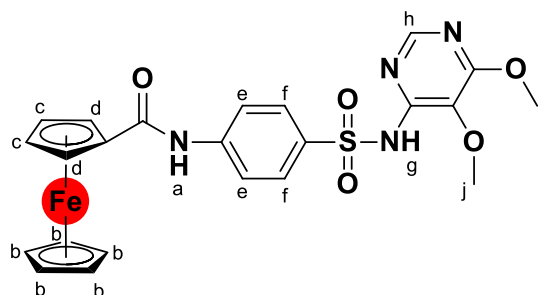
### 2.6.3 A general synthetic method

Ferrocene carboxylic acid (1 equiv.) was dissolved in dry dichloromethane (DCM) (20 mL) under inert ( $\text{N}_2$ ) conditions. The resulting yellow suspension was cooled to  $0^\circ\text{C}$ . Oxalyl chloride (2 equiv.) was added drop-wise to the yellow suspension followed by a catalytic amount of *N,N*-Dimethylformamide (DMF). The resulting mixture was stirred for 4 hours at room temperature. The solvent and excess oxalyl chloride were evaporated using Schlenk line techniques. The dark red crude residue was re-dissolved in dry acetonitrile (MeCN) (10 mL)

or tetrahydrofuran (THF) and cooled to 0°C. The crude, ferrocenoyl chloride, was subsequently used without further purification.

A solution of the appropriate amine (1.3 equiv.) and pyridine (2 equiv.) in dry acetonitrile (30 mL) was added drop wise to a stirred solution of ferrocenoyl chloride at 0°C. The reaction mixture was stirred for 24 hours at room temperature. The progress of the reaction was monitored by TLC. The solvent was evaporated and the crude residue re-dissolved in DCM. The solution was washed with saturated sodium bicarbonate (3x10 mL) followed by brine (1x10 mL). The combined organic phases were dried over anhydrous sodium sulphate, filtered, and concentrated under reduced pressure. The crude residue was dried overnight under reduced pressure and purified by recrystallisation or column chromatography to give the targeted complexes. The materials that precipitated out of solution were filtered and the product was washed with the reaction solvent to remove any unreacted starting materials. The remaining product was dried under reduced pressure.

### Ferrocenyl-amido-sulfadoxine (C1)



Ferrocene carboxylic acid (1.09 mmol, 250.0 mg) was reacted with oxalyl chloride (2.17 mmol, 1.08 mL) followed by the addition of sulfadoxine (1.31 mmol, 405.91 mg) and pyridine (2.17 mmol, 0.17 mL). The crude residue was purified by recrystallisation with DCM/Hexane (1:2) and the product was obtained as an orange powder.

**Yield:** 55%

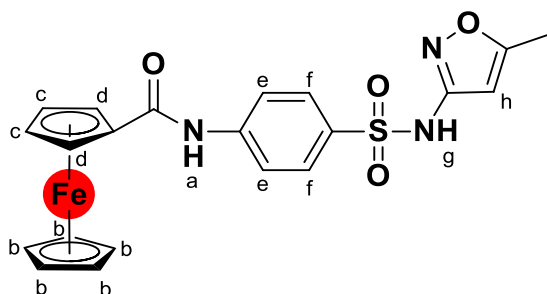
**Physical Appearance:** Orange powder

**<sup>1</sup>H NMR (400 MHz, DMSO-d<sub>6</sub>):** 11.04 (1H, s, H<sub>g</sub>); 9.76 (1H, s, H<sub>a</sub>); 8.10 (1H, s, H<sub>h</sub>); 7.92 (4H, m, J=8.8 Hz, H<sub>f</sub> and H<sub>e</sub>); 5.02 (2H, s, H<sub>d</sub>); 4.46 (2H, s, H<sub>c</sub>); 4.19 (5H, s, H<sub>b</sub>); 3.88 (3H, s, H<sub>i</sub>); 3.68 (3H, s, H<sub>j</sub>). **<sup>13</sup>C NMR (400 MHz, DMSO-d<sub>6</sub>):** δ (ppm) = 169.32; 161.98; 151.19; 150.94; 143.61; 134.93; 128.98; 127.64; 119.75; 76.08; 71.31; 70.00; 69.24; 60.61; 55.45.



**FTIR (ATR):** 3381.6; 3077.7 (NH); 1662.2 (C=O); 1525 (C=N); 1340 (SO<sub>2</sub>)<sub>asymmetric</sub>; 1134 (SO<sub>2</sub>)<sub>symmetric</sub>. **EI-MS:** m/z = [M+H]<sup>+</sup> 523.0739 (100%). **HPLC purity:** > 98% t<sub>R</sub> = 15.166 min.

### Ferrocenyl-amido-sulfamethoxazole (C2)

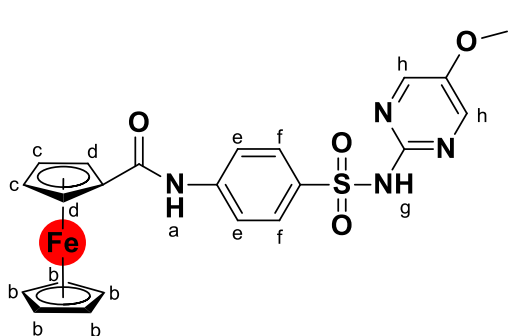


Ferrocene carboxylic acid (1.09 mmol, 250.0 mg) was reacted with oxalyl chloride (2.17 mmol, 1.08 mL) followed by the addition of sulfamethoxazole (1.31 mmol, 331.80 mg) and pyridine (2.17 mmol, 0.17 mL). An off-white product precipitated out of solution and the precipitate was filtered on hirch/buchner funnel and thoroughly washed with acetonitrile.

**Yield:** 64%

**Physical Appearance:** Off-white powder

**<sup>1</sup>H NMR (400 MHz, DMSO-d<sub>6</sub>):** 9.78 (1H, s, H<sub>a</sub>); 7.91 (d, J=8.2 Hz, 2H); 7.79 (4H, m, J=8.5 Hz, H<sub>e</sub> and H<sub>f</sub>); 6.11 (1H, s, H<sub>h</sub>); 5.02 (2H, s, H<sub>d</sub>); 4.47 (2H, s, H<sub>c</sub>); 4.20 (5H, s, H<sub>b</sub>); 2.27 (3H, s, H<sub>i</sub>). **<sup>13</sup>C NMR (400 MHz, DMSO-d<sub>6</sub>):** δ (ppm) = 170.46; 169.41; 158.49; 143.95; 133.79; 128.20; 120.18; 95.93; 76.02; 71.34; 70.02; 69.30; 12.53. **FTIR (ATR):** 3381.6; 3077.7 (NH); 1662.2 (C=O); 1525 (C=N); 1157 (SO<sub>2</sub>)<sub>asymmetric</sub>; 1313 (SO<sub>2</sub>)<sub>symmetric</sub>. **EI-MS:** m/z = [M+H]<sup>+</sup> 466.0523 (100%). **HPLC purity:** > 98% t<sub>R</sub> = 14.734 min.

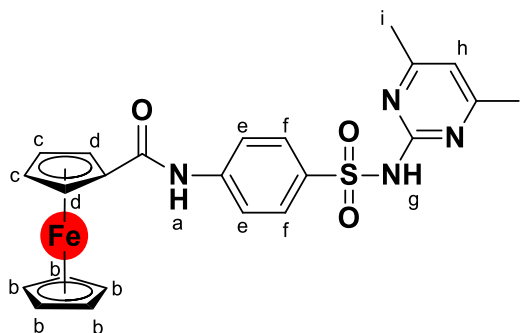
**Ferrocenyl-amido-sulfameter (C3)**

Ferrocene carboxylic acid (1.09 mmol, 250.0 mg) was reacted with oxalyl chloride (2.17 mmol, 1.08 mL) followed by the addition of sulfameter (1.31 mmol, 367.19 mg) and pyridine (2.17 mmol, 0.17 mL). An off-white product precipitated out of solution and the precipitate filtered and then thoroughly washed with acetonitrile.

**Yield:** 60%

**Physical Appearance:** Off-white powder

**<sup>1</sup>H NMR (400 MHz, DMSO-*d*<sub>6</sub>):** 11.37 (1H, s, H<sub>g</sub>); 9.95 (1H, s, H<sub>a</sub>); 8.28 (2H, s, H<sub>h</sub>); 7.98 (2H, d, J=8.6 Hz, H<sub>f</sub>); 7.90 (2H, d, J=8.6 Hz, H<sub>e</sub>); 5.09 (2H, t, J=1.9 Hz, H<sub>d</sub>); 4.44 (2H, t, J=1.8 Hz, H<sub>c</sub>); 4.18 (5H, s, H<sub>b</sub>); 3.77 (3H, s, H<sub>i</sub>). **<sup>13</sup>C NMR (400 MHz, DMSO-*d*<sub>6</sub>):** δ (ppm) = 169.44; 151.47; 150.06; 154.11; 143.78; 134.41; 128.85; 119.86; 76.09; 71.28; 69.99; 69.39; 56.73. **FTIR (ATR):** 3381.6; 3077.7 (NH); 1662.2 (C=O); 1525 (C=N); 1357 (SO<sub>2</sub>)<sub>asymmetric</sub>; 1128 (SO<sub>2</sub>)<sub>symmetric</sub>. **EI-MS:** m/z = [M+H]<sup>+</sup> 493.0641 (100%). **HPLC purity:** > 98% t<sub>R</sub> = 14.307 min.

**Ferrocenyl-amido-sulfamethazine (C4)**

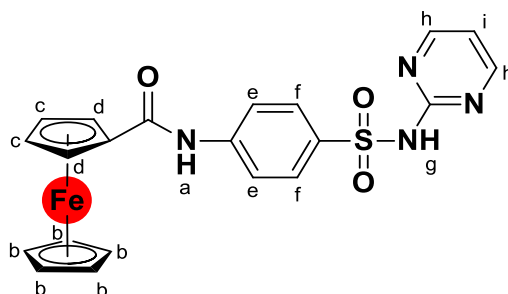
Ferrocene carboxylic acid (1.09 mmol, 250.0 mg) was reacted with oxalyl chloride (2.17 mmol, 1.08 mL) followed by the addition of sulfamethazine (1.31 mmol, 364.61 mg) and pyridine (2.17 mmol, 0.17 mL). The crude residue was purified by column chromatography on silica gel with ethyl acetate/hexane (70:30).

**Yield:** 49%

**Physical Appearance:** Orange powder

**<sup>1</sup>H NMR (400 MHz, DMSO-d<sub>6</sub>):** 9.72 (1H, s, H<sub>a</sub>); 7.95 (4H, m, H<sub>e</sub> and H<sub>f</sub>); 6.76 (1H, s, H<sub>h</sub>); 5.02 (2H, s, H<sub>d</sub>); 4.48 (2H, s, H<sub>c</sub>); 4.20 (5H, s, H<sub>b</sub>); 2.26 (6H, s, H<sub>i</sub>). **<sup>13</sup>C NMR (400 MHz, DMSO-d<sub>6</sub>):** δ (ppm) = 169.33; 153.47; 143.73; 134.29; 130.26; 129.11; 125.32; 119.77; 112.58; 76.07; 71.32; 70.01; 69.54; 11.87. **FTIR (ATR):** 3381.6; 3077.7 (NH); 1662.2 (C=O); 1525 (C=N); 1360 (SO<sub>2</sub>) asymmetric; 1142 (SO<sub>2</sub>) symmetric. **EI-MS:** m/z = [M+H]<sup>+</sup> 491.0842 (100%). **HPLC purity:** > 98% t<sub>R</sub> = 14.210 min.

### Ferrocenyl-amido-sulfadiazine (C5)



Ferrocene carboxylic acid (1.09 mmol, 250.0 mg) was reacted with oxalyl chloride (2.17 mmol, 1.08 mL) followed by the addition of sulfadiazine (1.31 mmol, 327.87 mg) and pyridine (2.17 mmol, 0.17 mL). An off-white product precipitated out of solution and the precipitate filtered and then thoroughly washed with the reaction solvent.

**Yield:** 62%

**Physical Appearance:** Off-white powder

**<sup>1</sup>H NMR (400 MHz, DMSO-d<sub>6</sub>):** 9.93 (1H, s, H<sub>a</sub>); 8.50 (2H, d, H<sub>i</sub>); 7.94 (4H, m, H<sub>e</sub> and H<sub>f</sub>); 7.01 (1H, m, H<sub>h</sub>); 5.07 (2H, s, H<sub>d</sub>); 4.47 (2H, s, H<sub>c</sub>); 4.21 (5H, s, H<sub>b</sub>). **<sup>13</sup>C NMR (400 MHz, DMSO-d<sub>6</sub>):** δ (ppm) = 169.33; 153.47; 143.73; 134.29; 130.26; 129.11; 125.32; 119.77; 112.58; 76.07; 71.32; 70.01; 69.24. **FTIR (ATR):** 3381.6; 3077.7 (NH); 1662.2 (C=O); 1525

(C=N); 1298 (SO<sub>2</sub>) asymmetric; 1144 (SO<sub>2</sub>) symmetric. **EI-MS:**  $m/z = [M+H]^+ 463.0534$  (100%).  
**HPLC purity:** > 98%  $t_R = 15.512$  min.

## 2.6.4 Electrochemical studies

Cyclic voltametric studies were performed at room temperature using a Bioanalytical Systems Inc. BAS 100W Electrochemical Analyser with a one compartment three-electrode system comprising of a glassy carbon working electrode, a platinum wire auxiliary electrode and a Ag/Ag<sup>+</sup> reference electrode (0.01 M AgNO<sub>3</sub> and 0.1 M [n-Bu<sub>4</sub>N][ClO<sub>4</sub>] in anhydrous acetonitrile). The reported  $E_{1/2}$  values are with reference to this electrode. Measurements were made using 5% dimethyl sulfoxide/acetonitrile solutions which were 1.0 mM in sample and contained 0.1 M [n-Bu<sub>4</sub>N][ClO<sub>4</sub>] as the background electrolyte. Unless otherwise stated, the scan rate used was 25 mV.s<sup>-1</sup>. Under these conditions the ferrocene/ferrocenium couple, which was used as a reference, had an  $E_{1/2}$  of 0.455 V and  $\Delta E_p$  of 0.11 V. All solutions were purged with nitrogen and the voltammograms were recorded under a blanket of nitrogen. The glassy carbon working electrode was polished before use.

## 2.6.5 HPLC method and purity determination

Analytical HPLC experiments were performed using a C18 column. A gradient elution was developed from 10% to 80% eluent B over a period of 45 min. Eluent A was 0.1% tetrafluoro acetic acid (TFA) in water, while eluent B contained 0.1% TFA in methanol. Experiments were carried out at a flow rate of 1 mL/min at room temperature. Samples were dissolved in a 10% methanol/water solution and the sample injections were half the loop volume (50  $\mu$ L); with needle washes (x3) of 50% methanol/water between injections. Peaks were detected at  $\lambda = 280$  nm and  $\lambda = 290$  nm. The sample concentration was 100  $\mu$ M and the peaks were manually integrated.

## 2.7 References

- 1 P. Chellan and P. J. Sadler, Enhancing the Activity of Drugs by Conjugation to Organometallic Fragments, *Chem. - A Eur. J.*, 2020, **26**, 8676–8688.
- 2 C. Biot, W. Castro, C. Y. Botté and M. Navarro, The therapeutic potential of metal-

- based antimalarial agents: implications for the mechanism of action, *Dalt. Trans.*, 2012, **41**, 6335–6349.
- 3 B. Đ. Glišić and M. I. Djuran, Gold complexes as antimicrobial agents: an overview of different biological activities in relation to the oxidation state of the gold ion and the ligand structure, *Dalton Trans.*, 2014, **43**, 5950–5969.
- 4 E. Kremer, G. Facchin, E. Estévez, P. Alborés, E. J. Baran, J. Ellena and M. H. Torre, Copper complexes with heterocyclic sulfonamides: Synthesis, spectroscopic characterization, microbiological and SOD-like activities: Crystal structure of  $[\text{Cu}(\text{sulfisoxazole})_2(\text{H}_2\text{O})_4] \cdot 2\text{H}_2\text{O}$ , *J. Inorg. Biochem.*, 2006, **100**, 1167–1175.
- 5 C. M. Sharaby, M. F. Amine and A. A. Hamed, Synthesis, structure characterization and biological activity of selected metal complexes of sulfonamide Schiff base as a primary ligand and some mixed ligand complexes with glycine as a secondary ligand, *J. Mol. Struct.*, 2017, **1134**, 208–216.
- 6 A. Ashraf, W. A. Siddiqui, J. Akbar, G. Mustafa, H. Krautscheid, N. Ullah, B. Mirza, F. Sher, M. Hanif and C. G. Hartinger, Metal complexes of benzimidazole derived sulfonamide: Synthesis, molecular structures and antimicrobial activity, *Inorg Chim. Acta*, 2016, **443**, 179–185.
- 7 H. Keypour, M. Shayesteh, M. Rezaeivala, F. Chalabian, Y. Elerman and O. Buyukgungor, Synthesis, spectral characterization, structural investigation and antimicrobial studies of mononuclear Cu(II), Ni(II), Co(II), Zn(II) and Cd(II) complexes of a new potentially hexadentate  $\text{N}_2\text{O}_4$  Schiff base ligand derived from salicylaldehyde, *J. Mol. Struct.*, 2013, **1032**, 62–68.
- 8 M. Zaki, F. Arjmand and S. Tabassum, Current and future potential of metallo drugs: Revisiting DNA-binding of metal containing molecules and their diverse mechanism of action, *Inorg Chim. Acta*, 2016, **444**, 1–22.
- 9 E. Bruno, M. R. Buemi, A. Di Fiore, L. De Luca, S. Ferro, A. Angeli, R. Cirilli, D. Sadutto, V. Alterio, S. M. Monti, C. T. Supuran, G. De Simone and R. Gitto, Probing Molecular Interactions between Human Carbonic Anhydrases (hCAs) and a Novel Class of Benzenesulfonamides, *J. Med. Chem.*, 2017, **60**, 4316–4326.
- 10 M. Mondelli, F. Pavan, P. C. De Souza, C. Q. Leite, J. Ellena, O. R. Nascimento, G.

- Facchin and M. H. Torre, Study of a series of cobalt(II) sulfonamide complexes: Synthesis, spectroscopic characterization, and microbiological evaluation against *M. tuberculosis*. Crystal structure of  $[\text{Co}(\text{sulfamethoxazole})_2(\text{H}_2\text{O})_2] \cdot \text{H}_2\text{O}$ , *J. Mol. Struct.*, 2013, **1036**, 180–187.
- 11 M. Mondelli, V. Bruné, G. Borthagaray, J. Ellena, O. R. Nascimento, C. Q. Leite, A. A. Batista and M. H. Torre, New Ni(II)-sulfonamide complexes: Synthesis, structural characterization and antibacterial properties. X-ray diffraction of  $[\text{Ni}(\text{sulfisoxazole})_2(\text{H}_2\text{O})_4] \cdot 2\text{H}_2\text{O}$  and  $[\text{Ni}(\text{sulfapyridine})_2]$ , *J. Inorg. Biochem.*, 2008, **102**, 285–292.
  - 12 C. Quintana, G. Silva, A. H. Klahn, V. Artigas, M. Fuentealba, C. Biot, I. Halloum, L. Kremer, N. Novoa and R. Arancibia, New cyrhetrenyl and ferrocenyl sulfonamides: Synthesis, characterization, X-ray crystallography, theoretical study and anti-*Mycobacterium tuberculosis* activity, *Polyhedron*, 2017, **134**, 166–172.
  - 13 P. Chellan, V. M. Avery, S. Duffy, J. A. Triccas, G. Nagalingam, C. Tam, L. W. Cheng, J. Liu, K. M. Land, G. J. Clarkson, I. Romero-Canelón and P. J. Sadler, Organometallic Conjugates of the Drug Sulfadoxine for Combatting Antimicrobial Resistance, *Chem. - A Eur. J.*, 2018, **24**, 10078–10090.
  - 14 T. J. Kotzé, S. Duffy, V. M. Avery, A. Jordaan, D. F. Warner, L. Loots, G. S. Smith and P. Chellan, Synthesis and antimicrobial study of organoiridium amido-sulfadoxine complexes, *Inorg Chim. Acta*, , DOI:10.1016/j.ica.2020.120175.
  - 15 M. Remko and C. W. Von Der Lieth, Theoretical study of gas-phase acidity,  $\text{pK}_a$ , lipophilicity, and solubility of some biologically active sulfonamides, *Bioorganic Med. Chem.*, 2004, **12**, 5395–5403.
  - 16 W. Nkoana, D. Nyoni, P. Chellan, T. Stringer, D. Taylor, P. J. Smith, A. T. Hutton and G. S. Smith, Heterometallic half-sandwich complexes containing a ferrocenyl motif: Synthesis, molecular structure, electrochemistry and antiplasmodial evaluation, *J. Organomet. Chem.*, 2014, **752**, 67–75.
  - 17 C. López, R. Bosque, S. Pérez, A. Roig, E. Molins, X. Solans and M. Font-Bardía, Relationships between  $^{57}\text{Fe}$  NMR, Mössbauer parameters, electrochemical properties and the structures of ferrocenylketimines, *J. Organomet. Chem.*, 2006, **691**, 475–484.

- 18 M. Ajmal, Review: electrochemical studies on some metal complexes having anti-cancer activities, *J. Coord. Chem.*, 2017, **70**, 2551–2588.
- 19 P. E. Kleyi, C. W. McClelland and T. I. A. Gerber, Solvent-free synthesis of bisferrocenyliumines and their rhodium(I) complexes, *Polyhedron*, 2010, **29**, 1095–1101.
- 20 R. Trivedi, S. B. Deepthi, L. Giribabu, B. Sridhar, P. Sujitha, C. Ganesh Kumar and K. V. S. Ramakrishna, Synthesis, crystal structure, electronic spectroscopy, electrochemistry and biological studies of carbohydrate containing ferrocene amides, *Appl. Organomet. Chem.*, 2012, **26**, 369–376.
- 21 A. J. Bard, L. R. Faulkner and H. S. White, *Electrochemical methods: fundamentals and applications*, John Wiley & Sons, 2022.
- 22 L. Di and E. H. Kerns, Biological assay challenges from compound solubility: strategies for bioassay optimization, *Drug Discov. Today*, 2006, **11**, 446–451.
- 23 E. Zitha-Bovens, P. Maas, D. Wife, J. Tijhuis, Q. N. Hu, T. Kleinöder and J. Gasteiger, COMDECOM: Predicting the lifetime of screening compounds in DMSO solution, *J. Biomol. Screen.*, 2009, **14**, 557–565.
- 24 X. L. Yang, J. Liu, L. Yang and X. Y. Zhang, Synthesis, characterization, and susceptibility of bacteria of selenium dioxide complexes with sulfadugs, *Synth. React. Inorganic, Met. Nano-Metal Chem.*, 2005, **35**, 761–766.
- 25 M. S. Refat, T. Sharshar, K. M. Elsabawy, M. Y. El-Sayed and A. M. A. Adam, Synthesis, physicochemical characterization and anticancer screening of sulfa drug ruthenium complexes as anticancer agent, *J. Mol. Liq.*, 2016, **222**, 334–349.

## Chapter 3: *In vitro* biological evaluation of ferrocenyl derivatives of sulfonamide complexes

### 3.1 Introduction

Sub-Saharan Africa and other developing nations are greatly affected by malaria and tuberculosis with the emergence of antimicrobial resistance (AMR).<sup>1,2</sup> AMR occurs when microbes such as bacteria, fungi, parasite, and viruses adapt and multiply in the presence of therapeutic agents that once destroyed them.<sup>3</sup> This type of resistance occurs through several mechanisms, however, gene mutations, whereby microbes modify the target enzyme or limit the permeability of drugs to the intracellular target site by decreasing or suppressing the outer membrane porin genes are among the common mechanisms of antimicrobial resistance.<sup>4</sup> Therefore, AMR emphasises the urgent need for novel antimicrobial agents with improved pharmacological activity.

One of the most common strategies used in drug discovery is the derivatisation (drug repositioning) of known clinical drugs, also known as “old drugs for new uses”.<sup>5–7</sup> Since diseases often share common metabolic pathways and many drugs contain multiple protein targets,<sup>8</sup> researchers use this strategy to identify new candidates which are ready for clinical trials faster than completely new drugs with unknown biological response. As shown in Figure 3.1, drug derivatisation is a quick, cost-effective, and low-risk strategy in contrast to the traditional approach of novel drug discovery and development.<sup>6</sup>

Moreover, the derivatisation of known clinical drugs with transition metals has already been explored as a method to combat AMR.<sup>9</sup> A metal-based derivative of chloroquine (CQ), ferroquine (FQ) as discussed in Chapter 1, is one such drug demonstrating the advantages of this strategy.<sup>10,11</sup> The ferrocene moiety is highly lipophilic and thus increases the concentration of the drug inside the cell by increasing the outer membrane permeability.<sup>12,13</sup> This is significant advance in the development of antimalarial agents as it allows the drug to be accumulated to a much greater extent within the digestive vacuole of the parasite. The same lipophilic effect also applies to the development of anti-TB agents as they often need to penetrate the lipid mycolic acid membrane of the bacteria in order to show any antimycobacterial activity.<sup>14,15</sup>



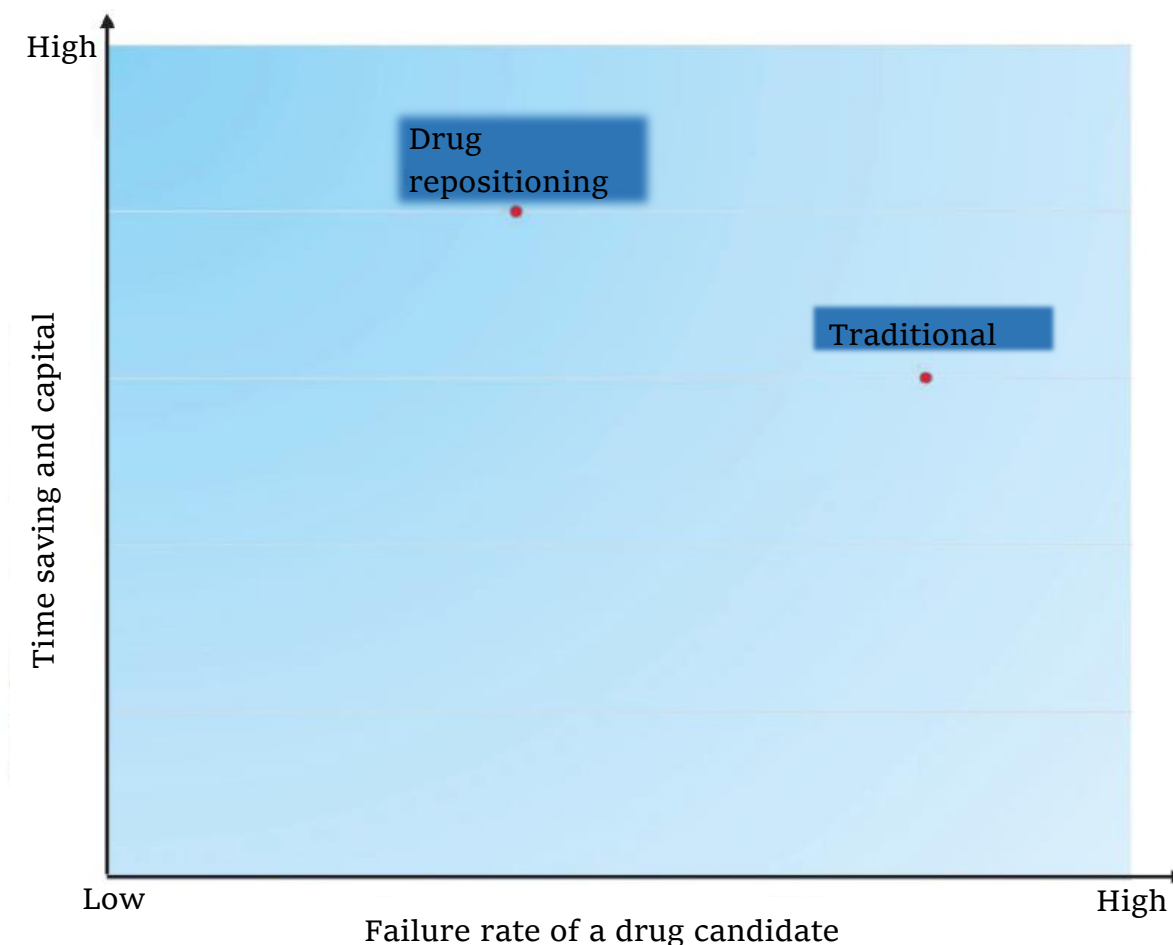


Figure 3.1: The Figure adapted from Xue et al., shows the comparisons of the risks and rewards in drug repositioning and traditional drug discovery.<sup>6</sup>

This chapter focuses on the biological activity of the ferrocenyl-sulfa drug derivatives **C1–C5**, synthesised in Chapter 2. The antimalarial activity of the complexes was evaluated *in vitro* against the chloroquine-sensitive (CQS) NF54 strain of *Plasmodium falciparum*. The screening against the chloroquine-resistant (CQR) strain of *Plasmodium falciparum* was not possible due to time constraints. The complexes were also screened against healthy human cell lines to determine their cytotoxicity and selectivity. The *in vitro* antimycobacterial activity of the complexes were also evaluated against the non-pathogenic mycobacterial strain *Mycobacterium smegmatis* (*M. smeg*) Mc<sup>2</sup>155 and the pathogenic strain *Mycobacterium tuberculosis* (*M. tb*) H37Rv. To gain further insight into the physicochemical properties of these complexes, the chemical stability was monitored under physiological conditions and

turbidimetric assays were also conducted to determine the aqueous solubility of the complexes. Lastly, a prediction analysis of the complexes' lipophilicity was also performed.

## 3.2 Results and discussion

### 3.2.1 Predicting lipophilicity

For a drug candidate to efficiently reach target sites, it must diffuse through various cellular membranes.<sup>16</sup> Lipophilicity can be expressed as a logP value when determined experimentally using an octanol-water partition coefficient assay. It is therefore considered an important physicochemical factor which not only influences membrane permeability but also the ADME (absorption, distribution, metabolism, elimination) parameters of a drug candidate.<sup>17</sup> However, several studies have shown that promiscuity (nonselective binding), which is often associated with attrition and toxicity, tends to increase with increasing lipophilicity.<sup>18</sup> In light of this, we investigated the relationship between lipophilicity, biological activity, and toxicity of the synthesised complexes. The clogP values of the sulfa drugs, **Sf1–Sf5**, seen in Figure 3.2, were estimated using Chemdraw Ultra 12.0. Due to the lack of solubility of the complexes **C1–C5** in water and octanol, the logP values could not experimentally be determined and thus, an alternative approach was used.

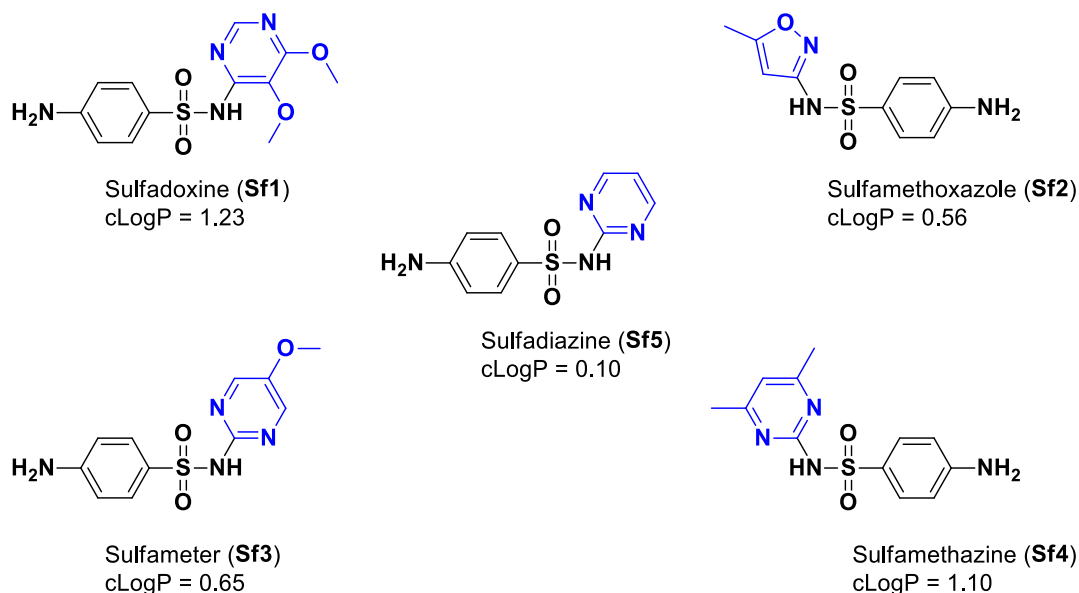


Figure 3.2: Sulfa drugs used as starting derivatives for this work with their estimated clogP values as determined using Chemdraw.

The lipophilicity of the synthesised ferrocenyl-sulfa drug derivatives could not be estimated in the exact same manner and for this reason, an alternative method was used.<sup>19,20</sup> Our alternative method involved a combination of the fragmental approach proposed by Mannhold and Rekker,<sup>21</sup> the ferrocenyl adaptation approach by Ahmedi and Lanez<sup>22</sup>, and the calculated logP values of the sulfa drugs from Chemdraw Ultra 12.0.

The fragmental approach proposed by Mannhold and Rekker, is based on the fragmentation of an organic molecule into smaller substructures with known theoretical hydrophobic constants. The constants are then added together, taking into consideration any correction factors, to give the calculated logP.<sup>21</sup> Since the fragmental method is only applicable to organic molecules, Ahemdi and Lanez adapted this method to calculate the logP of various ferrocene derivatives. They assumed the theoretical logP value of ferrocene (Fc) is equal to the experimental value, 2.66, since ferrocene does not contain any intermolecular interactions that might affect this value.<sup>22</sup> They determined the logP value of a ferrocenyl group (Fc-H) by subtracting the fragmental constant of a hydrogen atom ( $f_H=0.204$ ) from that of Fc, which gave a value of 2.456.<sup>22</sup>

In light of this, our modified approach used the logP value of Fc-H as determined by Ahemdi and Lanez, and calculated logP values of our synthesised drugs by subtracting the calculated logP values of the corresponding phenyl derivatives obtained from Chemdraw. Method validation was done by comparing our calculated logP values (Table 3.1) of several reference compounds (Figure 3.3) to the reported logP values found in the literature. The clogP values of ferrocene derivatives were calculated as follows:

$$\text{cLogP}_{(\text{Fc derivative})} = \text{cLogP}_{(\text{benzene derivative})} - f_{(\text{benzene fragment})} + f_{(\text{Fc-H})}$$

Where:

$\text{cLogP}_{(\text{benzene derivative})}$  is the calculated logP for the benzene derivative as predicted using Chemdraw.

$f_{(\text{benzene fragment})}$  is the logP of the benzene fragment obtained via the fragmented approach.

$f_{(\text{Fc-H})}$  is the logP of the ferrocenyl derivative obtained from Ahemdi and Lanez.

Consider the following ferrocenyl derivative reference compound and the corresponding benzene moiety in Figure 3.3, which was part of our library of reference compounds. The clogP value for this derivative using our method was calculated as follows:

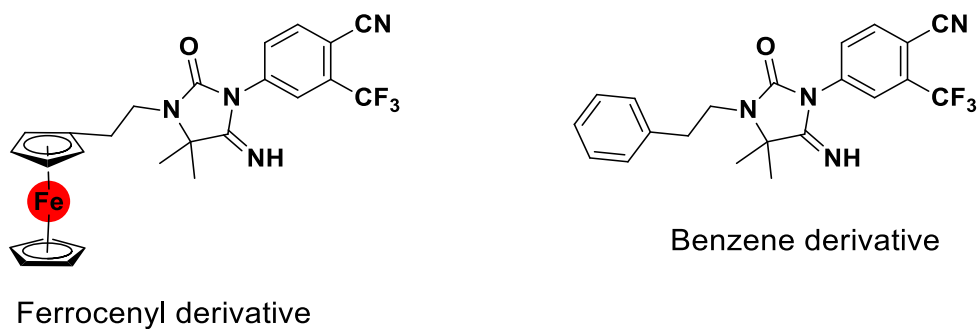


Figure 3.3: The ferrocenyl derivative and the corresponding benzene moiety used as an example to calculate the logP value.

$$\begin{aligned}
 \text{cLogP}_{(\text{Fc derivative})} &= \text{cLogP}_{(\text{benzene derivative})} - \mathbf{f}_{(\text{benzene fragment})} + \mathbf{f}_{(\text{Fc-H})} \\
 &= 4.291 - [6(0.110) + 5(0.204)] + 2.456 \\
 &= 5.07
 \end{aligned}$$

Our method was able to produce a clogP value within 0.6% error of the reported experimental logP of 5.04.

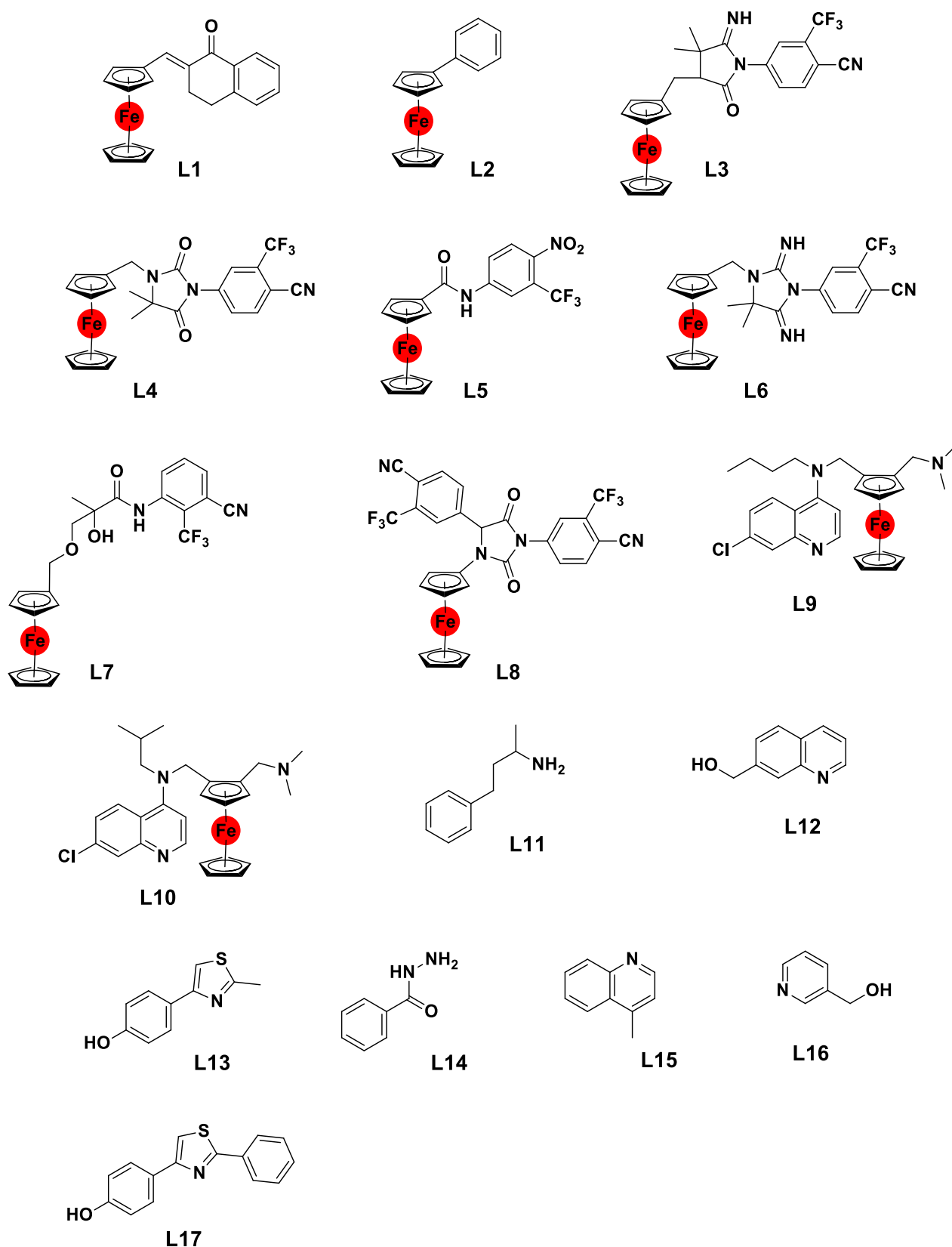


Figure 3.4: The selected reference compounds used to validate the method.<sup>21,22</sup>

Table 3.1: The experimental and calculated logP values of the reference compounds.

Compound	Experimental logP	Calculated logP
<b>L1</b>	5.27	4.93
<b>L2</b>	4.59	4.81
<b>L3</b>	5.04	5.07
<b>L4</b>	5.23	4.16
<b>L5</b>	4.42	4.76
<b>L6</b>	4.68	4.74
<b>L7</b>	4.63	2.86
<b>L8</b>	6.47	5.24
<b>L9</b>	6.70	7.48
<b>L10</b>	6.60	7.35
<b>L11</b>	2.12	2.12
<b>L12</b>	1.29	0.99
<b>L13</b>	2.82	2.62
<b>L14</b>	-0.70	-0.67
<b>L15</b>	2.61	2.53
<b>L16</b>	-0.02	0.06
<b>L17</b>	4.65	4.22

The experimental values were plotted against the above listed calculated values, resulting in a linear line of best fit (Figure 3.5). The correlation coefficient ( $R^2$ ) is 0.9157, indicating a good correlation between the two sets of values and a standard deviation (SD) of 0.059. Following the correlation of experimental and calculated logP values, our method was confirmed to be reasonable and representative of experimental observations. We therefore proceeded with calculating the logP values of **C1-C5**, which are listed in Table 3.2.

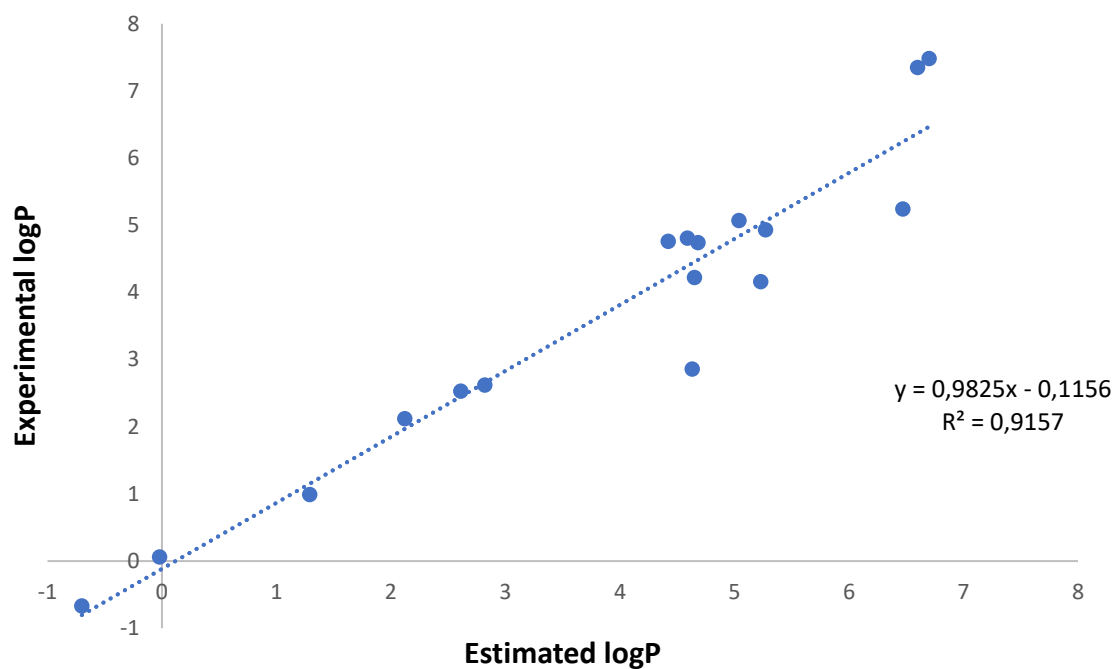
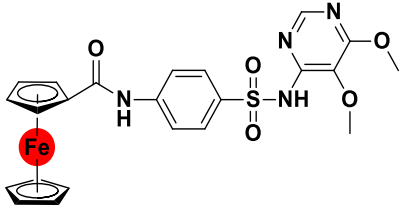
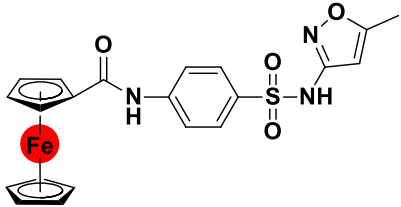
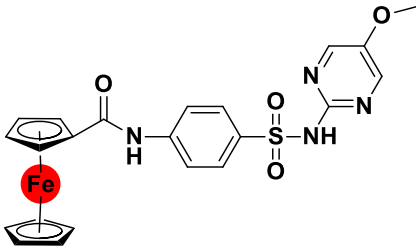
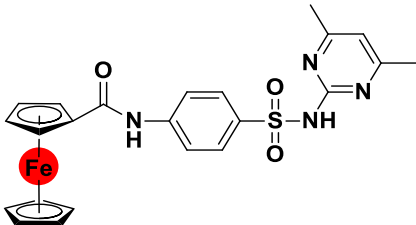
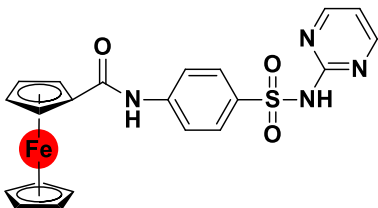


Figure 3.5: Correlated experimental and calculated logP values of reference compounds **L1** to **L17**.

Table 3.2: The calculated logP values of complexes **C1** – **C5**.

Complex	Structure	Calculated logP
<b>C1</b>		3.71
<b>C2</b>		3.05

<b>C3</b>	3.13
	
<b>C4</b>	3.58
	
<b>C5</b>	2.58
	

The logP values of complexes **C1-C5** were all calculated to be between 2.50 and 3.75, indicating that the complexes are lipid soluble compared to the unsubstituted sulfonamide derivatives with predicted clogP values between 0.10 and 1.25.

### 3.2.2 Turbidimetric solubility studies

Drug solubility in aqueous-based media is also considered an important factor for bioavailability in the initial stages of drug discovery, as the drug must completely dissolve and diffuse into the gastrointestinal (GI) epithelial cells in order to be absorbed. Solubility also validates the *in vitro* data obtained as lack of complete solubility at the test concentration might diminish the compound's true biological activity. Compounds are primarily arranged into three different classes based on their solubility ranges.<sup>23</sup> Compounds with a solubility range lower than 10 µg/mL are considered to have poor solubilities, with those between 10 and 60 µg/mL are considered partially soluble, and compounds displaying solubilities greater than 60 µg/mL are considered to have high solubilities.<sup>24-26</sup>



In this study a turbidimetric (kinetic) solubility assay was used to validate the aqueous solubility of **C1-C5** in phosphate-buffered saline (PBS) and 4-(2-Hydroxyethyl)-1-piperazineethanesulfonic acid (HEPES). PBS was chosen to mimic the physiological conditions, pH and ionic strength found in animals and humans, whereas HEPES is generally used in the *in vitro* *P. falciparum* assays. Hydrocortisone and reserpine (Figure 3.6), were used as positive and negative controls, respectively.<sup>23</sup> All complexes were highly soluble in DMSO as far as to 200  $\mu$ M, the highest concentration tested. However, they had poor solubility in both buffers, even at the least concentration tested (10  $\mu$ M). Table 3.1 lists the solubility ranges of **C1-C5**.

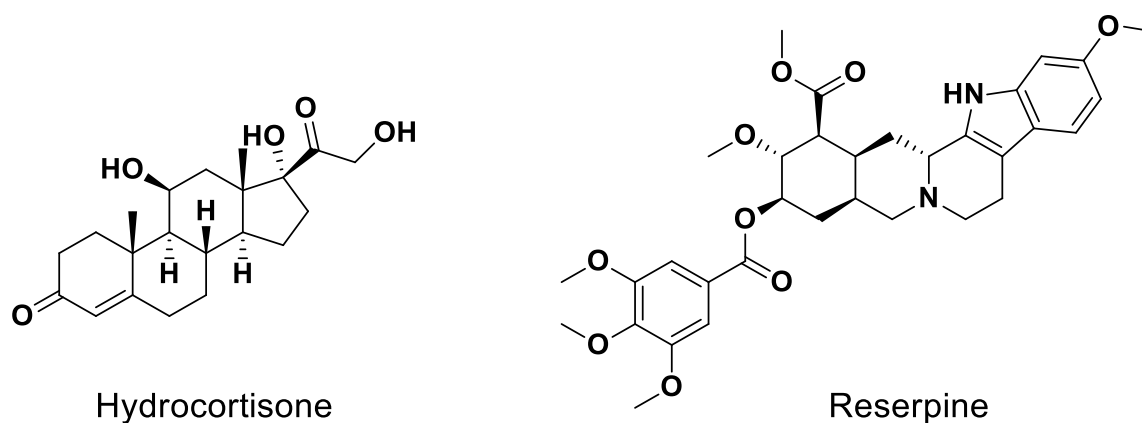


Figure 3.6: The two control drugs used for the study.

Table 3.3: Turbidimetric solubility data for **C1 – C5**.

Compound	PBS		HEPES	
	$\mu$ g/mL	$\mu$ M	$\mu$ g/mL	$\mu$ M
<b>C1</b>	<5.2	<10	<5.2	<10
<b>C2</b>	<4.7	<10	<4.6	<10
<b>C3</b>	<4.9	<10	<4.9	<10
<b>C4</b>	<4.9	<10	<4.9	<10
<b>C5</b>	<9.2	<10	<9.2	<10

### 3.2.3 *In vitro* antiparasmodial evaluation against *Plasmodium falciparum*

The sulfonamide compounds, **SF1-SF5**, and their Fe (II) complexes, **C1-C5**, were evaluated for antiparasmodial activity *in vitro* against the NF54 chloroquine sensitive strain of *P. falciparum*. A full dose-response experiment was performed for all the compounds in order to obtain the half-maximal inhibitory concentrations ( $IC_{50}$  values). The  $IC_{50}$  is defined as the concentration needed to inhibit 50% of the parasite growth. The *in vitro* antiparasmodial activity was determined via the *Plasmodium* lactate dehydrogenase assay using the method describe by Markler et al.<sup>27</sup>

*Plasmodium* lactate dehydrogenase (pLDH) is a terminal enzyme found in the glycolytic pathway of the parasite.<sup>28</sup> The enzyme is responsible for the conversion of lactate to pyruvate using the coenzyme nicotinamide adenine dinucleotide (NADH). The pLDH assay is based on the detection of the pLDH enzyme, which is associated with the percentage parasite viability in the blood.<sup>29</sup> Instead of NADH, the method used by Markler et al.,<sup>27</sup> uses the 3-acetyl pyridine analogue of the  $NAD^+$  (APAD<sup>+</sup>).<sup>30</sup> This is due to the ability of APAD<sup>+</sup> to bind more efficiently and faster to pLDH in comparison to the human lactate dehydrogenase enzyme (hLDH). This enables the assay to determine pLDH activity over hLDH activity.

The concept of the pLDH assay is shown in Figure 3.7. During the assay, pLDH oxidises lactate to pyruvate and this reaction is coupled with the reduction of APAD<sup>+</sup> to APADH. In turn, APADH reduces the yellow-coloured tetrazolium dye to dark blue formazan in the presence of phenazine ethosulfate.<sup>29,30</sup> The  $IC_{50}$  values obtained with the standard error of the mean values are shown in table 3.4. Chloroquine and artesunate (Arts) were used as reference drugs.

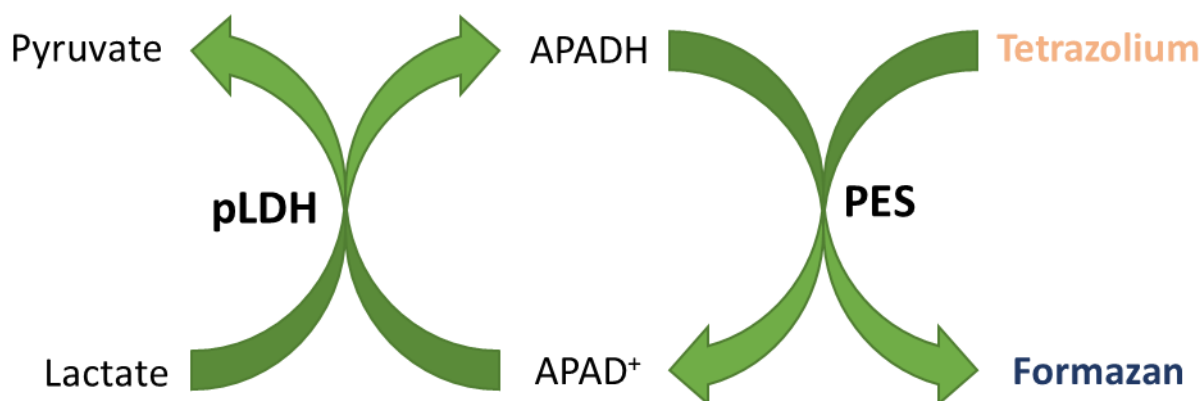


Figure 3.7: The principle of pLDH assay.<sup>30</sup>

Table 3.4: *In vitro* antiparasmodial activity of sulfonamide compounds, **Sf1-Sf5**, and the complexes, **C1-C5**, against the chloroquine-sensitive NF54 strain of *P. falciparum*.

Complex	IC <sub>50</sub> (μM)	SEM	Sulfonamides	IC <sub>50</sub> (μM)	SEM
<b>C1</b>	>6	*NA	<b>Sf1</b>	>6	*NA
<b>C2</b>	3.715	2.285	<b>Sf2</b>	4.984	1.016
<b>C3</b>	>6	*NA	<b>Sf3</b>	>6	*NA
<b>C4</b>	>6	*NA	<b>Sf4</b>	5.162	0.838
<b>C5</b>	5.822	0.178	<b>Sf5</b>	>6	*NA
<b>CQ</b>	0.007	0.001			
<b>Arts</b>	0.003	0.001			

\*NA – Not applicable. **Arts** – Artesunate.

Among the synthesised complexes, **C2** is the most active followed by **C5** with IC<sub>50</sub> values of 3.715 and 5.822 μM respectively. Moreover, these two complexes exhibited improved antiparasmodial activity in comparison to their respective unsubstituted sulfonamides compounds, **Sf2** and **Sf5**. This may be due to enhanced lipophilicity attributed by the hydrophobic ferrocenyl moiety. However, CQ (IC<sub>50</sub> = 0.007 μM) and Arts (IC<sub>50</sub> = 0.003 μM) were extremely active with IC<sub>50</sub> values in the sub-micromolar range compared to the synthesised complexes. It is evident that not merely is the lipophilic ferrocenyl moiety significant for achieving improved antiparasmodial activity, but the nature of the heterocyclic fragments also plays an important function in enhancing the activities of these compounds. This is demonstrated by the IC<sub>50</sub> value of **C2** (cLogP = 3.05) which is lower than that of **C1** (cLogP= 3.71). It is also observed that through the introduction of hydrophobic metal moieties greater antiparasmodial activities are not necessarily assured. This is demonstrated the IC<sub>50</sub> values of **Sf1** and **Sf3** that were still greater than 6 μM even after the introduction of the ferrocenyl moiety. Surprisingly, the activity of **Sf4** decreased upon the introduction of the ferrocenyl moiety, however it is important to note that the IC<sub>50</sub> of **Sf4** was close to 6 μM which is the upper concentration limit for the assay. This could infer that a delicate control of lipophilicity is essential to ensure cellular uptake by the parasite.

### 3.2.4 *In vitro* antimycobacterial evaluation against tuberculosis

The complexes, **C1-C5**, were further evaluated for their antimycobacterial activity against the non-pathogenic *M. smeg* Mc<sup>2</sup>155 and the pathogenic *M. tb* H37Rv strains of *mycobacterium tuberculosis*, by determination of their minimum inhibitory concentration (MIC) values using the modified broth microdilution method described by Leite <sup>31</sup> and resazurin dye was used. Resazurin is a blue/purple dye which is reduced to the pink, fluorescent resorufin, by aerobic respiration of metabolic active cells. The MIC value is defined as the lowest concentration that exhibit no growth at visual reading. Isoniazid, a currently used anti-TB drug, was used a positive control in this evaluation. The MIC results were interpreted as follows. For example, **C2** showed growth inhibition of *M. smeg* Mc<sup>2</sup>155 strain at 33.57  $\mu$ M (the wells in the 96 microplates were purple/blue) – 16.78  $\mu$ M (the wells were pink). Since we do not know the exact concentration where the bacteria are killed/inhibited, the MIC result was therefore reported as a range, **C2** 33.57 – 16.78  $\mu$ M. Table 3.5 summarises the data obtained for **C1-C5** and their respective sulfa drugs.

Table 3.5: The MIC values of the synthesised complexes, sulfa drugs and isoniazid as positive control against *M. smeg* Mc<sup>2</sup>155 and *M. tb* H37Rv.

	MIC (μM)	
	<i>Mycobacterium smegmatis</i>	<i>Mycobacterium tuberculosis</i>
	Mc <sup>2</sup> 155	H37Rv
<b>Isoniazid</b>	455.74 – 227.87	455.74 – 227.87
<b>C1</b>	119.65 – 59.83	59.83 – 31.82
<b>C2</b>	33.57 – 16.78	67.16 – 33.57
<b>C3</b>	253.90 – 126.95	31.73 – 15.86
<b>C4</b>	127.48 – 63.74	31.86 – 15.93
<b>C5</b>	135.19 – 67.60	33.79 – 16.89
<b>Sf1</b>	12.73 – 6.28	25.17 – 12.73
<b>Sf2</b>	1.90 – 0.95	15.60 – 7.70
<b>Sf3</b>	6.96 – 3.46	1.71 – 0.86
<b>Sf4</b>	56.12 – 28.02	56.12 – 28.02
<b>Sf5</b>	7.79 – 3.88	7.79 – 3.88
<b>Fc-COOH</b>	2172.78 – 1086.39	543.19 – 271.60

The sulfa drugs, **Sf1-Sf5** exhibited better activities than the synthesised complexes in both strains. The Mc<sup>2</sup>115 strain was inhibited at concentrations of 0.95 – 56.12 μM with sulfamethoxazole, **Sf2**, (MIC: 0.95 – 1.90 μM) being the most active. This may be due to the electron-donating nature of the amine functionality compared to the electron-withdrawing effects of the hydrophobic ferrocenyl moiety. Although the sulfa drugs exhibited better activities in the non-pathogenic strain, their activities significantly decreased in the pathogenic strain. Whereas the opposite effect was observed in **C1**, **C3**, **C4** and **C5**.

Among the synthesised complexes it was **C2**, bearing a five membered heterocyclic ring, which showed the highest activity against the Mc<sup>2</sup>155 strain, with MIC range of 33.57 - 16.78 μM,

followed by **C1** (MIC: 119.65 - 59.83  $\mu\text{M}$ ). This is contrary to what was expected as **C1** is more hydrophobic and therefore more lipophilic than **C2**, prompting the expectation that **C1** was to be more active than **C2** since increased lipophilicity is often translated into enhanced antimycobacterial activity. However, literature suggest that the ionic form of the sulfonamide is the active species. Thus, the pKa of the sulfonamide plays an important role in enhancing activity which is influenced by the nature of the heterocyclic ring.

As previously mentioned, **C1**, **C3**, **C4**, and **C5** showed moderate activities against the *Mycobacterium tuberculosis* H37Rv strain, with MIC values ranging between 15.86 and 59.83  $\mu\text{M}$ . Among these complexes, **C3** was the most active with an MIC range of 31.73 – 15.86  $\mu\text{M}$ , followed by **C4** and **C5** with MIC ranges of 31.86 – 15.93  $\mu\text{M}$  and 33.79 – 16.89  $\mu\text{M}$ , respectively. Other ferrocene derivatives were reported to display MIC<sub>90</sub> values of greater than 30  $\mu\text{M}$  but most displayed MIC<sub>90</sub> values of greater than 125  $\mu\text{M}$ .<sup>20,32–34</sup> Furthermore, all the complexes were found to be far more potent than INH in both strains, displaying activities greater than 10-fold.

### 3.2.5 *In vitro* cytotoxicity studies on healthy cells

One of the challenges experienced with the incorporation of metals into organic drug compounds, is the biological toxicity due to the metals. The complexes, **C1–C5**, were therefore investigated for their cytotoxicity against the human embryonic kidney 293 (HEK 293) and the human immortalised prostatic (PNT1A) cell lines using the rapid colorimetric tetrazolium dye procedure commonly referred to as the MTT (3-[4,5-dimethylthiazol-2-yl]-2,5-diphenyltetrazoliumbromide) assay.<sup>35</sup> The principle behind the MTT assay, shown in figure 3.7, is based on the conversion of a yellow MTT salt to purple formazan crystals by metabolically active cells. Thus, the darker the solution in the wells, the greater the number of metabolically active cells present.<sup>36,37</sup> The reduction results of MTT obtained are shown in Figure 3.8 below.

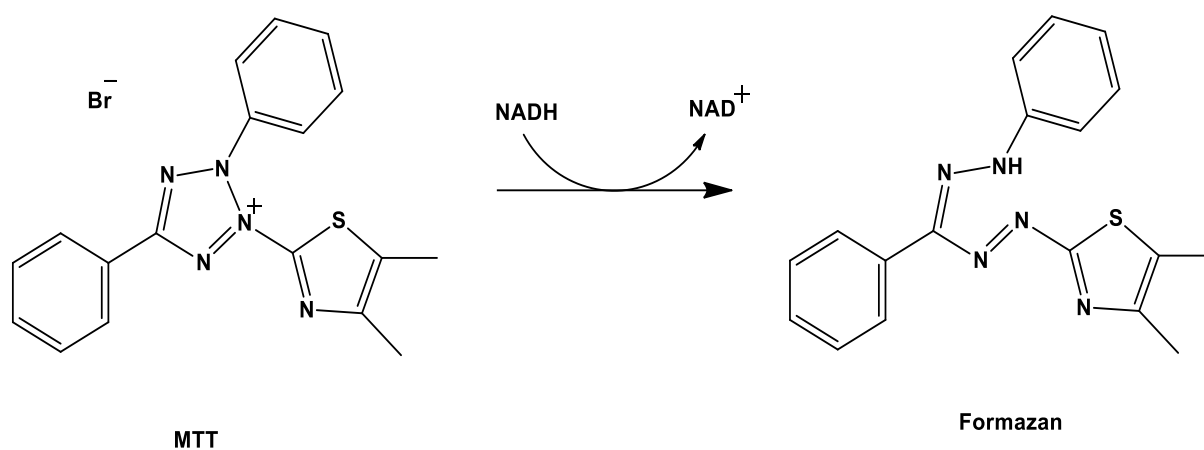


Figure 3.7: The conversion of MTT to formazan.<sup>37</sup>

From the graphs in Figure 3.8, it is evident that the complexes are not toxic to healthy cells up to 50  $\mu\text{M}$  ( $\text{IC}_{50} > 50\mu\text{M}$ ), the highest concentration tested. The different complexes exhibited similar patterns with no significant differences between the two cell lines. The sulfa drugs were not screened due to time constraints.

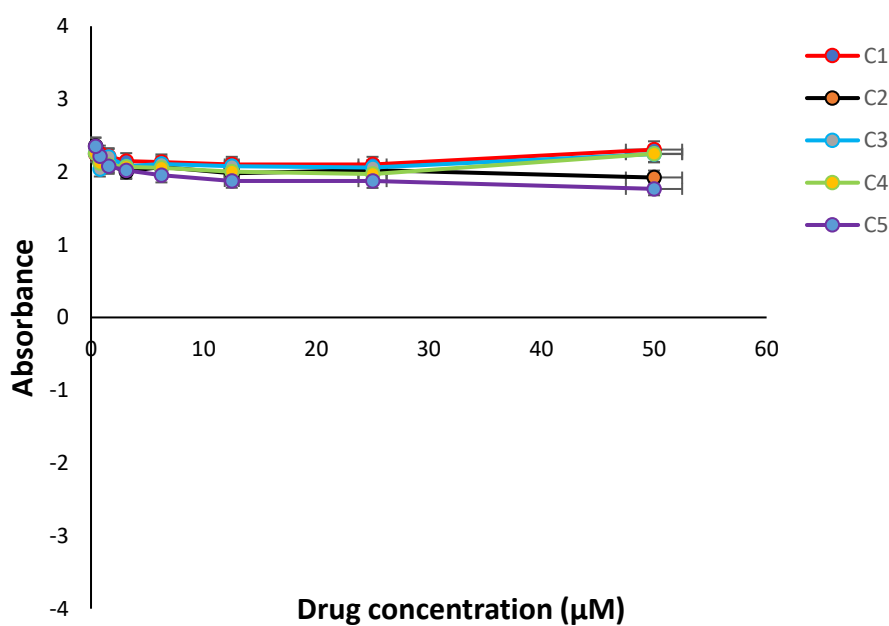


Figure 3.8: The effect of the complexes **C1-C5** on the reduction of MTT against HEK cell lines.

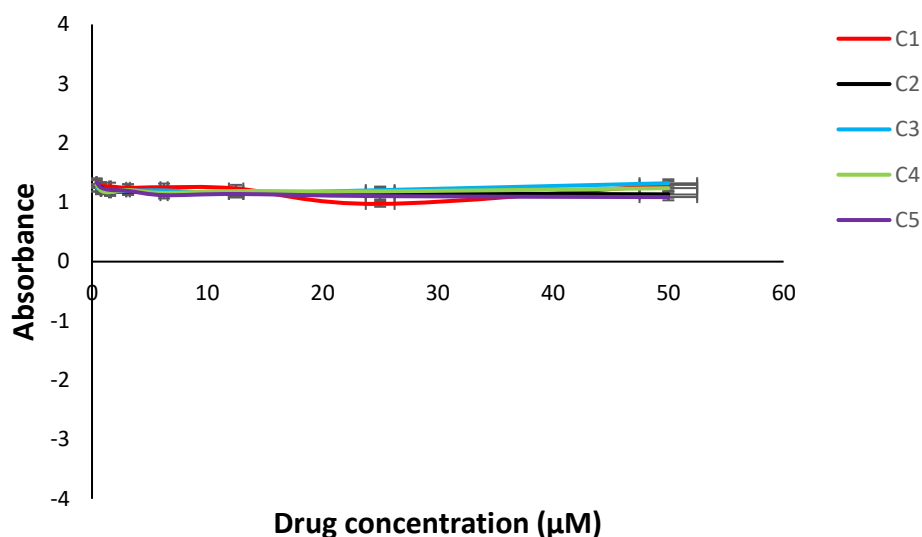


Figure 3.9: The effect of the complexes **C1-C5** on the reduction of MTT against PNT1A cell lines.

### 3.2.6 Aqueous stability studies

Stability plays a critical role in drug delivery systems. As lack of stability may significantly lower the intended dose and result in poor biological activity, which can potentially result in the drug being rejected. Therefore, it is of importance to study any instabilities in the initial stages of drug development. As mentioned in Chapter 2, DMSO is a widely used solvent in preparing drug stock solutions for biological assays. However, in this case, it was used to ensure complete dissolution in order to expose the complexes to solution conditions.

Time dependant hydrolysis studies were carried out in 2.5% DMSO/water and phosphate-buffered saline (PBS) systems over a period 24 h at 37°C. In 2.5% DMSO/water system, **C1**, **C2** and **C5** complexes showed changes in their spectra overtime. Changes was observed in the first 12h with little to no changes occurring after 12h (Figure 3.10). The UV scan (**C1**, **C2**, and **C5**) at 0 h displayed two absorption bands between 430 - 500nm and 240 - 300nm respectively. After 24 h, the absorption band between 430 - 500 nm completely disappeared and this may indicate possible structural changes as confirmed by ESI-MS in Chapter 2. In contrast, **C4** and **C3** appeared to be relatively stable.



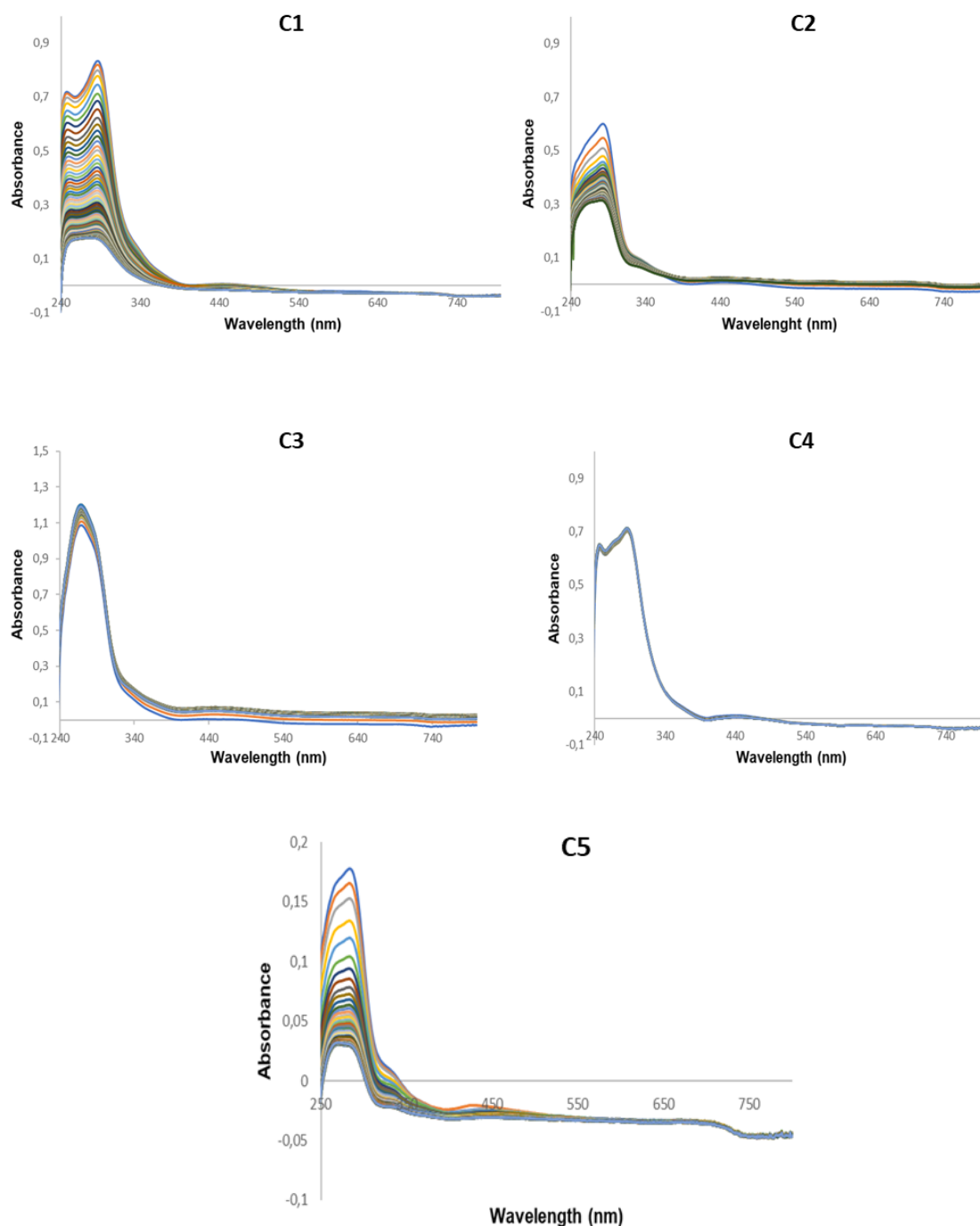


Figure 3.10: The UV-Vis spectra of **C1-C5** in 2.5% DMSO/water (v/v). The UV scan in each spectrum was taken every 10 min over a period of 24 hours.

However, in PBS, all complexes displayed no changes in their spectra overtime. The UV/Vis spectrum of **C3** is shown in Figure 3.11 as a representative example. This was unexpected as we thought the amide functional group would be deprotonated in buffer systems. This strongly

suggest that no chemical structural changes are taking place and this further substantiate that the sulfonamide and ferrocene moieties may remain intact in the blood plasma and cytoplasm.

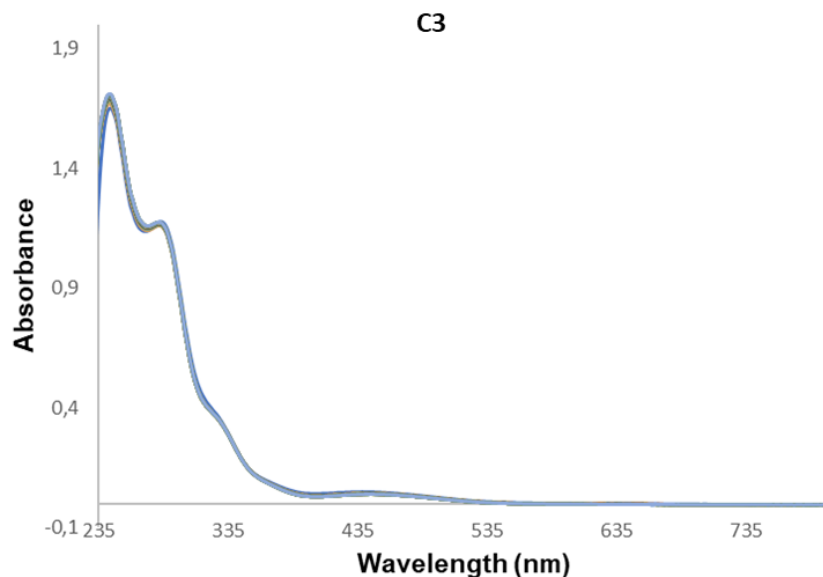


Figure 3.11: The UV-Vis spectra of **C3** in 2.5% DMSO/PBS (v/v) over a period of 24 hours.

### 3.3 Summary

The synthesised complexes and their respective sulfonamide compounds were evaluated *in vitro* for their antiplasmodial activity against the NF54 CQS strain of *P. falciparum*. Upon the introduction of the ferrocenyl moiety, the activity of selected sulfonamides was significantly enhanced, with some of the complexes being more active than their respective sulfonamides. Complex **C2** showed the best activity of all the complexes with an  $IC_{50}$  value of 3.714 followed by **C5**, having an  $IC_{50}$  value of 5.822  $\mu$ M. Unexpectedly, the antiplasmodial activity of **Sf4** decreased upon the introduction of the ferrocenyl moiety. The complexes and their respective sulfonamides were thereafter tested for their antimycobacterial activity against the non-pathogenic *M. smeg* and pathogenic *M. tb* strains of *M. tuberculosis*. For all of the complexes, the activities were higher in the pathogenic strain than in the non-pathogenic strain, with **C3** and **C4** exhibiting the highest activities. Complexes **C1-C5** were tested against the healthy HEK and PNT1A cell lines and were found not to be non-cytotoxic. To gain further insight into the physicochemical properties of these compounds, a turbidimetric assay was performed on all complexes. The complexes were highly soluble in DMSO but had poor solubility in both

the PBS and HEPES buffers. In order to investigate the relationship between lipophilicity and biological activity, the lipophilicity of the complexes was predicted. However, no linear correlation was established between lipophilicity, biological activity as well as the redox behaviour of the complexes

### 3.4 Experimental

#### 3.4.1 Turbidimetric Assay

A 0.01 M Phosphate Buffered Saline (PBS) solution (pH 7.4) was prepared by dissolving one PBS tablet (Sigma Aldrich) in 200 mL distilled water at 25 °C to yield a buffered solution containing 0.01 M phosphate buffer, 0.003 M KCl, and 0.14 M NaCl. The solution was filtered using a syringe filter after equilibrating at 25 °C for one hour upon which the pH was confirmed with a pH meter. A *N*-(2-Hydroxyethyl) piperazineethanesulfonic acid (HEPES) buffer solution was prepared by dissolving 1.191 g of HEPES free acid in 180 ml distilled water. Subsequently, a 0.1M solution of NaOH was added in 1mL equivalents to reach a pH of 7. The volume was then made up to 200 mL using distilled water.

A 10 mM stock solution in DMSO of each test compound was prepared and filtered through a 0.45 µm PVDF syringe filter prior to use. A preparation plate (96-well flat bottomed) was prepared by serially diluting each compound to achieve the desired concentrations (5.0 µM to 200 µM). The test plate was prepared by pipetting 196 µL DMSO into wells 1 – 6 and 196 µL PBS/ HEPES into wells 7 – 12. Each compound was tested in triplicate thus a single plate was used to evaluate two compounds. 4 µL of each concentration of the compound was pipetted from the preparation plate into the test plate in order to bring the total volume up to 200 µL and to ensure that a 2 % (v/v) DMSO/PBS and 2 % (v/v) DMSO/HEPES solution was achieved. Test plates were incubated for 2 hours at room temperature (25 °C) after which the UV-Vis absorbance readings were measured at 620 nm. The blank readings were subtracted from the absorbance for each concentration to obtain the corrected absorbance readings.

#### 3.4.2 Evaluation of *in vitro* activity against *Plasmodium falciparum*

The test samples were tested in triplicate on two separate occasions against the chloroquine-sensitive (NF54) strain of *P. falciparum*. Continuous *in vitro* cultures of asexual erythrocyte stages of *P. falciparum* were maintained using a modified method of Trager and Jensen.<sup>38</sup>

Quantitative assessment of antiplasmodial activity *in vitro* was determined via the parasite lactate dehydrogenase assay using a modified method described by Makler.<sup>27</sup> The test samples were prepared as a 10 mmol/L stock solution in 100% DMSO. Stock solutions were stored at -20 °C. Further dilutions were prepared on the day of the experiment. Chloroquine (CQ) and artesunate (Arts) were used as reference drugs in all experiments. A full dose-response was performed for all compounds to determine the concentration inhibiting 50% of parasite growth (IC<sub>50</sub> value). Test samples were tested at a starting concentration of 6 mmol/L, which was then serially diluted 2-fold in growth medium to generate the tested concentration range. The same dilution technique was used for all samples. CQ and Arts were tested from a starting concentration of 1 µg/mL.

The assay plate was incubated at 37°C for 72h in a sealed gas chamber under 3% O<sub>2</sub> and 4% CO<sub>2</sub> with the balance being N<sub>2</sub>. After 72h, the wells in the assay plate were gently resuspended, and 15 µL from each well was transferred to a duplicate plate containing 100 µL of Malstat reagent and 25 µL of nitroblue tetrazolium solution in each well. Plates were left to develop for 20 minutes in the dark and then absorbance of each well was quantified using a spectrophotometer at 620nm. The IC<sub>50</sub> values were obtained using a non-linear dose response curve fitting analysis via the Dotmatics software platform.

### 3.4.3 Evaluation of *in vitro* activity against *Mycobacterium tuberculosis*

A modified broth microdilution method by Leite et al., was used to determine the minimum inhibitory concentration (MIC) of five metal complexes against the non-pathogenic non-virulent *Mycobacterium smegmatis* (*M. smeg*) mc2155 in a bio-safety level 2 (BSL2) laboratory and *Mycobacterium tuberculosis* (*M. tb*) H37Rv in BSL3. Starter cultures was prepared by inoculating 1 mL of *M. smeg* mc2155 in 10 ml Middlebrook 7H9 broth (Difco, BD), supplemented with 0.5% glycerol and 10% Middlebrook oleic acid, albumin, dextrose and catalase (OADC) (Difco, BD). Following an overnight incubation of the starter culture, it was sub-cultured to an OD<sub>600</sub> of 0.005 and incubated till an OD<sub>600</sub> of 0.2-0.3 was reached. Aliquots of 50 µL of the metal complexes dissolved in dimethyl sulfoxide DMSO were added to a 96-well microplate to achieve a concentration of 500 µg/mL and serially diluted to 250, 125, 62.5, 31.25, 15.625, 7.1825, 3.91 and 1.955 µg/mL. Aliquots of 50 µL of inoculum (diluted 1:100) was added to the 96-well microplate. Middlebrook 7H9 medium with and without 1% DMSO was used as vehicle and sterility control. Plates was incubated for 72 hours

at 37 °C. Following the incubation period, 20 µL of 0.02% (w/v) resazurin was added to all the wells and incubated for four hours in the dark at 37 °C. Resazurin is a blue/purple dye which is reduced to the pink, fluorescent resorufin, by aerobic respiration of metabolic active cells. Viable cells will stain pink while non-viable cells stain blue. Plates will be visualised for a change in colour. Isoniazid was used as a positive control in the MIC assays. MIC is defined as the lowest concentration that exhibit no growth at visual reading (30)

The same assay was used to determine the MIC of the metal complexes against *M. tb* H37Rv, however starter cultures was prepared by inoculating 0.5 mL of *M. tb* H37Rv in 5 ml Middlebrook 7H9 broth (Difco, BD), supplemented with 0.5% glycerol and 10% OADC (Difco, BD). Following a 5–6-day incubation of the starter culture, cultures were sub-cultured to an OD600 of 0.005 and incubated till an OD600 of 0.2-0.3 is reached. *M. tb* plates were incubated for 7 days at 37 °C. Following the incubation period, 20 µL of 0.02% (w/v) resazurin was added to all the wells and incubated for 24 hours in the dark at 37 °C, after which the plates were visualised.

### 3.4.4 *In vitro* cytotoxicity on healthy cell lines

The cytotoxicity of the complexes was evaluated using the standard MTT 3-(4,5-Dimethylthiazol-2-yl)-2,5-diphenyltetrazolium bromide cellular viability assay as described by Kaschula et al. Briefly, the HEK 293 and immortalised human prostatic epithelial (PNT1A) cells were seeded in 96 well plates and allowed to settle overnight. Each complex, prepared in 100% DMSO, was added to the cells at relevant concentrations and incubated for 48 h. Thereafter, 10 µL of 5 mg/mL MTT was added to each well and incubated for further 4 hours at 37°C, followed by the addition of 100 µL of 10% sodium laurel sulfate in 0.01 M HCL, to solubilize the formazan crystals. The plates were read at 595 nm on a Multiscan FC plate reader (Thermo Fischer Scientific, Life Technologies, South Africa), and data was analysed using Graphpad Prism 4 software, sigmoidal dose–response variable slope curve fitting. The assay was done twice on different occasions.

## 3.5 References

- 1 World Health Organization, *World Malaria Report: 20 years of global progress and challenges*, 2020.

- 2 G. WHO, Global tuberculosis report 2020, *Glob. Tuberc. Rep.*
- 3 C. J. Murray, K. S. Ikuta, F. Sharara, L. Swetschinski, G. Robles Aguilar, A. Gray, C. Han, C. Bisignano, P. Rao, E. Wool, S. C. Johnson, A. J. Browne, M. G. Chipeta, F. Fell, S. Hackett, Global burden of bacterial antimicrobial resistance in 2019: a systematic analysis, *Lancet*, 2022, **399**, 629–655.
- 4 W. C Reygaert, An overview of the antimicrobial resistance mechanisms of bacteria, *AIMS Microbiol.*, 2018, **4**, 482–501.
- 5 N. Muralidharan, R. Sakthivel, D. Velmurugan and M. M. Gromiha, Computational studies of drug repurposing and synergism of lopinavir, oseltamivir and ritonavir binding with SARS-CoV-2 protease against COVID-19, *J. Biomol. Struct. Dyn.*, 2021, **39**, 2673–2678.
- 6 H. Xue, J. Li, H. Xie and Y. Wang, Review of drug repositioning approaches and resources, *Int. J. Biol. Sci.*, 2018, **14**, 1232–1244.
- 7 P. Chellan, V. M. Avery, S. Duffy, J. A. Triccas, G. Nagalingam, C. Tam, L. W. Cheng, J. Liu, K. M. Land, G. J. Clarkson, I. Romero-Canelón and P. J. Sadler, Organometallic Conjugates of the Drug Sulfadoxine for Combatting Antimicrobial Resistance, *Chem. - A Eur. J.*, 2018, **24**, 10078–10090.
- 8 M. Campillos, M. Kuhn, A. C. Gavin, L. J. Jensen and P. Bork, Drug target identification using side-effect similarity, *Science (80-. )*, 2008, **321**, 263–266.
- 9 P. Chellan and P. J. Sadler, Enhancing the Activity of Drugs by Conjugation to Organometallic Fragments, *Chem. - A Eur. J.*, 2020, **26**, 8676–8688.
- 10 J. Xiao, Z. Sun, F. Kong and F. Gao, Current scenario of ferrocene-containing hybrids for antimalarial activity, *Eur. J. Med. Chem.*, 2020, **185**, 111791.
- 11 Patra, M.; Gasser, G. The Medicinal Chemistry of Ferrocene and Its Derivatives. *Nat. Rev. Chem.* 2017, **1**, 9.
- 12 C. Biot, G. Glorian, L. A. Maciejewski, J. S. Brocard, O. Domarle, G. Blampain, P. Millet, A. J. Georges, H. Abessolo and D. Dive, Synthesis and antimalarial activity in vitro and in vivo of a new ferrocene– chloroquine analogue, *J. Med. Chem.*, 1997, **40**, 3715–3718.

- 13 F. Dubar, T. J. Egan, B. Pradines, D. Kuter, K. K. Ncokazi, D. Forge, J.-F. Paul, C. Pierrot, H. Kalamou and J. Khalife, The antimalarial ferroquine: role of the metal and intramolecular hydrogen bond in activity and resistance, *ACS Chem. Biol.*, 2011, **6**, 275–287.
- 14 M. Niederweis, O. Danilchanka, J. Huff, C. Hoffmann and H. Engelhardt, Mycobacterial outer membranes: in search of proteins, *Trends Microbiol.*, 2010, **18**, 109–116.
- 15 P. C. Karakousis, in *Antimicrobial drug resistance*, Springer, 2009, pp. 271–291.
- 16 X. Liu, B. Testa and A. Fahr, Lipophilicity and its relationship with passive drug permeation, *Pharm. Res.*, 2011, **28**, 962–977.
- 17 M. K. Bayliss, J. Butler, P. L. Feldman, D. V. S. Green, P. D. Leeson, M. R. Palovich and A. J. Taylor, Quality guidelines for oral drug candidates: dose, solubility and lipophilicity, *Drug Discov. Today*, 2016, **21**, 1719–1727.
- 18 J. U. Peters, J. Hert, C. Bissantz, A. Hillebrecht, G. Gerebtzoff, S. Bendels, F. Tillier, J. Migeon, H. Fischer, W. Guba and M. Kansy, Can we discover pharmacological promiscuity early in the drug discovery process?, *Drug Discov. Today*, 2012, **17**, 325–335.
- 19 T. Stringer, D. Taylor, C. De Kock, H. Guzgay, A. Au, S. H. An, B. Sanchez, R. O'Connor, N. Patel, K. M. Land, P. J. Smith, D. T. Hendricks, T. J. Egan and G. S. Smith, Synthesis, characterization, antiparasitic and cytotoxic evaluation of thioureas conjugated to polyamine scaffolds, *Eur. J. Med. Chem.*, 2013, **69**, 90–98.
- 20 T. Stringer, R. Seldon, N. Liu, D. F. Warner, C. Tam, L. W. Cheng, K. M. Land, P. J. Smith, K. Chibale and G. S. Smith, Antimicrobial activity of organometallic isonicotinyl and pyrazinyl ferrocenyl-derived complexes, *Dalton Trans.*, 2017, **46**, 9875–9885.
- 21 R. Mannhold and R. F. Rekker, The hydrophobic fragmental constant approach for calculating log P in octanol/water and aliphatic hydrocarbon/water systems, *Perspect. Drug Discov. Des.*, 2000, **18**, 1–18.
- 22 R. Ahmed and T. Lanez, Calculation of octanol/water partition coefficients of ferrocene derivatives, *Asian J. Chem.*, 2010, **22**, 299–306.

- 23 P. Chellan, K. M. Land, A. Shokar, A. Au, S. H. An, D. Taylor, P. J. Smith, K. Chibale and G. S. Smith, Di- and trinuclear ruthenium-, rhodium-, and iridium-functionalized pyridyl aromatic ethers: A new class of antiparasitic agents, *Organometallics*, 2013, **32**, 4793–4804.
- 24 L. Di and E. Kerns, *Drug-like properties: concepts, structure design and methods from ADME to toxicity optimization*, Academic press, 2015.
- 25 C. A. Lipinski, Lead-and drug-like compounds: the rule-of-five revolution, *Drug Discov. today Technol.*, 2004, **1**, 337–341.
- 26 C. A. Lipinski, F. Lombardo, B. W. Dominy and P. J. Feeney, Experimental and computational approaches to estimate solubility and permeability in drug discovery and development settings, *Adv. Drug Deliv. Rev.*, 1997, **23**, 3–25.
- 27 M. T. Makler, J. M. Ries, J. A. Williams, J. E. Bancroft, R. C. Piper, B. L. Gibbins and D. J. Hinrichs, Parasite lactate dehydrogenase as an assay for *Plasmodium falciparum* drug sensitivity., *Am. J. Trop. Med. Hyg.*, 1993, **48**, 739–741.
- 28 C. F. Markwalter, K. M. Davis and D. W. Wright, Immunomagnetic capture and colorimetric detection of malarial biomarker *Plasmodium falciparum* lactate dehydrogenase, *Anal. Biochem.*, 2016, **493**, 30–34.
- 29 R. Piper, J. LeBras, L. Wentworth, A. Hunt-Cooke, S. Houzé, P. Chiodini and M. Makler, Immunocapture diagnostic assays for malaria using *Plasmodium* lactate dehydrogenase (pLDH), *Am. J. Trop. Med. Hyg.*, 1999, **60**, 109–118.
- 30 M. T. Makler, R. C. Piper and W. K. Milhous, Lactate dehydrogenase and the diagnosis of malaria, *Parasitol. Today*, 1998, **14**, 376–377.
- 31 C. Q. Fujimura Leite, A. L. Remédio Zeni Beretta, I. Shizuko Anno and M. A. Da Silva Telles, Standartization of Broth Microdilution Method for *Mycobacterium tuberculosis*, *Mem. Inst. Oswaldo Cruz*, 2000, **95**, 127–129.
- 32 S. Siangwata, N. Baartzes, B. C. E. Makhubela and G. S. Smith, Synthesis, characterisation and reactivity of water-soluble ferrocenylimine-Rh(I) complexes as aqueous-biphasic hydroformylation catalyst precursors, *J. Organomet. Chem.*, 2015, **796**, 26–32.
- 33 N. Baartzes, T. Stringer, J. Okombo, R. Seldon, D. F. Warner, C. de Kock, P. J. Smith



- and G. S. Smith, Mono- and polynuclear ferrocenylthiosemicarbazones: Synthesis, characterisation and antimicrobial evaluation, *J. Organomet. Chem.*, 2016, **819**, 166–172.
- 34 A. Mahajan, L. Kremer, S. Louw, Y. Guéradel, K. Chibale and C. Biot, Synthesis and in vitro antitubercular activity of ferrocene-based hydrazones, *Bioorganic Med. Chem. Lett.*, 2011, **21**, 2866–2868.
- 35 I. Mitra, S. Mukherjee, P. B. Reddy Venkata, S. Dasgupta, C. K. Jagadeesh Bose, S. Mukherjee, W. Linert and S. C. Moi, Benzimidazole based Pt(II) complexes with better normal cell viability than cisplatin: Synthesis, substitution behavior, cytotoxicity, DNA binding and DFT study, *RSC Adv.*, 2016, **6**, 76600–76613.
- 36 S. P. Langdon, Cancer Cell Culture, *Cancer Cell Cult.*, 2003, **731**, 237–245.
- 37 T. L. Riss, R. A. Moravec, A. L. Niles, S. Duellman, H. A. Benink, T. J. Worzella and L. Minor, Cell Viability Assays, *Assay Guid. Man.*, 2004, 1–25.
- 38 W. Trager and J. B. Jensen, Human malaria parasites in continuous culture, *Science* (80)., 1976, **193**, 673–675.

## Chapter 4: Conclusions and future work

### 4.1 Conclusions

This project successfully synthesised a small library of ferrocenyl conjugates of sulfa drugs and evaluated the activity of the complexes as antimicrobial agents. The structure of these complexes varied in degrees of electron-donating or withdrawing effects of the different heterocyclic rings. The ferrocene moiety was introduced via an amide linker to increase the lipophilic character of the sulfa drugs, thus allowing the drugs to diffuse more efficiently through the hydrophobic membranes of the microbes. It was also incorporated for its ability to produce ROS (reactive oxygen species) causing cellular membrane damage.

The complexes were prepared via a two-step reaction using commercially available reagents. The reaction started with nucleophilic acyl substitution to form ferrocenoyl chloride from ferrocene carboxylic acid directly followed by aminolysis. All the complexes were successfully characterised using various analytical and spectroscopic techniques including  $^1\text{H}$  and  $^{13}\text{C}$  { $^1\text{H}$ } nuclear magnetic resonance (NMR) spectroscopy, infrared (IR) spectroscopy, and electrospray ionisation mass spectrometry (ESI-MS). Reversed phase HPLC (RP-HPLC) was used to assess the purity of the complexes while the redox behaviours were evaluated using cyclic voltammetry (CV).

All synthesised complexes were screened *in vitro* for potential antiplasmodial activity against the chloroquine-sensitive NF54 strain of *P. falciparum*. Complexes **C1**, **C3**, and **C4** exhibited low antiplasmodial activities while complexes **C2** and **C5** exhibited moderate activities, displaying  $\text{IC}_{50}$  values of 3.715 and 5.822  $\mu\text{M}$  respectively. However, the complexes could not be screened for antiplasmodial activity against the chloroquine-resistant strain due to unforeseen contamination and time constraints.

The complexes were additionally screened *in vitro* for antitubercular activity against the non-pathogenic *M. smeg* strain of *M. tuberculosis*. The parent sulfa drugs exhibited good antitubercular activity with MIC values  $< 26 \mu\text{M}$ . This was attributed to the presence of the primary amine functionality which assisted in the accumulation of the drug within the bacterium. Upon incorporating ferrocene into the structures of these sulfa drugs, the antitubercular activity decreased. This is likely due to increased lipophilicity causing strong interactions between the complexes and the hydrophobic membranes of the parasite. Despite

this, **C2** (MIC: 33.57 – 16.78  $\mu$ M) showed enhanced activity over sulfamethazine (MIC: 56.12 – 28.02  $\mu$ M) and was also found to be the most active among the complexes in this strain.

The complexes were further screened for antitubercular activity against the pathogenic *M. tb* H37Rv strain of *Mycobacterium tuberculosis*. Interestingly, the complexes displayed increased activity compared to that in the non-pathogenic strain. Complexes **C3**, **C4**, and **C5** displayed similar activities. Surprisingly, the activity of complex **C2** decreased. The cytotoxicity of the complexes was evaluated against the healthy, human embryonic kidney (HEK 293) along with the human immortalised prostatic (PNT1A) cell lines, which were all found to be non-cytotoxic, indicating selectivity towards the microbial strains.

## 4.2 Future work

Based on the results of this study, the sulfonamide complexes exhibited promising antimicrobial activity. However, future mechanistic studies and structural modifications can be made in order to gain insight into possible mode(s) of action, to improve solubility and enhance efficacy.

### 4.2.1 Mechanistic studies

Stage specific assays could be undertaken to determine which stage of the parasite's life cycle the complexes target. The inhibition of haemozoin formation, in the erythrocytic stage, can lead to the death of the parasite due to the build-up of haematin in the digestive vacuole of the parasite. Therefore, the ability of a compound to inhibit haemozoin formation is important and can be evaluated by the use of Nonidet P-40 mediated assay to determine  $\beta$ -haematin inhibition activity.<sup>1,2</sup> The ability of the ferrocenyl derivatives to produce ROS, as an additional mechanism of action, can be evaluated by incubating the complexes with an antioxidant like N-acetylcysteine (NAC), a free radical scavenger. If the activity of the compounds is enhanced by means of oxidative damage, the use of NAC would then decrease the activity (increase  $IC_{50}$  values) of the compounds and thus providing insight into whether ROS formation is a possible mode of action.<sup>3</sup>

Recently, it was discovered that laboratory adapted strains such as the H37Rv, CDC 155, and Erdman have the ability to survive and grow by using the cytochrome bd oxidase complex during chemical inhibition of the bc1 complex.<sup>4</sup> This was further supported by Renier et al.,<sup>5</sup>

when they tested several compounds in the glycerol-aniline-salts with iron (GAST-Fe) medium using the *mtb::gfp* strain and found to be active. However, the same compounds were inactive when tested following the 14-days incubation standard middle-brook 7H9 medium supplemented with ADC. Similarly, Stringer et al.,<sup>6</sup> found promising antimycobacterial activities in the GAST-Fe medium in comparison to the glucose-based Middlebrook 7H9-ADC, suggesting that the complexes may inhibit the growth of *Mycobacterium tuberculosis* by disrupting glycerol metabolism, resulting in the accumulation of toxic metabolites within the bacteria.<sup>6</sup>

In light of these, the complexes can be tested against *M. tuberculosis* cytochrome bd oxidase, depletion mutant ( $\Delta$ cyd/KO), strain in order to evaluate if cytochrome bd oxidase is a potential cellular target for these complexes. The MIC values can be determined via the microplate-based alamar blue assay (MABA) using the method described by Franzblau et al.<sup>7</sup>

#### 4.2.2 Structural modifications

Structural modifications can be made in order to improve the solubility and enhance biological activity. Since low solubility was encountered in this study, it is suggested that incorporating water-soluble groups may improve the solubility and potentially other physicochemical properties resulting in increased biological activity of these complexes.<sup>8</sup> Furthermore, by changing the amide linker to a secondary amine one may achieve increased activity by enhancing the accumulation of the compound in the digestive vacuole of the parasite, counteracting lipophilicity through pH trapping which refers to the degree of ionization of the drug in physiological medium.<sup>9</sup> Proposed structural modifications of one complex, which may enhance activity and overall solubility is presented in Figure 4.1

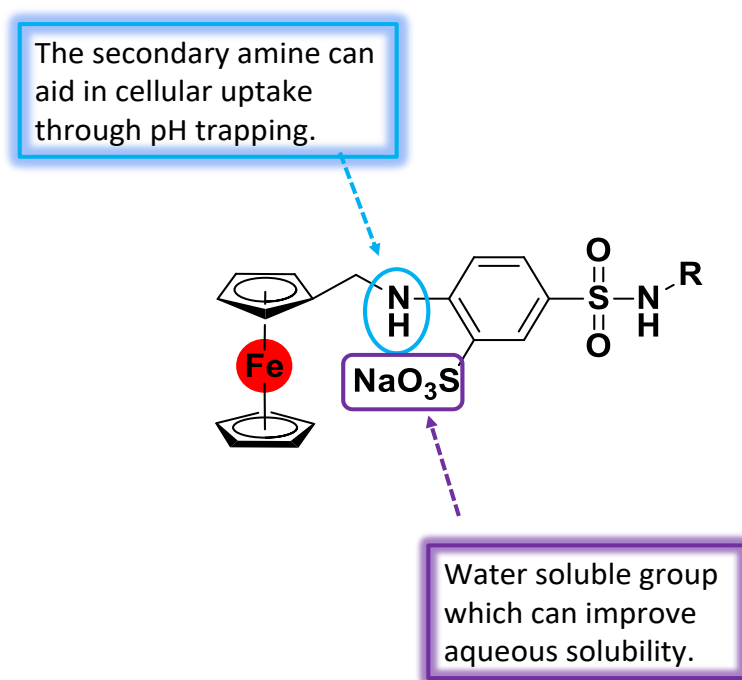


Figure 4.1: Proposed structural modification to enhance antimicrobial activity and overall solubility.

### 4.3 References

- 1 P. Chellan, K. M. Land, A. Shokar, A. Au, S. H. An, C. M. Clavel, P. J. Dyson, C. de Kock, P. J. Smith and K. Chibale, Exploring the versatility of cycloplatinated thiosemicarbazones as antitumor and antiparasitic agents, *Organometallics*, 2012, **31**, 5791–5799.
- 2 D. R. Melis, C. B. Barnett, L. Wiesner, E. Nordlander and G. S. Smith, Quinoline-triazole half-sandwich iridium (III) complexes: Synthesis, antiplasmodial activity and preliminary transfer hydrogenation studies, *Dalt. Trans.*, 2020, **49**, 11543–11555.
- 3 A. A. L. G. Marianna Halasi, Ming Wang, Tanmay S. Chavan, Vadim Gaponenko, Nissim Hay, ROS inhibitor N-acetyl-L-cysteine antagonizes the activity of proteasome inhibitors, *Biochem J.*, 2008, **23**, 1–7.
- 4 K. Arora, B. Ochoa-Montaña, P. S. Tsang, T. L. Blundell, S. S. Dawes, V. Mizrahi, T. Bayliss, C. J. Mackenzie, L. A. T. Cleghorn, P. C. Ray, P. G. Wyatt, E. Uh, J. Lee, C. E. Barry and H. I. Boshoff, Respiratory flexibility in response to inhibition of cytochrome C oxidase in *Mycobacterium tuberculosis*, *Antimicrob. Agents*

- Chemother.*, 2014, **58**, 6962–6965.
- 5 R. Van Der Westhuyzen, S. Winks, C. R. Wilson, G. A. Boyle, R. K. Gessner, C. Soares De Melo, D. Taylor, C. De Kock, M. Njoroge, C. Brunschwig, N. Lawrence, S. P. S. Rao, F. Sirgel, P. Van Helden, R. Seldon, A. Moosa, D. F. Warner, L. Arista, U. H. Manjunatha, P. W. Smith, L. J. Street and K. Chibale, Pyrrolo[3,4-c]pyridine-1,3(2H)-diones: A novel antimycobacterial class targeting mycobacterial respiration, *J. Med. Chem.*, 2015, **58**, 9371–9381.
  - 6 T. Stringer, R. Seldon, N. Liu, D. F. Warner, C. Tam, L. W. Cheng, K. M. Land, P. J. Smith, K. Chibale and G. S. Smith, Antimicrobial activity of organometallic isonicotinyl and pyrazinyl ferrocenyl-derived complexes, *Dalt. Trans.*, 2017, **46**, 9875–9885.
  - 7 S. G. Franzblau, R. S. Witzig, J. C. McLaughlin, P. Torres, G. Madico, A. Hernandez, M. T. Degnan, M. B. Cook, V. K. Quenzer and R. M. Ferguson, Rapid, low-technology MIC determination with clinical *Mycobacterium tuberculosis* isolates by using the microplate Alamar Blue assay, *J. Clin. Microbiol.*, 1998, **36**, 362–366.
  - 8 A. D. M. Mohamad, E. R. El-Shrkawy, M. F. I. Al-Hussein and M. S. S. Adam, Water-soluble Cu (II)-complexes of Schiff base amino acid derivatives as biological reagents and sufficient catalysts for oxidation reactions, *J. Taiwan Inst. Chem. Eng.*, 2020, **113**, 27–45.
  - 9 C. Biot and D. Dive, Bioorganometallic chemistry and malaria, *Med. Organomet. Chem.*, 2010, 155–193.